UNIVERSITY OF SOUTHAMPTON

FACULTY OF ENGINEERING, SCIENCE AND MATHEMATICS

School of Ocean and Earth Science

On steady and variable buoyancy forcing in the Atlantic, an idealised modelling study.

by

Marc A. Lucas

Thesis for the degree of Doctor of Philosophy

February 2005

Graduate School of the
Southampton Oceanography Centre

This PhD dissertation by

Marc A. Lucas

has been produced under the supervision of the following persons:

Supervisor:

Prof. Jochem Marotzke

Chair of Advisory Panel:

Prof. Harry L. Bryden

Member of Advisory Panel:

Prof. John G. Shepherd

Declaration of Authorship

I, Marc A. Lucas, declare that the thesis entitled ‘On steady and variable buoyancy forcing in the Atlantic, an idealised modelling’ and the work presented in it are my own. I confirm that:

• this work was done wholly or mainly while in candidature for a research degree at this University;

• where any part of this thesis has previously been submitted for a degree or any other qualification at this University or any other institution, this has been clearly stated;

• where I have consulted the published work of others, this is always clearly attributed;

• where I have quoted from the work of others, the source is always given. With the exception of such quotations, this thesis is entirely my own work;

• I have acknowledged all main sources of help;

• where the thesis is based on work done by myself jointly with others, I havemade clear exactly what was done by others and what I have contributed myself;

• Chapter 4 has been published as:

Lucas, M. A., J. J. Hirschi, J. D. Stark, and J. Marotzke, 2005: The response of an idealized ocean basin to variable buoyancy forcing. *Journal of Physical Oceanography*, in press.

Signed: .....
Date: .....

UNIVERSITY OF SOUTHAMPTON

ABSTRACT

FACULTY OF SCIENCE, SCHOOL OF OCEAN AND EARTH SCIENCE

Doctor of Philosophy

ON STEADY AND VARIABLE BUOYANCY FORCING IN THE ATLANTIC, AN IDEALISED MODELLING STUDY

By Marc A. Lucas

This study examines the response of the thermohaline circulation in the north Atlantic to steady and variable buoyancy forcing. The model used is a version of the MOMA model (Webb, 1996), updated to include a free surface and Gent & McWilliams mixing. The model's resolution is coarse, 4 x4 degrees with 15 levels in the vertical. In a first instance, the model's response to 14 different fixed thermal profiles is investigated, by systematically keeping the equator temperature fixed and then the northernmost temperature fixed. The results show that the models response differs for these two sets of experiments as one setup favours stratification while the other favours convection. In a second instance, the restoring field is made to oscillate over 17 different periods, ranging from 6 months to 32,000 years. The model's meridional overturning circulation (MOC) exhibits a very strong response on all timescales greater than 15 years, up to and including the longest forcing timescales examined. The peak-to-peak values of the MOC oscillations reach up to 125% of the steady-state maximum MOC and exhibit resonance-like behaviour, with a maximum at centennial to millennial forcing periods (depending on the vertical diffusivity). This resonance-like behaviour stems from the existence of two adjustment time scales, one of which is set by the vertical diffusion and another, which is set by the basin width. Finally, the study is extended to a double hemisphere basin. Again, the model's MOC exhibits a very strong response on all timescales in both hemispheres, up to and including the longest forcing timescales examined for either set of experiments with the amplitude of the oscillations reaching up to 140% of the steady-state maximum MOC and exhibiting resonance-like behaviour, with a maximum at centennial to millennial forcing periods. This resonance like behaviour is identical to what has been observed in a single hemisphere and occurs for the same reasons. What is novel is that when the forcing in the southern subordinate hemisphere lags that of the northern by half a period, the amplitude of the response is substantially greater for large forcing periods (millennial and above), particularly in the subordinate (southern) hemisphere. This happens because the basin has in effect two sources of deep water. This leads to colder bottom waters and thus greater stratification, which in turn stabilises the water column and thus reduces the value of the minimum overturning. The considerable deviation from the quasi-equilibrium response at all timescales above 15 years for both the single hemisphere and the double hemisphere experiments is surprising and suggests a potentially important role of the ocean circulation for climate even at Milankovich timescales.

Acknowledgements:

First of all, I would like to thanks Prof. Jochem Marotzke for giving me this opportunity to delve into the realm ocean modelling. His enthusiasm over these three years is gratefully acknowledged as is his insistence on addressing zero order problems. If I have learnt anything, then it must the importance of scientific rigour in all the aspects of research.

I would also like to thank Joel Hisrchi, without whom much of this work would not have happened. His passion for all aspects of oceanography is truly infectious and his constant probing and fascination for the various problems encountered, either theoretical or numerical are exemplary. The whole group benefited from his insights and I owe him much in terms of the analytical approaches used during my PhD. He was also a much appreciated and efficient "secondary supervisor" when Jochem left for MPI.

I would also like to thank John Stark for setting up the model and adding the various pieces of code to bring it up to date. He greatly reduces the amount of time I spent staring at an insipid piece of code in frustration.

Special thanks also to the member of my advisory panel, Prof. Harry Bryden and Prof. John Shepherd who insured that my research stayed on course and encouraged me to look at the bigger picture, beyond the realm of numerical modelling.

A special mention must go to Matt Palmer. Sharing an office with him meant that we could share our day to day frustrations and discuss various aspects of our work. I also learnt a lot about music, surfing and the Indian Ocean.

The physical oceanography group must also be mentioned, particularly Clotilde, Fiona and Johanna as well as Rachel, Hannah, Adam and Zoë. The weekly meetings allowed me to broaden my knowledge of oceanography in a friendly and relaxed environment.

Thanks also to all the fellow students at the SOC, particularly the Mediterranean crowd for providing and enjoyable social environment while I was in Southampton.

Finally, I would like to thank my parents and family for their support and of course, I have to thank Başak, who walked this road with me…

Table of Contents

Table of Figures

Chapter 1: Introduction

Summary:

In this chapter, the motivation behind this thesis is addressed. This is followed by a brief review of relevant topics namely, the North Atlantic and the Thermohaline circulation, the variability in data, the variability in models and fundamental modelling issues. Finally, a brief outline of the thesis is given.

1.1) Motivation:

The advent of numerical modelling has allowed the physical oceanographic community to take great steps in understanding problems that mathematical analysis cannot solve. Enormous progress in modelling has been made but some of the fundamental processes are still far from understood.

Simple theoretical models have been around since the 1950's. The box model of Henry Stommel (1961) was particularly notable in that it clearly demonstrated the strength of using equations to solve a physically relevant oceanographic problem. The next crucial step was the comparatively simple code of Bryan (1969). With the work of Cox (1984) the code was improved and has evolved into today's high resolution complex ocean models. Although the complexity of these models has dramatically increased, it is fair to say that the greater amount of progress has been due to the improvement of computing power rather than from a revolutionary approach. This might be changing with the development of

finite element adaptive grids models such as the one being developed at Imperial College, London (ICOM, 2004). However, these models are still in their infancy and most of today's state-of-the-art ocean models are still based on the Bryan code written some 35 years ago.

This is not to say that there have not been significant improvements to the code. Particularly notable are the works of Redi (1982) of Gent and McWilliam (1990) in the domain of diffusion and eddy parameterisation. There has also been the development of isopycnal coordinates models such as MICOM (Miami Isopycnal Ocean Model), sigma coordinates models (Princeton Ocean Model) and Hybrid coordinates models such as Hybrid Coordinate Ocean Model (Bleck, 2002).

However, the lion's share of improvements is the results of an increase in the resolution from coarse, $4^{o}x4^{o}$ non-eddy-permitting grids at the beginning of the last decade to the $1/12^{o}$ eddy-resolving grid of OCCAM (Ocean Circulation and Climate Advanced Modelling)(Webb, 1995). The increase in resolution is a direct result of the increase in processor speed and this increase was such that very quickly, physical oceanographers went from very basic ocean only process modelling with no or very simple topography to fully coupled ocean atmosphere scenarios with realistic topography. This was in part due to the growing awareness by the funding authorities of the uncertainties regarding a possible global warming and the need to have an idea of the possible scenarios (IPCC, 2001).

The result is that although the scientific community now possesses a catalogue of scenarios for the earth's climate in the coming century, some of the basic processes that take place in the ocean are still not properly understood. The effect of buoyancy forcing is a prime example. A scaling law linking the equator to pole thermal gradient to the meridional overturning circulation, derived from the basic equation does not seem to hold (Marotzke 1997, Scott 2000). And to date, the response of the ocean to an oscillatory pure buoyancy forcing has not been

investigated. The aim of the present study is to address this particular gap in the modelling community's understanding of the ocean circulation's behaviour.

1.2) The North Atlantic and the THC:

The North Atlantic is the only region in the world where pure deep-water formation takes place. This is not a continuous process and occurs intermittently, during the coldest months of the year through deep convective events (Dickson & Brown, 1994). This does not mean that no deep water is formed anywhere else: there is deep-water formation in the Mediterranean for instance and of course in the Weddell Sea, where the world densest waters are formed. However, both the Mediterranean deep water and as the Weddell Sea Water are profoundly modified by cabelling and lose their distinct T-S signature very rapidly as they are carried away from the site of formation. By contrast the North Atlantic Deep Water (NADW) retains its T-S signature fairly well.

This deep water formation, which results from a combination of sinking and then cooling of the sinking waters is made possible by the high salinity of the Atlantic surface waters, which hovers around the 36 PSU mark, up to 3 PSU higher than North Pacific waters at similar latitudes (Pickard & Emery, 1990).

One of the reasons for this higher salinity is the moisture transport over the Isthmus of Panama. Crudely put, water evaporates in the Atlantic and is carried into the Pacific, where it precipitates, making the Pacific fresher and the Atlantic saltier. Another contributing factor to the high salinity levels in the Atlantic is the input of highly saline Mediterranean water as well as the contribution from the warm and saline Indian ocean through the shedding of Agulhas rings (Pickard & Emery, 1990).

As to why higher evaporation occurs in the Atlantic, this could be due to the net northward transport of heat throughout the ocean basin which incorporates a uniquely northward transport of heat across the equator (Rahmstorf, 1995).

Recent studies have shown that it is impossible to study the North Atlantic in term of freshwater budgets without considering the South Atlantic basin. Rahmstorf (1996) conducted a series of experiments which showed that the net evaporation in the subtropical South Atlantic and the southward fresh water transport by the conveyor belt are both compensated by a wind driven northward freshwater transport. This is in keeping with the conclusion of Schiller (1995). This means that freshwater budget north of 30^{o}S is crucial to what happens in the north, i.e. how salty the North Atlantic will be. However, the freshwater water budget south of 30^{o}S is function of the surface flow into the South Atlantic, via the Drake Passage and the Agulhas input through the shedding of the mesoscale rings.

Another factor affecting the salinity of the North Atlantic is the input of a fresh-water source through the Bering Strait. Its precise importance is not yet understood and there are diverging opinions regarding it. While Wijffells et al (1992) consider it highly important others like Reason & Power (1994) do not think it has any significant impact at all.

The issue of freshwater forcing is important, as studies have shown that the circulation in the North Atlantic is very sensitive to perturbations in the freshwater budget (Ramhstorf, 1996). For instance, although the melting of glaciers at the end of the last ice age might not have affected the NADW formation as it was far too slow (Rahmstorf, 1995), a sudden release of melt water due to the bursting of an ice dam could have briefly shut down NADW formation (Broecker, 1998). Furthermore, there are indications that the release of fresh water due to intense ice rafting during the younger Dryas some 12,000 years ago caused the shutdown of NADW formation. (McManus et al, 2004). In any case, it seems that the global freshwater flux governs where most of the deep water will be formed, i.e. in the Northern or in the Southern Hemisphere (Wang et al, 1999).

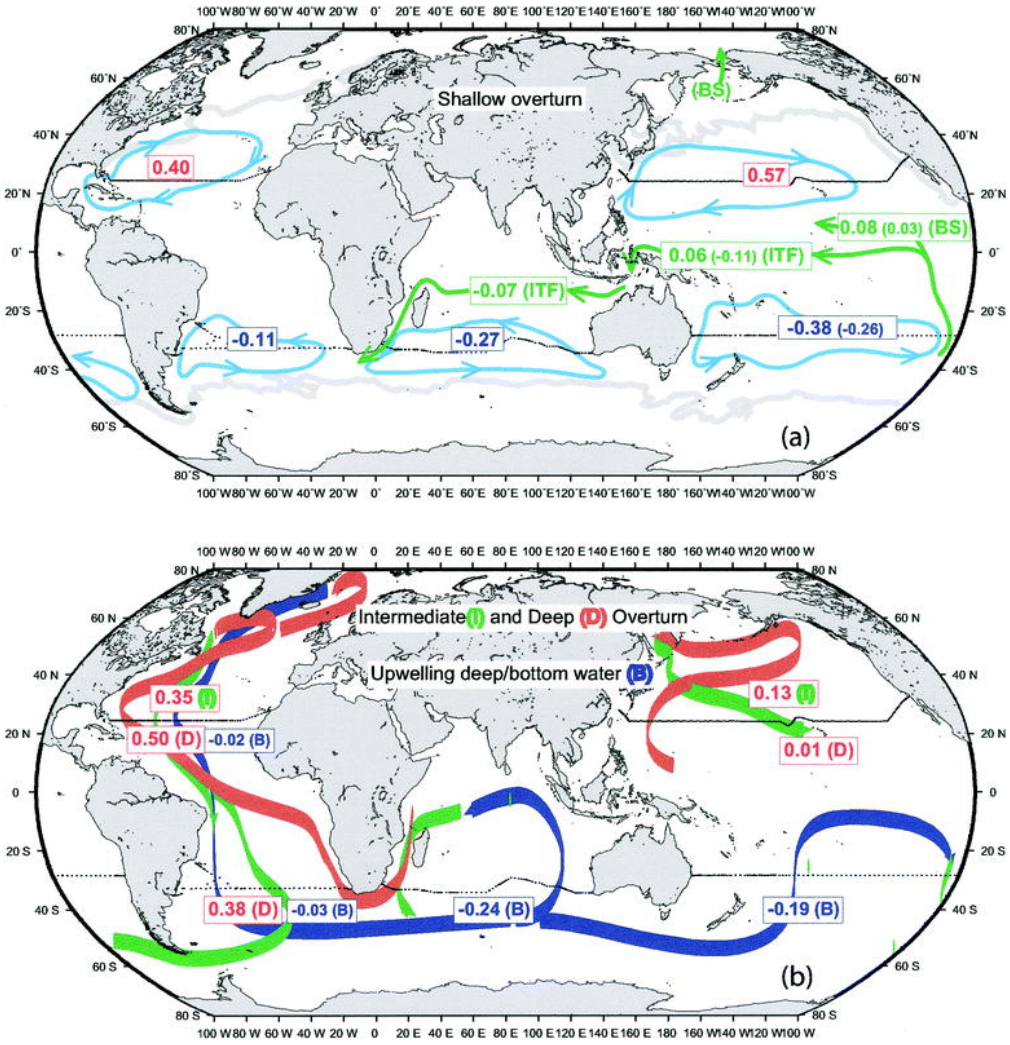

Figure1-1: Schematic of the oceanic circulation, panel a) shallow, panel b) intermediate and deep (Talley, 2003).

This deep-water formation is a critical element of what is called the Thermohaline Circulation (THC). This term refers to the density driven circulation of water masses throughout the world ocean. Coupled to the wind driven circulation, the THC is responsible for the transport of heat and salt through dynamic features such as the western boundary currents. It is impossible in observations to fully decouple the effect of the THC and those due to the wind driven part of the circulation. However, as density in the ocean is a function of temperature and salinity (and also pressure) (Pickard &Emery, 1990), changes in the surface forcing of the two tracers will directly impact on the THC, thus determining the properties of the deep waters and where they are formed. These deep waters then progressively upwell through the effect of mixing and Ekman

pumping and return to the regions of deep-water formation as surface waters, thus closing the circulation (figure 1.1).

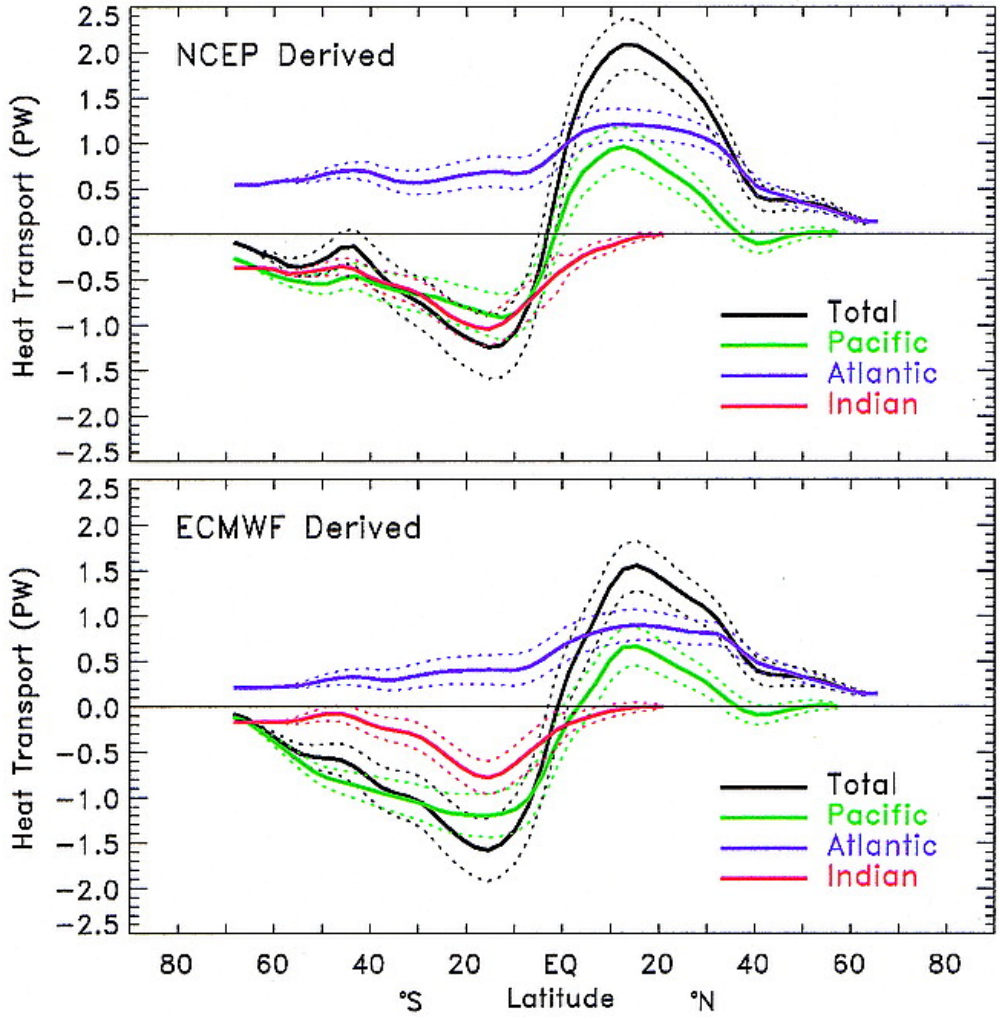

Figure1-2: Poleward heat transport in the ocean basins (Trenberth and Caron, 2001).

In terms of the global climate, the THC is thought to be responsible for a significant amount of heat transport between the low latitudes and high polar latitudes (1.1 PW at 25°N in the Atlantic, Trenberth and Caron, 2001, see figure1-2). Hence any changes in the THC would have a significant climatic impact. This is in part why there is so much concern about global warming inthe scientific community. An increase in global temperatures could severely alter the global distribution of freshwater and consequently the behaviour of the THC. This could have an unforeseen climatic impact (IPCC, 2001).

It is widely reported is that the THC has several stable equilibria as has been shown in relatively simple ocean only model studies (Stommel, 1961, Rooth, 1982, Birchfield, 1989, Bryan, 1986, Kallen & Huang, 1987 Marotzke et al, 1988, Rahmstorf, 1995) and that a different THC configuration has existed in the past (Broecker, 1998). More complex coupled models have also exhibited these multiple equilibria (Manabe & Stouffer, 1988).

Today's circulation is characterised by sinking in the high latitudes and is classified as thermally driven. This means that the flow is driven primarily by temperature differences. Theoretically, the sinking of water at low latitudes, driven by increasing salinity due to high evaporation is a perfectly sustainable alternative circulation set-up. Such a circulation is classified as haline driven but is thought to be highly unlikely (NRC 2002). It seems that the initial conditions determine which equilibrium will be achieved (Bryan, 1986). Moreover, some suggest that the present THC is very close to a bifurcation point. Increasing the freshwater input could well lead to a shutdown or a switch to an oscillatory regime (Rahmstorf, 1995).

The North Atlantic is thus a critical region in terms of the THC as it is one of the principal regions of deep-water formation. Any change to the properties of its surface waters will have a profound impact on the THC and hence on the global climate.

1.3) Variability in data:

1.3.1)From decadal to Milankovitch climatic signals:

There has been great awareness in recent years of the existence of interannual and decadal oscillations in the climate system. The most famous example is The El Nino Southern Oscillation (ENSO), which is routinely blamed for almost all

"abnormal" weather behaviour throughout the world even though oscillations, especially in temperature are common throughout the globe (Moron et al, 1998).

Another well studied interannual variability is the North Atlantic Oscillation, also called the northern hemisphere annular mode, which has been responsible for the succession of warm winters that Europe has experienced in the last 10 years. During its positive phase, the strength of mid-latitude zonal winds increase, trapping the cold Artic air in the northern Latitudes. As a result, winters in Europe are mild and wet (Thompson & Wallace, 2001). The NAO's most common feature is a variation in sea level pressure around the Azores and Iceland but it can also be picked up in by variations in surface temperatures (Curry and McCartney, 2001). A detailed study of the interdecadal variations and the Atmospheric conditions that accompany them was conducted by Kushnir (1994). He found that there was not a lot of coherence between the SST anomalies behaviour and sea level pressure anomalies and associated wind anomalies. This hinted in his opinion to the fact that the interdecadal variabilities were controlled by a basin wide dynamical interaction between oceanic circulation and atmospheric processes.

Numerical AGCM studies suggest that the NAO is a predominantly atmospheric phenomenon that arises from internal non-linear dynamics (Hurrell et al, 2003, Seager et al, 2000). The ocean acts as a low pass active filter, responding to the atmospheric fluctuations in a persistent almost oscillatory way. Some suggest that this is a result of the effect of the low variability of the oceanic heat capacity (Manabe & Stouffer, 1996) while others advocate that the mean oceanic advection acts to redden the variability (Saravanan & McWiliams, 1998). The ocean impact on the NAO can also be remote. For instance, it is thought that the location and strength of rainfall over the tropical Atlantic impact on the mid-latitude circulation and thus on the NAO (Sutton et al, 2001). Some even propose that the tropical Indian Ocean forces the NAO on long time scales (Sutton & Hodson, 2002). More contentious is the effect of ENSO on the NAO. A direct effect has not been detected in statistical analyses (Hurrell et al, 2003) but an

indirect effect through the ENSO impact on tropical North Atlantic SST has been presented in some studies (Chiang et al, 2000, 2002)

Hydrographic studies over the last 30 years, particularly analysis of repeat sections of the ocean have also suggested a certain amount of fluctuation in the properties of the deep ocean, in the Atlantic (Lavin et al, 2003) and in the Indian Ocean (Bryden et al, 2003). Such studies have underlined variations in temperature, salinity and meridional transport (Lavin et al, 1998). However, the precise nature of these fluctuations, i.e. whether they are oscillations, red noise or trends is still uncertain.

All the variations discussed so far are of relatively high frequency. There are other oscillations of longer periods, which have been exposed by the study of Palaeodata, such as the Dansgaard/Oeschger and Heinrich Events, which oscillate on a millennial time scale. These events are known to influence the behaviour of the THC in the North Atlantic by varying the penetration of the sinking of surface waters and, as a result, the nature of the deep water (Alley et al, 1998). Succinctly, a Heinrich event corresponds to a period of massive ice rafting leading to a freshening of the surface waters. This means that the waters do not sink as deep. There is therefore an influx at depth of deep water from the Southern Hemisphere (Vidal et al, 1997). Dansgaard/Oeschger cycles refer to millennium scale climatic oscillations detected in ices cores from Greenland (Dansgaard et al, 1993). This translates to rapid warming or cooling of up to $16^{o}C$ in the air temperature. Overlying these cycles is the longer period Bond Cycle, which has a period of roughly 6000 years (Alley, 1998) and corresponds to a warming/cooling of air temperature. The important point is that these events are thought to be independent of the glacial interglacial climate state, and are as such “pervasive millennial scale events” (Bond, 1997).

Beyond the millennial time scale are the time scales of the various components of orbital forcing, namely precession, obliquity and eccentricity. These cycles are also called Milankovitch cycles and are known to affect climate insofar as they appear to regulate ice ages (Broecker, 1966, Rial, 1999).

Precession refers to the angle of the earth's axis to the stars; it has a period of 19,000 to 23,000 years depending on the eccentricity. The obliquity is the angle between the plane of the equator and the earth's orbiting plane. Its period is roughly 41,000 years. Finally, the eccentricity refers to the elliptical shape of the earth orbits and its fluctuation between an almost perfect circle and a stretched out ellipse. The periods of the eccentricity are 54, 106 and 410 Ka (House, 1994).

There is evidence that these cycles affect climate in more ways than just by regulating the size of the ice sheets. Accurately forecasting their effect on the earth system is not an easy task and requires advanced climate models. A simple energy balance feedback model will not take into account all the various feedbacks, which influence the SST (North et al, 1981).

In a more recent attempt to fully model the orbital variations effect on the Sea Surface Temperature (SST), a numerical experiment by Sloan and Huber (2001) involving an Atmosphere coupled to a single layer shallow ocean showed that SST varied by as much as $6^{o}C$ for two extreme points of the obliquity orbital cycle. They concluded that most of this variation was due to the presence of sea ice. Added to these SST variations was also a strong fluctuation in the wind fields at the surface of the sea.

However, analysis of deep sediments cores from the North Atlantic by Raymo et al (1989) has led them to conclude that the deep-sea circulation in the North Atlantic is also controlled by climatic variations unrelated to ice sheets. This does not mean that ice sheets do not exert any control. On the contrary, in the period studied, 2.8 to 1.6 MA ago, they found that the dominant component seemed to be obliquity. However, the analysis of the $\delta^{13}C$ isotope signal within the three cores studied led them to conclude that, further to this ice sheet control, there are some variations in the deep circulation which are wholly independent of ice sheet behaviour.

1.3.2) Amplitude of the SST variabilities:

By analysing the $\delta^{18}O$ isotope records from various sites in the North Atlantic for the last 1.1 MA, Ruddiman et al (1986) concluded that maximum SST variations at about 60^o north were in excess of 10^oC for summer and winter temperatures. This is also the estimate obtained by the Climex project in their world maps of the last two climatic extremes, namely 18,000years ago, the last glacial maximum and 8,000 years ago, the Holocene optimum (CGCM, 1999).

The same order of magnitude for variations can be found for temperatures over Antarctica in the last 400,000 years. Although these are land temperatures, they vary by up to 16^oC (IPCC, 2002). This indicates that SST variations of about 6^oC at 60^o of latitude are plausible. Such an indicator is useful because of recent developments in palaeostudies, which imply that many previous findings might have been flawed (Pearson et al, 2001).

1.3.3) Palaeoceanography Methods:

There have been several approaches in Paleoceanography to determine SSTs in the past. In the late seventies, the chosen method was identification of foramanifera, a calcite shelled zooplankton found in a sediment core and comparing it with present day species. Working on the assumption that similar species live in similar habitats, i.e. similar temperature and depth, researchers were able to determine the SST bracket in which the forams found in the core lived. Thus, after dating the core, either through carbon dating or deposition rates, they could work out past SSTs. It was through this method that most of the Climap data was obtained. For 60^o North, Climap gives a range of SST temperatures of about 8^oC (IRI, 2002) between the two climatic maxima.

However, this micropalaeontology transfer function method was highly inaccurate and was soon replaced by the oxygen isotope method pioneered by Emiliani (1955). There are two stable naturally occurring isotopes of oxygen: oxygen 16 (^{16}O) and oxygen 18 (^{18}O). The vastly predominant isotope is the ^{16}O with a natural abundance of 99.757 %. Because of the weight difference between

the two isotopes, the lighter isotope escapes more easily during evaporation, while the heavier isotope precipitates more easily. At low latitudes, net evaporation produces vapour which is depleted in ^{18}O. As atmospheric circulation transports this vapour poleward, the on going precipitation en route causes the remaining water vapour to become progressively depleted in ^{18}O. This process is also called Rayleigh Distillation (Libes,1992) The Rayleigh Distillation of water vapour also causes polar ice to be depleted in ^{18}O relative to seawater. Thus, during an ice age, an increase in ice volume causes the ocean to be enriched in ^{18}O. In addition to recording the oxygen isotope signature of ice volume, biogenic carbonates also reflect the water temperatures under which the foram shells were deposited.

The oxygen fractionation in a foram shell varies from specie to specie but can also be affected by the presence of symbionts, light levels and other factors (Bemis et al, 1998). But the comparison of data from various sites as well as laboratory experiments on modern species has enabled scientists to dissociate the various effects and work out reasonably accurate empirical equation giving the temperature of the waters in which the forams lived. Providing that the species examined are surface water dwelling and that their ages are known, past SST temperatures can be inferred (Savin et al, 1985).

The method however is not without its problems, as can be demonstrated by the cool tropics paradox (D'Hondt and Arthur, 1996). Succinctly, paleostudies had led to estimates of SST in the late creatceous as low as 16^{o}C in the tropics from the oxygen isotope record. This seriously clashed with climate modelling studies, which had never produced such low estimates. Pearson et al (2001) claimed to have solved this paradox through the analysis of a core from a lake in Tanzania. The critical aspect of this core is that it lies beneath anoxic mud. As a result the forams are exceptionally well preserved and thus have not undergone any diagenesis. Estimate for temperatures at the surface of the lake during the late cretaceous are far higher than previously found, i.e. between 28^{o}C and 32^{o}C. The authors therefor suggest that previous estimates were distorted due to the fact that the forams had suffered from post depositional chemical alteration.

The bottom line seems to be that care must be taken when looking at SST as derived from Oxygen isotope analysis. Furthermore, it is important to remember that the data obtained in cores is very localised and that care must be taken when extrapolating the results obtained for a few sites to a whole sea or portion of an ocean.

Finally, extra care must be taken when looking at very long SST records such as those available for Antarctica. It is possible to get SST estimates for the past 60 Ma. However, during this period, the world experienced significant tectonic alteration such as the closure of the Tethyan gateway and the opening of the Drake Passage. These changes were probably responsible for a drop of up to 18^{o}C in SST, swamping any orbital and smaller period fluctuations (Open University, 1997). Furthermore, the oceanic circulation, prior to those changes was significantly different to today and therefore not really comparable. Indeed, some studies suggest that in the presence of a closed or shallow Drake Passage, there would be no production of NADW (Sijp and England, 2004) and as a result, the northern hemispheres temperatures would be colder.

A very useful parameter for determining past oceanic circulation is the deep-sea temperatures. Many oxygen based studies suggest that in the past, the deep waters were warmer than at present, by as much as 12^{o}C 70 million years ago. (Zachos et al, 2001). The use of other proxies such as the Magnesium calcium ratio confirms this idea (Lear et al, 2000) and allows the dating of the major icing events in Antarctica.

Warmer deep waters temperatures imply a different oceanic circulation set-up than today's (Kennett, 1977, Haupt & Seidov, 2001). The nature of that set-up is heavily influence by the temperature of the high latitude surface waters. Some consider that these were relatively warm (Bice & Marotzke, 2001) while others believe that the high latitudes surface temperatures remained relatively cool. However, for that latter scenario, finding a mechanism that allows the formation of warm deep water is problematic. Nevertheless, Haupt & Seidov (2001) conducted a series of numerical experiments confirming that such as set-up was

feasible. It is even possible for the ocean to switch from one circulation pattern to another (Stocker, 1998). Such an event could have brought about the release an enormous amount of gas hydrates and thus caused the relatively sudden PETM (Palaeocene Eocene Thermal Maximum) warming 55 million years ago (Bice & Marotzke, 2002).

Recent methods now allow scientist to have a better handle on the past behaviour of the THC in the North Atlantic. McManus et al, (2004) suggest that the strength of the THC in the North Atlantic is highly correlated with temperature. Hence a cooling event is associated with a decrease in the overturning and conversely, a warming with a speeding up of the circulation.

It is clear that observational analysis, either by direct measurements or by the use of proxies reveals many variabilities in oceanic quantities such as temperature, salinity and forcing fields. The question is how well models can reproduce these and if they can provide a reasonable explanation for them.

1.4) Variabilities in Models

The study of variabilities in the ocean has largely involved numerical simulation, mostly because of a "*lack of understanding of the physics of this type of variability*" (te Raa & Dijkstra, 2002). Of all the variable time scales mentioned earlier, the most studied appears to be the decadal to interdecadal scale. This is because to study longer time scales requires longer integration time not really feasible in the past.

Early on in the modern history of numerical modelling, Marotzke (1990) reported the presence of interdecadal variabilities in General Circulation Models under temporally constant mixed boundary conditions. These oscillations arose spontaneously and were not the result of any variable forcing. Weaver and

Sarachik (1991) went on to show the advective origin of the oscillations but were unable to pinpoint the precise mechanism. Weaver et al (1993) showed that these oscillations were still present under varying evaporation-precipitation fluxes.

The three dimensional aspect of the oscillations was established by Winton (1996) as he found that they did not appear in 2D models. This is in disagreement with the results of Aeberhardt et al. (2000), who found oscillations in a zonally average ocean atmosphere coupled model. Winton (1996) also found that weak stratification at high latitudes, common in earlier models, impeded wave propagation and could thus lead to the decadal variabilities.

It was later suggested by Greatbatch and Peterson (1996) that the oscillations in the THC were generated by the propagation of a boundary trapped Kelvin wave and that therefore the western boundary was crucial to the existence of the oscillations.

The importance of the western boundary current seems to have been disproved by Huck et al (1999) who found that none of the boundaries was fundamental to the oscillatory behaviour. They also found that the wider the ocean basin, the greater the amplitudes and the periods of the oscillations. Their conclusion was that the dynamical link between the north-south pressure gradient and the overturning induced a time lag, which was fundamental to the oscillatory behaviour. Furthermore, in agreement with Winton (1997) and Weaver et al (1996) they found that realistic bottom topography damped out these oscillations: it is therefore unlikely that they would be found in the real ocean.

Huck et al (1999) also found that the oscillations were damped out by horizontal diffusion. All this leads to the question of whether the oscillations observed in the models actually represent some real variability or are just an artefact of the modelling technique used. This does not mean that there are no decadal and interdecadal oscillations in the real world. The question is whether the

oscillations present in models are generated by the models themselves or by the phenomena modelled.

However, there are cases of studies where the oscillations found in the models roughly match those observed. For instance, Delworth and Mann, (2000), found in their runs oscillations of a seventy year period similar to those observed by Kushnir(1994). They noted however that the SST anomaly pattern was far closer to observations than the SLP (Sea Level Pressure) anomaly pattern, which exhibited a definite time lag compared to the patterns observed. Delworth and Mann (2000) concluded that these variabilities resulted from low frequency atmospheric noise interacting with feedbacks from the THC.

In the particular case of the North Atlantic, until recently there has been generally less awareness and interest of naturally occurring interdecadal variabilities among both the scientific and lay communities. This is mainly because the phase and amplitude of the oscillations observed were thought to be totally unpredictable (Hurrell et al, 2001).

This does not mean that no research was conducted. In the early 90's, Delworth et al (1993) noted that a coupled GCM model of the North Atlantic exhibited interdecadal oscillation, albeit highly irregular, in the atmospheric signals similar to those observed in the real ocean. They concluded that these oscillations were driven by density anomalies in the vicinity of the sinking region.

Another NAO based study was conducted by Visbeck et al (1998). They examined the response of a GCM to NAO like wind forcing and found that the greatest response occurred for forcing periods in the decadal band. Visbeck and Krahmann (2000) went to study the phenomenon further, still using NAO-like wind forcing. Their results suggested that for an interannual forcing period, the response in the SST field was dipole like whereas for longer forcing time scales, the response was monopole like. In other words, for interannual time scales, there was an increase in high latitudes SST whereas the low latitudes SST

decreased and for an interdecadal forcing period, there was either a basin wide increase or decrease. The authors also showed that under persistent forcing, the ocean could switch from a dipole to monopole SST pattern.

More recently, Delworth and Greatbatch (2000) revisited the NAO issue by using ocean only and coupled model runs. They concluded that a strong ocean-air interaction was not necessary to the generation of multidecadal variabilities. However, this does not mean that this is not the case in the real world.

The NAO does not only have an effect on SST and winds. It has also a distinct variability in the pressure distribution. Curry and McCartney (2001) looked at the effect of the varying pressure field and found that these considerably influence the gyre circulation in the North Atlantic.

Other studies have looked at the interdecadal oscillation problem from a numerical point of view. One such study was conducted by te Raa and Dijkstra (2002). They used a spherical coordinate implicit model to try to determine the physics behind the interdecadal oscillations. They pointed out that it was first necessary to distinguish between the growth of perturbations under unstable conditions from the physical mechanism that causes oscillatory behaviour, i.e. isolate what is specific to interdecadal oscillations.

They then found that the oscillations resulted from the westward propagation of temperatures anomalies. This led to a phase difference between the temperature anomalies and the velocity anomalies. This in turn created a phase difference between the two components of the variation in basin wide potential energy, the variation in potential energy due to the propagation of temperature anomalies and that due to the effect of flow on the background stratification. This phase difference drove the oscillatory behaviour of the ocean integrated buoyancy work and hence the oscillations in the 3D flow. The period of the oscillations was determined by the phase speed of the temperature anomaly as it crosses the ocean basin. Their conclusions are fairly close to that of Colin de Verdiere and

Huck, (1999), if not a bit more elaborate. The latter pair concluded that the driving mechanism behind the oscillations were baroclinic instabilities, the term they give to the instability in the buoyancy work term.

There have also been efforts to study the oceanic response to Milankovitch orbital forcing. Brickman et al (1999) conducted a study using a 2.5D atmosphere ocean model run for 3.2 Ma. They found that the strongest response was in the obliquity band while the response in the eccentricity band was suppressed. Their explanation for this was that the main effect of obliquity was to control the seasonal contrast, and as deep water formation happens in winter, the harsher the winter, the greater amount of deep water formed and the stronger the overturning. Their results also showed that in the obliquity band, the global ocean average temperatures were negatively correlated with the atmospheric ones, due to a rectifying effect by the ocean. Their main conclusion was to highlight the complexity of the ocean system response and that, hence, care should be taken when interpreting deep-sea sediment cores.

1.5) Modelling Issues:

1.5.1) Mixing:

Mixing is believed to be one of the fundamental processes taking place in the ocean. It is the process by which heat is transferred down to the deep waters, changing their properties and allowing them to slowly upwell. The canonical value used is of $10^{-4}m^2/s$ as determined by Munk (1966) through calculations based on the depth of the thermocline in the Pacific. This estimate is a global average and says nothing about the distribution of mixing. Indeed, measurements in the open ocean suggest that the mixing there is of about of $10^{-5}m^2/s$, roughly an order of magnitude below what is needed to close the meridional circulation (Ledwell et al, 1998). Recent work suggest that the shortfall might be made up in part by the activities of internal tides particularly when these encounter rough deep topography which causes them to dissipate (Munk and Wunsch, 1998). This idea is supported by the work of Polzin et al. (1997) who found increase mixing

in the vicinity of rough topography in the Brazil basin. It is still unclear however, as to whether or not tidal energy and its dissipation is sufficient enough to close the MOC. Some studies suggest that the tilting of isopycnal in the southern ocean due to intense Ekman pumping may also play an important role in closing the MOC (Webb & Suginohara, 1997).

Within the numerical community, simultaneously to trying to understand various processes through the use of models, a lot of effort has been put into developing and improving numerical models. Most model used nowadays are derived from the original code written by Bryan (1969) and then further improved by Semtner and Cox (Kantha & Clayson, 2000).

In the last two decades, one of the most significant developments has been the improvement of the mixing scheme. The first step was to parameterise the fact that, in the ocean, a large part of tracer mixing consists of down gradient diffusion along isopycnals (Redi, 1982), which are not necessarily horizontal, especially at high latitudes (Danabasoglu and Mc William, 1995). In the original code, the mixing was handled by horizontal and vertical diffusion coefficients. As a result, the diapycnal mixing tended to be overestimated. Cox (1987) produced an isopycnal mixing parameterisation but the scheme contained a numerical instability, which meant that it could not be run without a non-negligible amount of background diffusion. As a result, the models tended to over diffuse and tracer properties were not well preserved over great distances, in contrast to observations (Griffies et al, 1998)

Another improvement to the mixing scheme stemmed from the observation that most of the mixing in the ocean can be attributed to mesoscale eddies (Gent & McWilliam, 1990). Resolving these instead of parameterising them would have required very high horizontal and vertical resolution, unattainable even on modern computers (Danabasoglu and McWilliam, 1995). The Gent-McWilliam mixing scheme basically parameterised the effect of eddies by the introduction of an eddy advection flux (Gent & McWilliam, 1990).

Griffies (1998) later found that GM mixing could also be handled through eddy skew diffusive fluxes. The advantage of this approach lies in the fact that it can be relatively easily combined with Redi (1982) diffusion and thus not only improve ocean modelling but also reduce the computational cost of the Redi (1982) diffusion scheme alone by a factor of 2.

The results are cooler deep waters, a shallower and sharper thermocline and a slight reduction in the overturning. Generally, model runs with isopycnal mixing yield results closer to observations than horizontal mixing runs. (Danabasoglu and McWilliam, 1995, Kamenkovich et al, 2000). These findings are very similar to those of Park and Bryan (2001) who compared three types of models: z layered with horizontal mixing, z layered with GM mixing and an isopycnal layered model. They looked at velocitiy fields, temperature profiles and the flow at the boundaries. They concluded that, although the three models had almost identical zonally averaged properties, the isopycnal model yielded the results, which were the closest to observations.

Danabasoglu and Mc William (1995) also found an increase in heat transport, in contrast to Kamenkovich et al (2000) who reported that the heat transport varies only very slightly, even though the overturning does decrease. Their explanation is that the decrease in overturning is compensated by the greater surface to bottom temperature gradient. They also suggest that the strength of the overturning results from the interaction of two competing effects. On one hand, reduced mixing in the high latitudes leads to a decrease in the mass overturning at low latitudes and hence a reduction in the overturning. On the other hand, reduced diapycnal mixing allows a greater amount of NADW to reach the low latitudes. They concluded that details in the model configuration such as topography, determine which of the two effects dominate, and whether the overturning will increase or decrease by comparison with a horizontal mixing setting.

The issue of mixing in numerical models is far from resolved, even with advances such as Gent-McWilliam mixing. One of the major problems resides in

the fact that, in the ocean, mixing is not uniform, far from it. It has been known for some time that a lot of the mixing takes place in shallow shelf seas, at the edges of ocean basins, driven by tidal and wind forces. As mentioned earlier, recent work suggests that a considerable amount of mixing also takes place in the deep ocean, as tidal and internal waves break on steep topography (Egbert & Ray, 2000). This suggest that some of today's models basic parameterisations are fundamentally wrong and that the main control on the strength of the THC within an ocean basin is not the pole to pole surface density difference, a common concept amongst physical oceanographers (Rahmstorf, 1996) but rather the tidal and wind distributions (Wunsch, 2000).

This contrasts slightly with the findings of Marotzke and Scott (1999), who undertook the study of the convective mixing term. Using a 3D model, they investigated the oceanic circulation with 3 values of the convective mixing term: 0.1, 1 and 10 cm^2/s. They found that the maximum overturning varied by only 1.5% for changes in the mixing term of 2 orders of magnitude. This led them to conclude that the strength of the overturning is primarily controlled by the strength of the diapycnal mixing but also by the surface density difference. They also found that increasing the convective mixing leads to a decrease in the overturning. In effect, mixing is important at low latitudes as it allows the deep waters to upwell but the rate of convective mixing, which occurs at high latitude has little impact on the strength of the overturning (NRC, 2002).

There have been some efforts in the numerical community to implement a more realistic mixing parameterisation scheme, such as the work by Simmons et al, (2004) where they use a global tidal model to compute the turbulent energy levels in the ocean and incorporate their parameterisation in a coarse resolution ocean model. The results are promising but such work is still in its infancy.

1.5.2) Sinking:

Another important development in the field of numerical studies of oceanic circulation has been the analysis of the sinking and cooling of waters at high

latitudes. For many years, the general assumption was that water was cooled by the atmosphere, its density increased, and as a result it sank (Gordon, 1986).

Winton (1996) used a 2D model to study the processes that led to very narrow sinking regions. He showed that a narrow sinking / broad upwelling system had two interesting energetic properties: upwelling occurred over a wide area to allow for the maximum penetration of heat through diffusion, thus the greatest overturning for a given forcing and a system with a narrow sinking region had the lowest potential energy possible because the deep is filled with the coldest possible waters, formed where the surface temperature is the coldest. As highlighted by Marotzke and Scott (1999), his approach is slightly flawed in that he used a 2D model, which is unable to resolve the 3D behaviour of the processes involved.

Clearly, in a 2D model, sinking and cooling are co-located. In a 3D environment, this has been shown not to be the case. Sinking and cooling are not necessarily co-located (Marotzke, 2000).

This issue was first highlighted by Marotzke and Scott (1999), who were looking at varying values of convective mixing. They point out that in the open ocean, cooling creates a depression and that, because of geostrophy, the waters go round this depression rather than down. This question of where sinking occurs was further investigated by Spall and Pickart (2001) who looked at the velocities fields in an idealised ocean basin. They underlined the fact that deep sinking is a net vertical mass flux whereas deep cooling was a net vertical heat flux. This is in keeping with the work of Marshall and Schott (1999) who state that during deep cooling events in the open ocean, the deep waters are cooled through the activity of narrow convection plumes. The downward mass flux is compensated locally by an upward mass flux so in effect, there is no net no mass flux transport. Spall and Pickart (2001) also found that sinking in the North Atlantic took place in two locations: north of 55^{o} N near the western boundary and south of 45^{o}N, where the deep flowing western boundary current subducts under the gulf stream. They also point out, as did Marotzke and Scott (1999) that sinking

and convective mixing, can be co-located in regions of steep topography, i.e. in the Labrador sea.

1.6) Thesis layout:

As discussed above, the North Atlantic has some unique characteristics, which set it aside from the rest of the world's oceans. Furthermore, the climate system has many variabilities ranging from the seasonal to the decadal to millennial timescales. This thesis examines the effect that simple buoyancy forcing has on the THC in the Atlantic, whether the forcing is steady or oscillatory. Specifically, the objectives of this study are:

- To examine the response of an idealized ocean basin to steady buoyancy forcing and provide an explanation for the observed breakdown of the scaling law.

- To examine and analyse the behaviour of the MOC in a single hemisphere basin submitted to oscillatory buoyancy forcing.

- To examine and analyse the response of the MOC to oscillatory buoyancy forcing in a double hemisphere basin.

In chapter 2, the models used are presented. The fundamental properties of the principal model, MOMA (Webb, 1996) are described in detail. A brief discussion of the effect of resolution is also given. Finally, the issue of visualisation is succinctly addressed in term of two fundamental quantities, the meridional overturning stream function and the heat transport.

In chapter 3, the response of a single hemisphere ocean basin to constant buoyancy forcing is addressed. The scaling law relating the north-south

temperature gradient to meridional overturning stream function is revisited and investigated in term of the distribution of convection. The experiments are carried out with two models, MOMA and the MIT model (Marshall et al, 1997) in order to determine whether or not the observed behaviour is model dependent.

In chapter 4, the response of the circulation to variable buoyancy forcing in a single hemisphere is investigated. Different diffusion and basin configurations are applied. In total 17 forcing period ranging from 6 month to 32,000 years are studied. The sensitivity of the response to basin width and diffusion is highlighted.

In chapter 5, the basin is increased to a double hemisphere. The response of the circulation to an oscillatory buoyancy forcing is investigated under two restoring scenarios: one where the forcing is synchronous in both hemispheres, the other with a lag of half a period. For each scenario, a range of north-south temperature gradient is examined.

Finally, in chapter 6, a summary of the main findings is given. Implication and future work are also considered.

Chapter 2: Model descriptions and visualisation

Summary:

This chapter presents a detailed overview of the MOMA model used in this study. A description of the initial fields is provided as well as an analysis of the important features of the model such as the equation of state. The method of visualising the model outputs is also examined, as is the effect of resolution. Finally, a brief description of the MIT model used in chapter 3 is given.

2.1) The MOMA model:

2.1.1) Introduction:

The model used is a parallelised version of the GFDL MOM model which can distribute the various processes on an array of processors (Webb 1996). The free surface numerics have been updated by including the free surface numerical code of OCCAM (Webb 1995). The model also includes the eddy parameterisation scheme of Gent and McWilliams (1990). This is implemented using the Griffies (1998) approach (see appendix for the model code tree). Again, most of the code comes from OCCAM. The dynamics of the ocean are represented through the evolution of the salinity, potential temperature and horizontal velocities. The model uses a 3-D advection diffusion equation for momentum, temperature and salinity.

The equations used, often called the primitive equations, are as described by Bryan (1969). As in most ocean models, in order to reduce the computational workload, three major approximations are used:

- In the continuity equation, the ocean is assumed incompressible.
- In the vertical momentum equation, the vertical acceleration is assumed negligible (hydrostatic approximation).
- The density is replaced by a constant value except in the terms involving the gravitational constant (Boussinesq approximation).

2.1.2) Ocean Grid:

The ocean is subdivided into small 3D boxes: in the Horizontal, the model uses a Arakawa B grid, where the horizontal velocities are defined at identical points offset from the tracers (see figure 2.1). This grid is well adapted to coarse resolution models although it does not represent well poorly resolved inertial gravity waves. It also offers a good representation of geostrophy as the velocity points are co-located (Griffies et al, 2000). One of its draw-back is that it slows down very fast waves such as Kelvin waves. It does however handle Rossby waves very satisfactorily (Wajsowicz, 1986, Dukowicz, 1995, Webb, 1996).

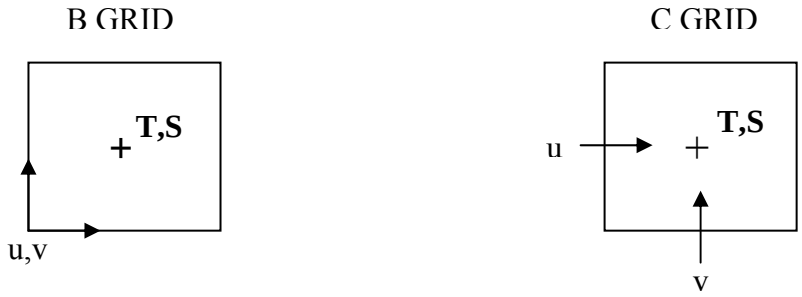

Figure2-1: schematic of the horizontal discretisation of two types of grids.

The lateral boundary conditions in all the runs are no slip, non porous, which are naturally implemented in an Arakawa B grid. In the vertical, the ocean is divided into 15 levels. In order to have greater resolution near the surface, the level thickness increases with depth, varying from about 30 metres at the surface to more than 800 metres at the bottom (table 2-1). Topography is modelled by designating each box either as an ocean box or a Land box.

Level 1	30.0 metres
Level 2	46.15 metres
Level 3	68.93 metres
Level 4	99.93 metres
Level 5	140.63 metres
Level 6	192.11 metres
Level 7	254.76 metres
Level 8	327.95 metres
Level 9	409.81 metres
Level 10	497.11 metres
Level 11	585.36 metres
Level 12	669.09 metres
Level 13	742.41 metres
Level 14	799.65 metres
Level 15	836.1 metres

Table 2- 1: thickness of grid cells at each level

2.1.3) Free surface:

MOMA uses a free surface code, which allows for the propagation of barotropic gravity waves as well as the direct introduction of freshwater to the model. It also avoids all the issues relating to the rigid lid approximation such as solving elliptic problems with realistic surface forcings and topography (Griffies et al, 2000).

2.1.4) Initial salinity and temperature fields:

In the original MOMA code, the salinity is initially set at 34.9 throughout the ocean. The temperature field is slightly more complex in the original program code. At all grid points below 2000 metres of depth, the temperature is set at 2^{o} centigrade. In the upper 2000 metres, an estimation is produced for each tracer grid point from a 7^{th} order polynomial. The polynomial is the best-fit curve obtained from the Levitus surface temperature. At three reference latitudes, a depth profile is given. These are used to anchor the polynomial at every depth.

2.1.5) Surface boundary conditions:

MOMA allows the user to choose between restoring boundary conditions for both tracers and mixed boundary conditions. In all the experiments in this study, mixed boundary conditions are used. This means that the salinity is forced through fluxes while the temperature is restored through a Newtonian dampening scheme. In all the experiments in this study, the restoring time scale used in is 40 days and the salinity fluxes set to zero. In the original model code, the restoring surface temperature field is interpolated in the same way as the salinity from the Levitus database. However, in all the experiments in this study, an oscillating restoring field is used. The details can be found in chapters 4 and 5.

A surface restoring salinity field is then prescribed, using the surface salinity values as in Levitus (1982), although this was switched off in all the experiments in this study. The wind forcing is set up by generating for each surface grid points an east-west and a south-north wind stress value. In most of the experiments in this study, the wind forcing is switched off by setting the wind

stress to zero. In chapter 4, a zonal wind stress is used in one of the experiments. It is identical to that of Weaver & Sarachik (1990).

2.1.6) Time-step:

The model is integrated forward in time by leapfrogging (Webb, 1996). However, this leads to instabilities for the diffusive terms so an Euler forward time step scheme is used for those. Furthermore, to avoid the splitting of the solutions, every 20 time step, an Euler backward time step is used. The main advantage of an Euler backward method is that it prevents the model from becoming unstable due to the diffusive terms in the equations (Griffies et al, 2000).

Parameter	Value
Basin Width, length	60^o, 60^o
Basin depth	5000 m
Number of vertical levels	15
Longitude, latitude grid spacing	4^o, 4^o
Vertical, horizontal diffusion coefficient	$1.10^{-4} m^2 s^{-1}$, 0 $m^2 s^{-1}$
Isopycnal thickness diffusivity	$2.10^3 m^2 s^{-1}$
Lateral eddy diffusivity, viscosity	$2.10^3 m^2 s^{-1}$, 1.10^5 $m^2 s^{-1}$
Temperature restoring time scale	40 days
Baroclinic Time step	14400 s
Barotropic Time step	600 s
Tracer time step	150000 s

Table 2- 2: Summary of numerical parameters and diffusivities in MOMA.

To make the best possible use of the computational resources available, the time step should be as large as possible. The limiting condition placed upon the time step is that any disturbance must be contained within a cell during a time step. Consequently, the greater the resolution, the smaller the cell dimensions and the smaller the time step will have to be. In MOMA, the tracers and the barotropic and baroclinic velocities have independent time steps. This allows the model to be far more efficient as the tracer can handle much greater time steps without becoming unstable. This greatly reduces the amount of computations needed, since it integrates forward in time with the tracer time step, and then determines the variation of the horizontal velocities by using a single velocity time step. In such a configuration however, the model is only suited for the study of steady equilibrium solutions and not of transient behaviour (Griffies et al, 2000).

2.1.7) Equation of state:

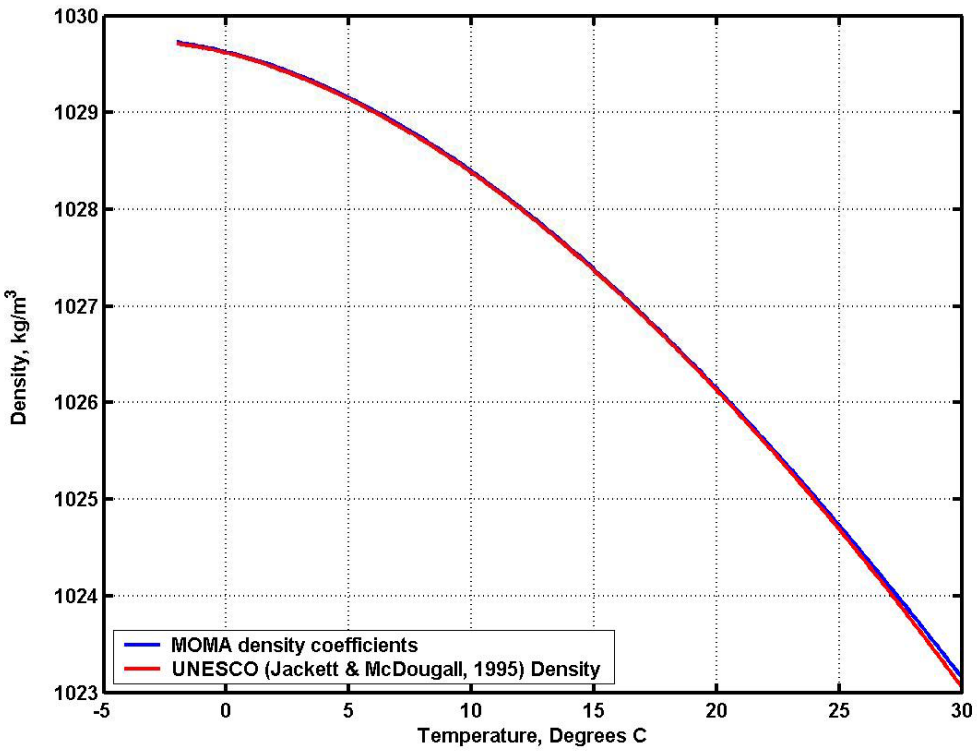

Figure2-2: Density against temperature at level 5, S=35

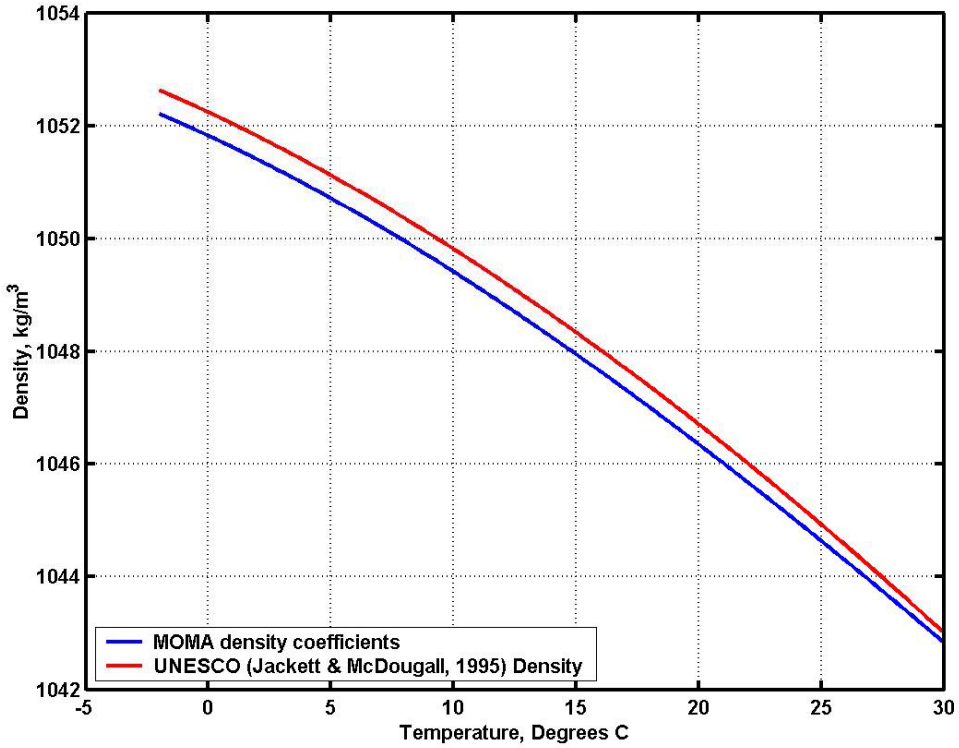

Figure2-3: Density against temperature at level 10, S=35

The model uses an approximation of the UNESCO equation of state by fitting a cubic polynomial at each of the discrete levels of the model. The advantage of using an approximation rather than the full UNESCO equation is that is saves on average up to 20% of the total computational load (Griffies et al, 2000). Figures 2-1 and 2-2 show plots of the density against temperature as calculated from the UNESCO equation of state and from the cubic polynomial in our model for a salinity of 35 PSU and at depth level 5 for figure 2-1 and depth level 14 for figure 2-2. The fit is almost perfect for the surface layers. It becomes less accurate at deeper levels. The density obtained from the polynomial is slightly smaller than the one given by the UNESCO equation. This means that the model might underestimate the surface to bottom density difference and be slightly more prone to convection than with the exact equation of state

2.1.8) Gent-Mc William Mixing

All the runs in this study include Gent McWilliams mixing (Gent & McWilliams, 1990) implemented through the Griffies (1998) parameterisation.

The aim of GM mixing is to parameterise the mixing effect of highly energetic eddies in the ocean. This is combined with the work of Redi (1982) which implemented the observation that most of the mixing occurs along density surface and not through them. The scheme involves introducing isopycnal tracer diffusivity ($2.10^3 m^2 s^{-1}$) and correcting the vertical and horizontal effect of diffusion accordingly. There is also a cut off angle for the slope of the isopycnal above which the GM scheme is not applied. This is to avoid spurious vertical mixing when the isopycnals are very steep such as in the high latitudes. Using GM mixing usually results in cooler bottom temperature as less heat from the surface diffuses down and a sharper thermocline as a consequence of the reduced diapycnal mixing (Kamenkovich et al, 2000). Furthermore, a slightly weaker overturning is found as a result of the weaker east-west density gradients due to the relative increase in the horizontal fraction of the mixing (Griffies et al, 2000).

2.1.9) Convection scheme

The MOMA model uses convective adjustment to deal with unstable stratification. After each times steps, the model checks from the top down the stratification stability at each level. When an unstable stratification is found, it mixes the two cells thus reducing the potential density difference. The number of time this procedure occurs is set by the user. However, the greater the number of passes, the heavier the computational load. Hence, in all the runs in this study, the number of passes was set to one. As a result instabilities can persist, with a cell with a cooler potential temperature overlying a cell with a warmer potential temperature.

2.2)Visualisation:

2.2.1) Meridional overturning:

There are many ways of visualising the circulation in the ocean. However, in the case of a THC circulation, visualising the sinking and upwelling regions is of particular interest.

In order to so while simultaneously looking at the meridional behaviour of the circulation, one option is to calculate a proxy, called the meridional overturning. This scalar is defined from a triple integration of the continuity equation:

$$\frac{\partial u}{\partial x}+\frac{\partial v}{\partial y}+\frac{\partial w}{\partial z}=0$$

where u, v, w are the zonal, meridional and vertical velocities respectively. The first integration is along the x-axis, i.e. from east to west of the u and v terms. This leads to the following expression:

$$-\int_{W}^{E}\frac{\partial w}{\partial z}\partial x=\int_{W}^{E}\frac{\partial v}{\partial y}\partial x$$

where W is the western boundary of the ocean basin and E is the eastern one.

The following two integrations are along the vertical and the meridional length leading to the final expression of the meridional overturning:

$$\Phi(y,z)=-\int_{-Z}^{0}\int_{W}^{E}\int_{0}^{Y}\frac{\partial w}{\partial z}\partial y\partial x\partial z=\int_{-z}^{0}\int_{W}^{E}\int_{0}^{Y}\frac{\partial v}{\partial y}\partial y\partial x\partial z$$

$$\Phi(y,z)=-\int_{-z}^{0}\int_{W}^{E}v\partial x\partial z$$

where Φ, the term on the left is known as the meridional overturning.

By definition, the meridional overturning is equal to zero at the bottom. In the case a free surface model, i.e where the surface is allowed to move up and down, it is easier to integrate the meridional overturning from the bottom upwards, especially when the bottom of the ocean is featureless, without any topography. Furthermore, in the case where there is no net mean transport, the meridional overturning is also equal to zero at the other vertical boundary.

2.2.2) Heat Transport:

Another important quantity to visualise is heat transport, particularly in the case of a double hemisphere basin as trans-equatorial heat transport in the ocean has a substantial impact on the global climate and deep-water formation. Bryan (1962) defines the total energy transport (F_q) in the ocean as follows:

$$F_q = \int_0^L \int_{-H}^0 \rho c_p v \theta dz dx$$

where ρ is the density, cp the heat capacity at constant pressure, θ the potential temperature, H and L the depth and width of the section respectively. In models, this can be approximated by the following expression used for example by Stammer et al (2003):

$$F_q = \rho c_p \int_0^L \int_{-H}^0 v \theta dz dx$$

Calculating the heat transport in a model with a rectangular section without topography is fairly straightforward.

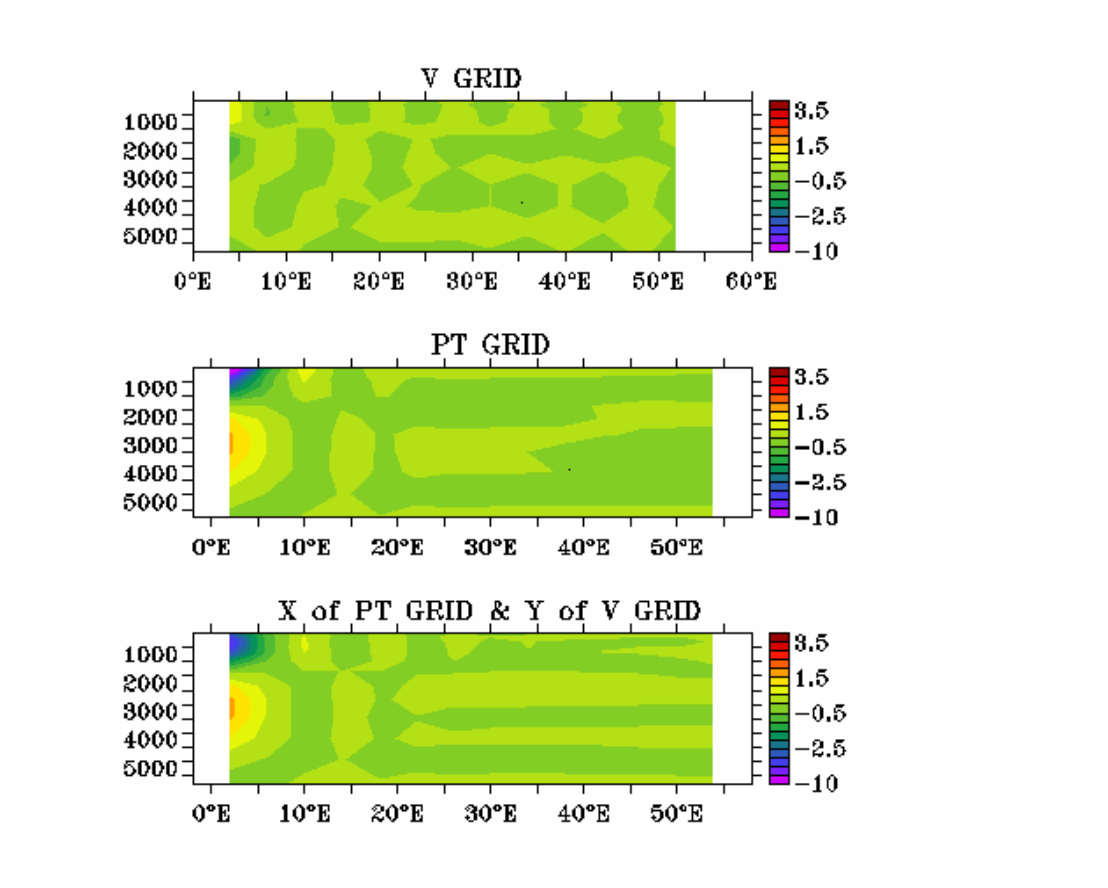

Figure2-4: Meridional velocity contours at the equator on 3 grids. Colour contours are in cm/s.

There is however an issue with the model grid. The MOMA model uses an Arakawa B grid and as a result the meridional velocity and the potential temperature are not co- located. For the calculation to be as exact as possible, both quantities should be on the same grid. There are then three options: recalculate the value of v, the meridional velocity onto the potential temperature (θ) grid, recalculate the values of θ on the v grid or to recalculate both quantities onto an intermediate grid. Although this might appear trivial at first glance, in a model with coarse resolution, the differences can be quite substantial.

This is clearly demonstrated by figure2-4, which shows the v velocity at the equator, plotted on three grids. Obviously, the equator is a region where the velocity changes significantly; it is positive to the north and negative to the south. Hence the averaging used will have a significant impact on the heat transport calculation. The choice of gridding will not have such an impact at

higher latitudes but this example underlines the care needed when computing quantities such as heat transport.

As the potential temperature field varies very little about the equator, the choice was made to recalculate PT and V on an intermediate grid, the x axis of which is that of PT and the y axis of which is that of V and then compute the heat transport. This strategy was deemed to yield the most sensible answer.

2.3) Comparison between 2^o and 4^o lateral resolution:

Lateral resolution can have a profound affect on the behaviour of an ocean model. In this study, a resolution of 4^ox 4^o is chosen mainly because of the integration time required to run the experiments. Indeed, halving the resolution not only reduces by a factor of four the number of cells, it also allows the timestep to be double. As a result, the total time gain obtained by halving the resolution is of a factor of 8.

Two identical runs but with two different resolutions are conducted to ascertain how substantial the difference are between a resolution of 4^ox 4^o and a resolution of 2^ox 2^o. Run Res1 has a resolution of 4^ox 4^o and run Res2 has a resolution of 2^ox 2^o. Both runs have a fixed restoring temperature profile which decreases sinusoidally with latitude from 28 degrees at the equator to 2 degrees at 60 degrees north. The vertical mixing is of 10 m^{-4}/s in both cases and both runs have the free surface enabled as well as the Gent-McWilliams mixing.

Figure 2-5 shows the evolution of the maximum overturning during a spin up of 10,000 years for the two resolutions. The two curves show the same qualitative behaviour throughout the 10,000 years and quantitatively, the values for the maximum overturning have a constant difference of 0.2 Sverdrups (1 $Sv=10^6 m^3/s$). The end value is of 11.84 Sv for the resolution of 2 degrees and

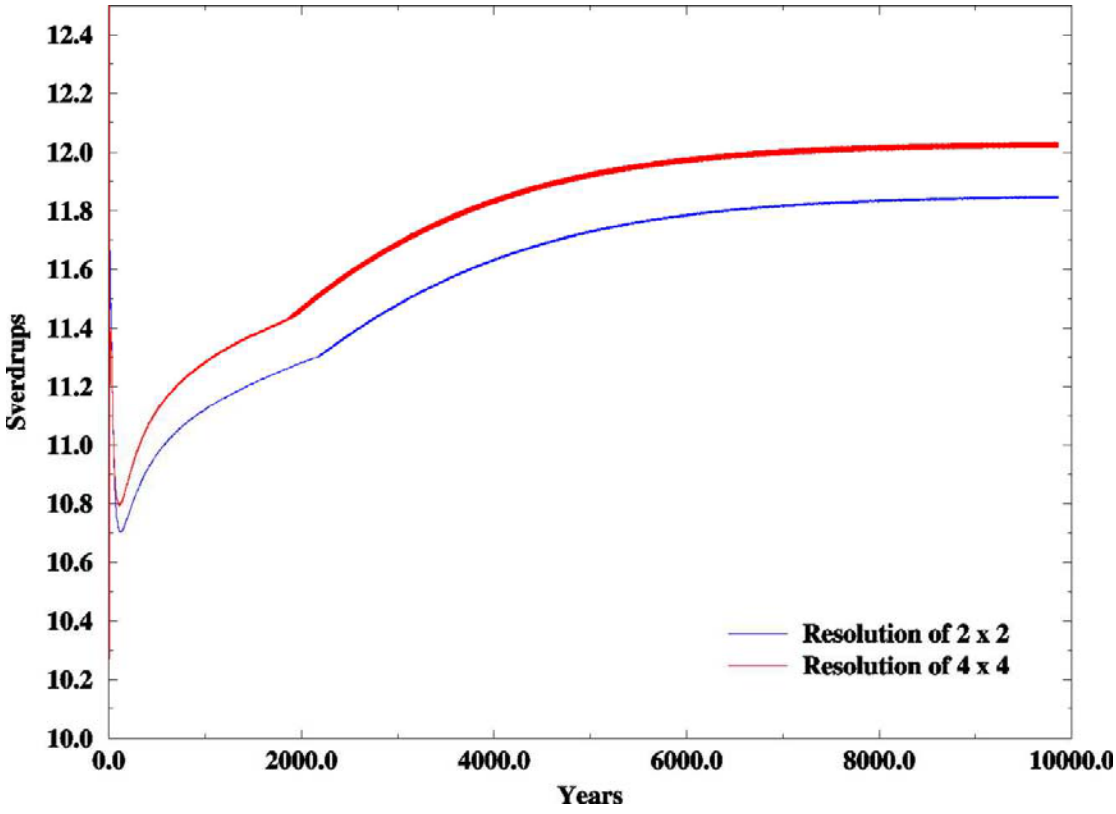

Figure2-5: Maximum overturning during Spin-up for Res1 and Res2

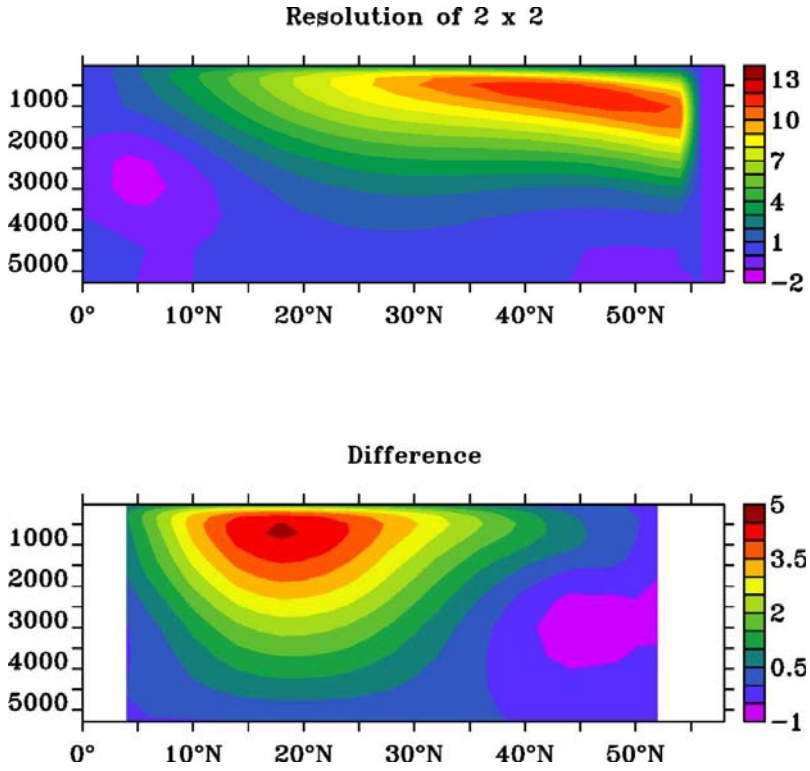

Figure2-6: Meridional overturning stream function (sv) for 2x2 resolution (res2) case and difference with 4x4 resolution (res1)

12.04 Sv for the resolution of 4 degrees. This amount to a difference of 1.6 %, which is very small.

Figure 2-6 and figure 2-7 show respectively the structure of the meridional overturning and the structure of the potential temperature in the upper 700 metres at the end of the two runs. It is clears that there are some differences between the two runs. Figure 2.6 shows that the major differences in the overturning happen at low latitudes. This occurs because the overturning core extends further south for the resolution of $4^{o}x4^{o}$ resolution than for the $2^{o}x2^{o}$ resolution (not shown). The actual shape and maximum intensity of the overturning cell are almost identical in both runs. Furthermore, in both cases, the maximum overturning is located at $45^{o}N$ and 1000 metres depth. Figure 2-7 shows that the isotherms behave similarly in both runs. As for the overturning, the greater differences occur at low latitudes, hence the difference in the amount of deep water formed at high latitude is very small (less than 1.5%).

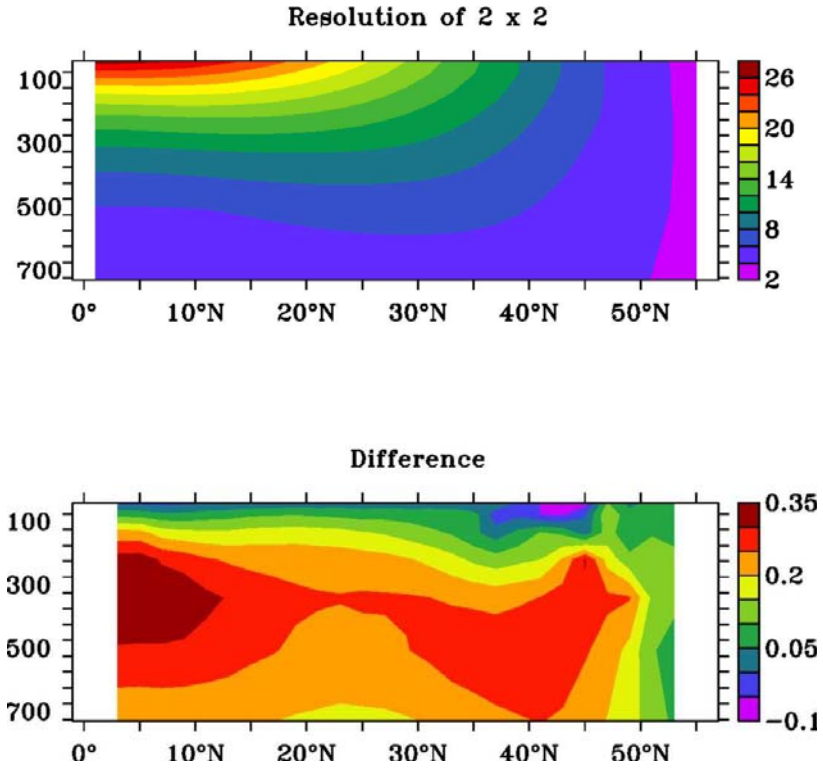

Figure2-7: Zonally averaged temperature field (^{o}C) in the upper 700 metres for 2x2 and difference with 4x4 resolution

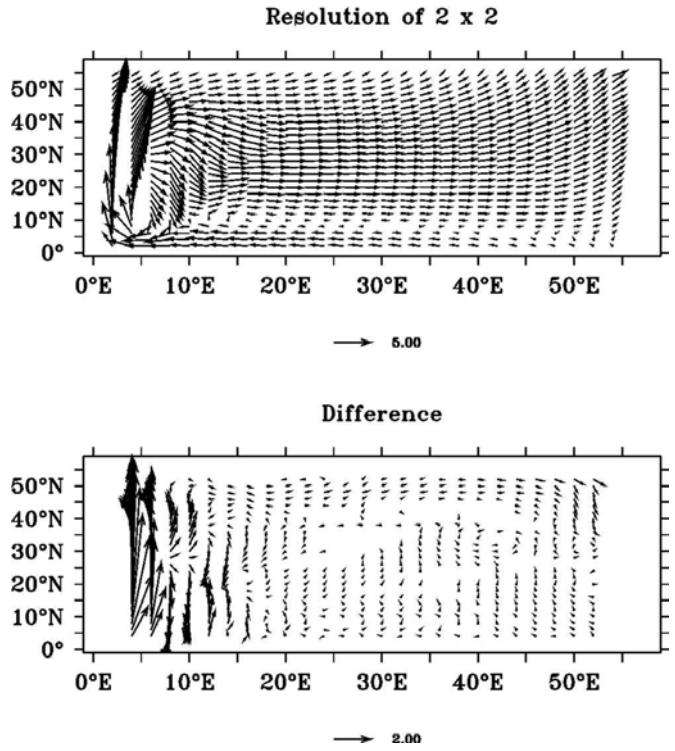

Figure2-8: Surface currents for the two resolutions. The units are cm/s.

In figure 2-8, the surface currents are displayed. The western boundary current transport has approximately the same maximum value for both resolution, although it slightly greater for the 2x2 resolution. This occurs because in the 4x4 resolution, the WBC is only 1 cell wide whereas in the 2x2 resolution, it is 2 cells wide. This allows for a narrower WBC and thus, in order to get a similar mass transport, a greater velocity (in Res2, v_{max}= 16.44 cm/s, in Res4, v_{max}=13.10cm/s). It is interesting to note that the greater velocity occurs for the run with the smaller overturning. Outside the western boundary, the currents are almost identical for both resolutions.

2.4) The MIT model:

In chapter 3 of this study, experiments are conducted with the MIT model (Marshall et al, 1997). As is made clear in that chapter, this is in order to examine whether some aspects of the MOMA model response is model dependent.

The MIT model is used in an identical setting as the MOMA model, with the same resolution, same forcing configuration (no wind, no salt fluxes, free surface and GM mixing implemented). It is however a far more modern model and many of its numerics are different from that of the older model. At a more fundamental level, it differs through the use of a horizontal C grid instead of a B grid for MOMA (figure 2-1). It also uses a third order Adams-Bashforth scheme instead of leapfrogging and synchronous time step for the velocity and tracers. These differences have repercussions in the representation of wave processes.

Parameter	Value
Basin Width, length	60^o, 60^o
Basin depth	5000 m
Number of vertical levels	15
Longitude, latitude grid spacing	4^o, 4^o
Vertical, horizontal diffusion coefficient	$1.10^{-4} m^2s^{-1}$, 0 m^2s^{-1}
Horizontal, vertical eddy viscosity	1.10^5 m^2s^{-1}, $2.10^{-3} m^2s^{-1}$
Temperature restoring time scale	30 days
Momentum equation time step	3600 s
Tracer time step	86400 s

Table 2-3: Summary of numerical parameters and diffusivities in the MIT model.

In terms of convection, the MIT model uses an implicit diffusion scheme to deal with unstable stratification. This involves ramping up the diffusion coefficient to 10^2m/s to simulate the intensive mixing that would occur in such situation. This

is different from the MOMA approach which uses convective adjustment to deal with unstable stratification.

For a detailed description of the MIT model it is recommended to consult Marshall et al. (1997). The main parameters used in all experiments are listed in table 2.3.

Chapter 3: On the scaling law in OGCMs

Summary:

This study presents results that stem from the observation that increasing the north-south temperature gradient does not necessarily lead to an increase in the strength of the meridional overturning stream function. Four sets of results are presented, sets 1 and 1M, where the north to south temperature gradient is decreased by increasing the northern most temperature and keeping the equator temperature fixed and sets 2 and 2 M where the north to south temperature gradient is decreased by decreasing the northern most temperature and keeping the northern most temperature fixed. Sets 1 and 2 are experiments conducted with the MOMA model while set 1M and set 2M are conducted with the MIT model. Sets 1 and 2 are analysed in detail and show that the strength and behaviour of convection vary substantially between the two sets and that they control the intensity of the stratification. As a result, the strength of the overturning in set 1 increase before it decreases as the temperature gradient decrease while for set 2, the strength of the overturning decease almost linearly with a decrease in the temperature gradient. These experiment show that the scaling law derived by Bryan & Cox (1967) and the object of many a study does not hold in these experiments, particularly when the temperature of the coldest water is varied. Furthermore, the spatial distribution of the convection is more important in setting the strength of the overturning than its actual intensity.

3.1) Introduction:

The complexity of the primitive equations that govern the oceanic thermohaline circulation has driven efforts to find a simple relationship that allows some form of prediction of the strength of the overturning given some simple climate parameters such as the equator to pole temperature difference. Very early on, Bryan and Cox (1967) suggested that the vertical "advection-diffusion" balance (3.1) and the thermal wind balance (3.3) could be combined with the continuity equation (3.2) to produce a scaling relationship giving the dependence of V, the horizontal velocity to ΔT, the equator to pole temperature difference and κ, the vertical diffusivity:

$$W \sim \frac{\kappa}{D} \qquad (3.1)$$

$$\frac{V}{L} \sim \frac{W}{D} \qquad (3.2)$$

$$\frac{V}{D} \sim \frac{g\alpha}{f}\frac{\Delta T}{L} \qquad (3.3)$$

where W is the vertical velocity, L is the horizontal length scale, D is the vertical length scale, g is the gravitational acceleration and f is the Coriolis parameter. Now,

$$(1)\,\&\,(2) \Rightarrow \frac{V}{L} \sim \frac{\kappa}{D^2} \qquad (3.4)$$

$$(3) \Rightarrow V \sim \frac{g\alpha}{f}\frac{\Delta T}{L}D \qquad (3.5)$$

which lead to the following expressions:

$$(4) \Rightarrow D \sim \left(\frac{\kappa L}{V}\right)^{\frac{1}{2}} \qquad (3.6)$$

$$(5)\,\&\,(6) \Rightarrow V \sim \left(\frac{g\alpha\Delta T}{f}\right)^{\frac{2}{3}}\left(\frac{\kappa}{L}\right)^{\frac{1}{3}} \qquad (3.7)$$

$$(7)\,\&\,(6) \Rightarrow D \sim \left(\frac{\kappa f}{g\alpha\Delta T}\right)^{\frac{1}{3}} L^{\frac{2}{3}} \qquad (3.8)$$

Assuming that the meridional velocity is proportional to the zonal velocity and as $\Psi \sim VDL$, it follows that $\Psi \sim \Delta T^{1/3} \kappa^{2/3}$.

The dependence of Ψ to $\kappa^{2/3}$ has been verified in a few numerical studies, including that of Zhang et al (1999) and Park and Bryan (2000). However, the robustness of this scaling law had already been questioned in numerical studies such as the one of Bryan (1987), where he found that Ψ scaled to $\kappa^{1/3}$ and not to $\kappa^{2/3}$,although as pointed out by Huang (1999), the integration time might not have been sufficient for the model to reach equilibrium. Scott (2000), in his detailed study concludes that the success of the scaling law, which he also observes, is rather *"fortuitous"*. Furthermore, it is not clear in a more realistic setting how well this formula works or, indeed simply how to apply this scaling in a situation where the ocean domain has more than one basin.

The dependence of Ψ to $\Delta T^{1/3}$ has always been far more problematic. As discussed in detail by Scott (2000), deriving a scaling relationship for a *meridional* overturning stream function implicitly involves assuming that the *east-west* temperature gradient is proportional to the north-south temperature gradient. Marotzke (1997) showed analytically that this was indeed the case, a result that was confirmed by Park & Bryan (2000) in a series of numerical experiments. The other issue discussed by Scott (2000), which also applies to the scaling of the meridional overturning to the vertical diffusivity is that of D, which in expression (1) refers to the advective-diffusive height scale but in (3) refers to the level of no motion. It is not at all clear that these two depths are proportional to each at other. Furthermore, depending on the numerical study, the authors use different approaches to estimate a scaled height: Park and Bryan (2000) used a temperature weighted average height while Bryan (1987) used the e-folding height of the top to bottom density difference and neither of these "*directly measures the advecticve-diffusive height or the zero crossing depth*" (Scott 2000).

Finally, as pointed out by Park and Bryan (2000), using a scaling law assumes self similarity in the system, in other words that the major features of the circulation stay qualitatively the same from one experiment to the next.

These issues go some way towards explaining why Scott's (2000) results did not show the expected dependency of Ψ to $\Delta T^{1/3}$. In fact, with a similar set-up but with a fixed mixing energy input, Huang (1999) observed a decrease in the overturning for an increasing temperature gradient. Scott (2000) suggested that this behaviour results from a weakening of the effective κ in the upper waters, which lead to a weakening of the MOC.

These studies clearly show that the issue of the scaling argument is far from resolved. It is nonetheless important to know the response of the MOC to smaller temperature gradients as most future climate studies predict a warming of high latitudes SSTs.

3.2) Method:

3.2.1) Models description:

A detailed description of the models can be found in chapter 2.

3.2.2) Experimental strategy.

Four sets of experiments are carried out, two with each of the models. The surface temperature is restored to a zonally averaged field, which decreases sinusoidally with latitude. In set 1, the surface restoring temperature at the equator is fixed to 28°C while the northern most restoring temperature is varied from 0°C to 22°C. The latitudinal distribution varies according to the following algorithm:

$$T(\Phi,t) = A\times(\cos(\Phi\times 3)-1)+28 \qquad (3.9)$$

where T is the restoring temperature, Φ is latitude and A is half the amplitude, varying from 14 to 3.

In set 2, the restoring temperature at the northern most latitude is set to 0 °C while the equator restoring temperature varies from 28°C to 6°C degrees. The latitudinal distribution varies according to the following algorithm:

$$T(\Phi,t) = B/2\times(\cos(\Phi\times 3)-1)+B \qquad (3.10)$$

where T is the restoring temperature, Φ is latitude, t is time and B is the northern most value of the restoring temperature, varying from 28°C to 6°C.

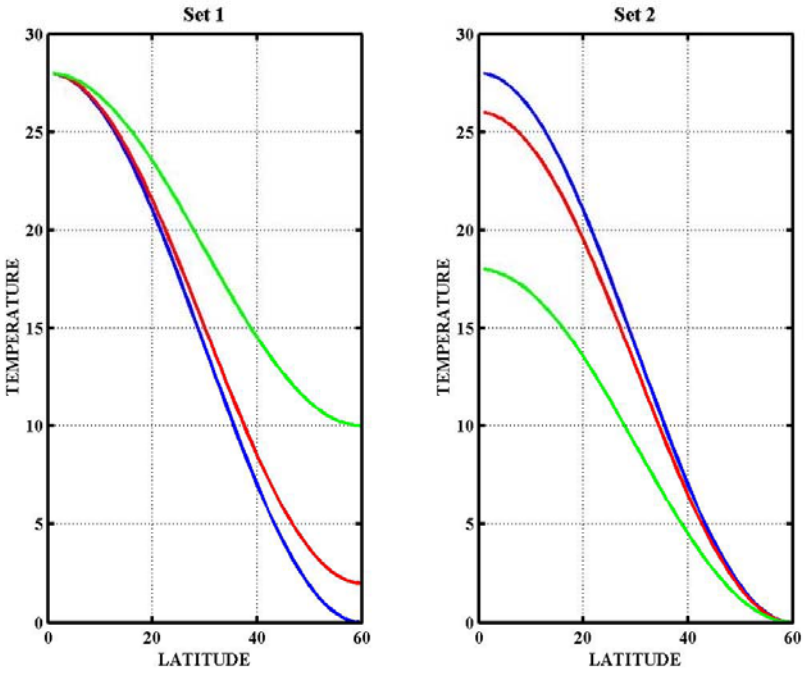

Figure3-1: Example of the restoring temperature profile (°C) for 3 temperature gradients, 28 in blue, 26 in red and 18 in green for set 1 and 1M(left panel) and set 2 and 2M (right panel).

The set-up of set 1M and set 2M are identical to that of set 1 and set 2 respectively but are run using the MIT model. Figure 3-1 shows 3 forcing profiles for each set.

For each experiments, the temperature field is initialised at the surface to Levitus (1982)) values. The temperature then progressively decreases with depth until 2000 metres whereupon, the temperature is set everywhere to 2°C. Equilibrium is often reached after 10,000 years but the model is integrated for 20,000 years.

In the following sections, the results from set 1 and 2 are analysed in detail. The results from set 1M and set 2M are succinctly presented as an example of the behaviour of another model. A convection index is defined as the number of times a cell undergoes convective adjustment between two sampling events. For the experiments, the sampling interval is 1000 years.

3.3) Results:

Figure 3-2 shows the strength of the maximum overturning stream function for all 4 sets of experiments. The two sets do not have the same values or the same behaviour, a result that is independent of the model used. Set 1 has a maximum overturning for a temperature gradient of 22^{o}C with a decrease in the strength of the overturning for larger or smaller temperature gradients. Set 2 has a maximum overturning for a temperature gradient of 28 ^{o}C and shows an almost linear decrease in the strength of the maximum overturning for a decrease in the north-south temperature gradient.

Set 1M and set 2M show that the qualitative behaviour observed is not model dependent although the actual values are. Indeed, the MIT model shows a similar increase and decrease in the value of the overturning as the restoring temperature gradient decreases for set 1M. For set 2M, the values decrease with decrease in the amplitude of the restoring temperature gradient.

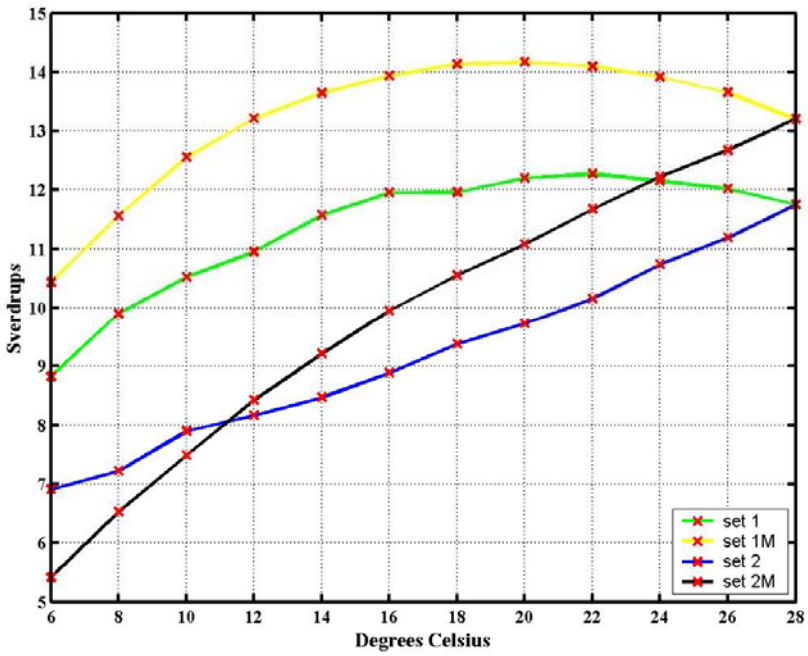

Figure3-2: Maximum overturning stream function against restoring temperature gradient for the 4 sets.

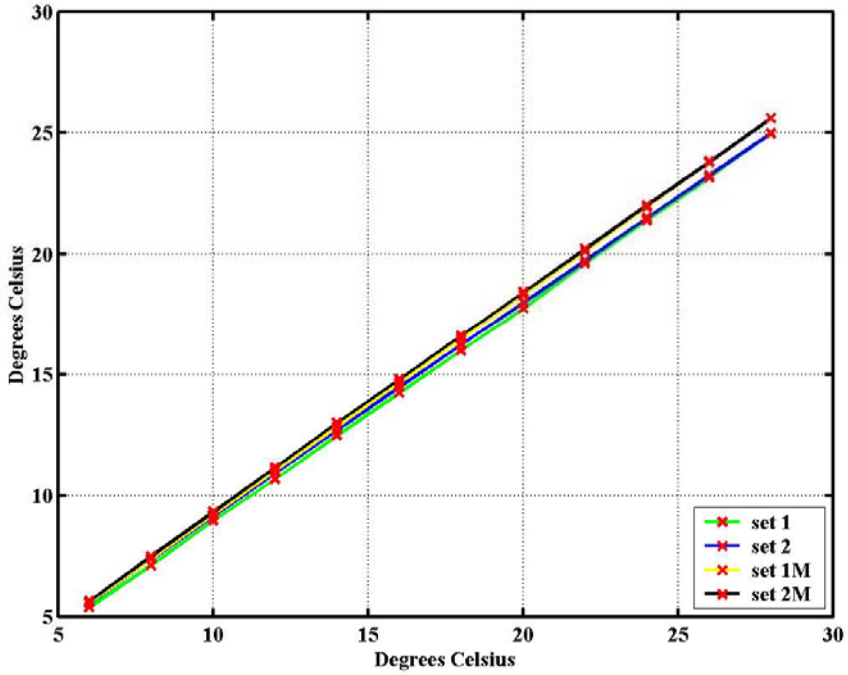

Figure3-3: SST gradient (y-axis) against restoring temperature gradient (x-axis) for the 4 sets.

Figure 3-3 shows the actual surface temperature gradient in the model versus the restoring temperature gradient. Set 2 and 2M experiments always display a greater north-south SST gradient than set 1 and 1M respectively even though in most cases the overturning in set 1 and 1M is greater than the overturning in set 2 and 2M. The difference though is quite small, in the order of 0.1-0.2 degrees Celsius.

3.4) Discussion

3.4.1) Behaviour of set 1:

The important feature of set 1 is the presence of the maximum overturning for a restoring temperature profile of 28°C at the equator to 6°C at 60°N. To understand why this occurs, four experiments of set 1 are analysed in detail, respectively with a temperature gradient of 26°C, 24°C, 22°C and 20°C.

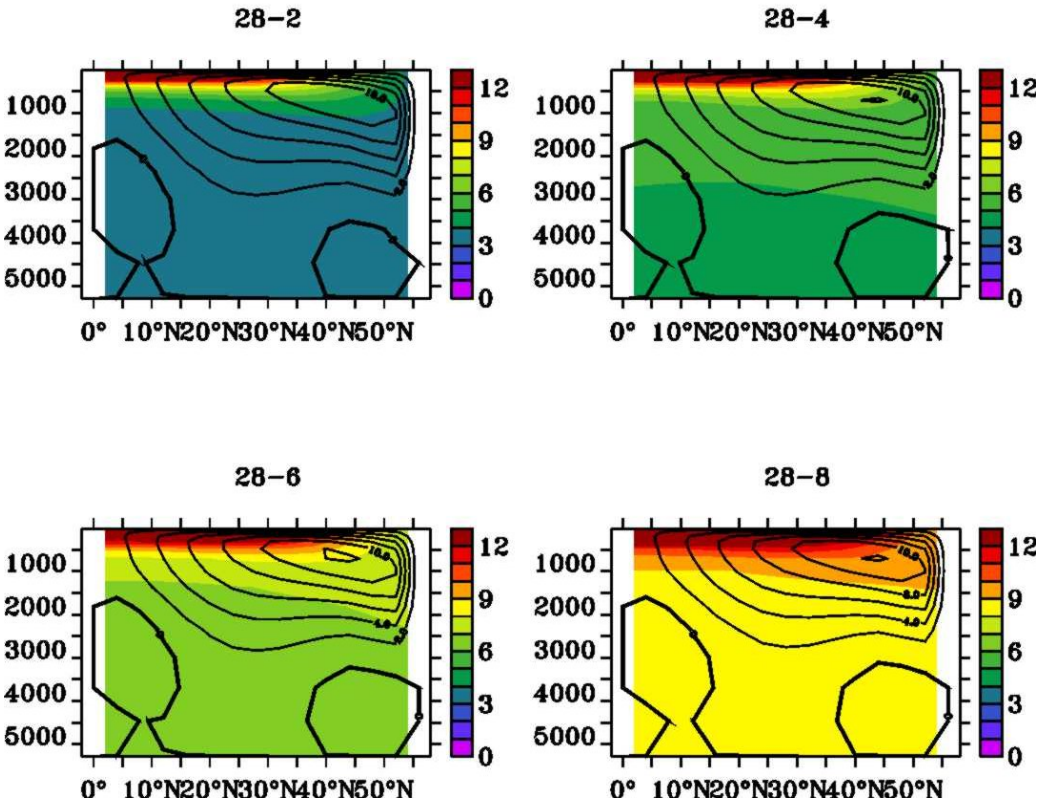

Figure3-4: Zonally average temperature field in °C (colour shading) and meridional overturning stream function in Sv (black contours) for 4 experiments of set 1.

	Equator Values		60° N Values		Gradient	
Restoring	SST	ρ	SST	ρ	SST	ρ
28-2	26.8	1022.9	3.634	1027.9	23.116	5
28-4	26.89	1022.8	5.484	1027.7	21.406	4.9
28-6	26.99	1022.8	7.357	1027.5	19.633	4.7
28-8	27.09	1022.8	9.327	1027.2	17.763	4.5

Table 3- 1: SST and density at the equator and northernmost latitude for 4 experiments in set 1. The temperatures are in °C and the densities in kg/m^3.

As shown in figure 3-2 and table3-4, in set 1, the maximum overturning occurs for the temperature gradient of 22°C. In the light of previous studies (Park & Bryan, 2000) suggesting a 2/3 power scaling between ΔT and Ψ, this is unexpected, the more so as most fields display the expected structure, with a weakening of the north-south SST gradient as the northern most restoring temperature increases. There are no substantial differences in the structure of the

meridional overturning stream function for the three different forcing profiles as clearly shown in figure 3-4. In all four cases, the maximum is at 44°N and at about 1500 metres depth. All four cases also have a small counter-rotating cell at depth near the equator. As illustrated by figure3-3, the surface temperature trend is still in keeping with the expected behaviour although the surface eastward flowing surface current (not shown) is clearly stronger in the for the 28-6 profile.

Figure 3-5 shows the depth-integrated distribution of the convection index between two sampling events. Generally, as the temperature gradient decreases, the convection shifts eastward. The 28-8 case has no convection west of 27° east. The other three cases exhibits convection right across the basin although for the 28-6 case, the far western side of the basin is convection free.

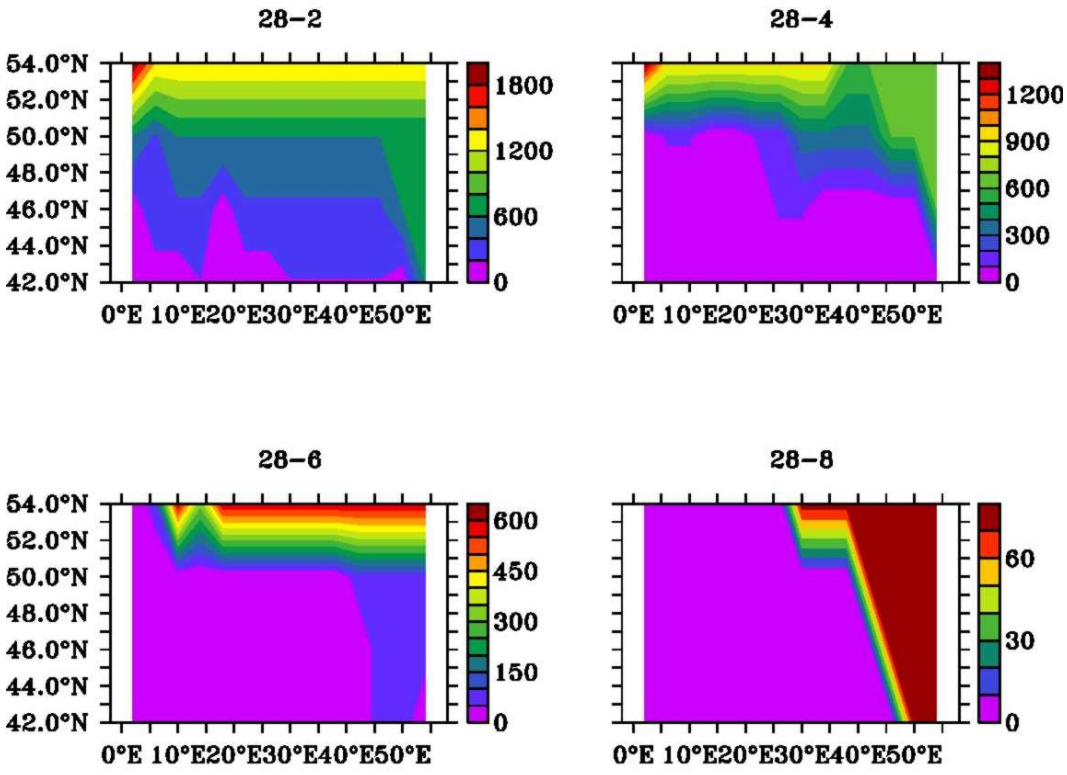

Figure3-5: Depth integrated distribution of the convection index in the high latitudes (45°-60°N)

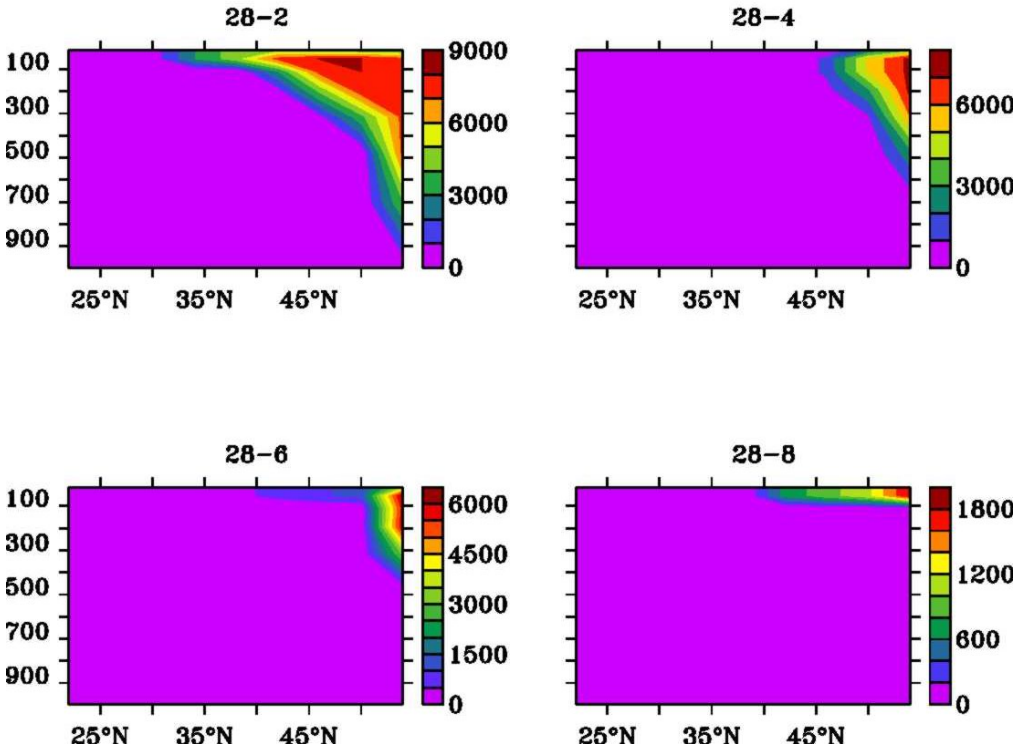

Figure3-6: meridional distribution of the zonally integrated convection index in the high latitudes (45°-60°N) from the surface to 1000 metres.

The meridional distribution of the zonally integrated convection index between 45°N and 60°N (figure3-6) also shows substantial differences between the 28-8 and the other three cases. Clearly, the 28-8 case has a very weak and shallow convection relative to the other three. It does not go much deeper than 150 metres and extends all the way south to 40°N. In the other three cases, the convection is much stronger, deeper and concentrated in the high northern latitudes.

In fact, as the temperature is increased, there is a definite evolution of the distribution of the convection, which shallows and shifts eastward. Furthermore, for a forcing profile of 28-10, there is no convection in the model, an extreme case of the swallowing of the convection (not shown). This occurs because the diffusion is efficient enough to handle all the adjustments necessary in response to the thermal forcing.

As is shown in figure 3-5, the maximum overturning occurs for the forcing profile that displays the most uniform distribution of convection at very high

latitudes. The exact mechanisms involved are difficult to pinpoint but some elements of explanation are provided in section 3.4.4.

It is the structure and strength of the convection that varies most between the four experiments. For the 28-0, 28–2 and 28-4 experiments, the convection is stronger than for the 28-6 experiment. It is also predominantly on the western side of the basin. As the northernmost temperature is increased, the relative convection strength increases in the west side of the basin. As explained in section 3.4.4, this favours an increase in the overturning, which is what is observed. Experiment 28-6 displays a distribution of convection that is localised in the high latitudes but also fairly, uniform zonally. For experiment 28-8, the convection is shifted to the east and is very shallow and much weaker than for experiment 28-6. Because it is so shallow, it does not have a substantial impact on the eastern temperatures. For north-south temperature gradients less than 20^{o}C in set 1, there is no convection to strengthen (or weaken) the east-west temperature gradient.

3.4.2) Behaviour of set 2:

In this section, the experiments with a temperature gradient of 24, 20 and 14^{o}C are used to illustrate the generic behaviour of set 2. Here, the expected behaviour is observed, i.e. a decrease in the strength of the overturning as the temperature gradient is reduced. The convection field for the three experiments shows that the greater the temperature gradient, the more asymmetric the zonal distribution of the convection index becomes (figure3-7), with more and particularly deeper convection on the eastern side of the basin than on the west thus leading to a weaker overturning (see section 3.4.4). Furthermore, the position of the maximum convection migrates southward as the restoring temperature gradient decreases (figure3-8). This means that more and more of the basin undergoes convection. As the convection is now evenly distributed across the longitudes, the east-west pressure gradient is weakened. This leads to a weaker meridional overturning.

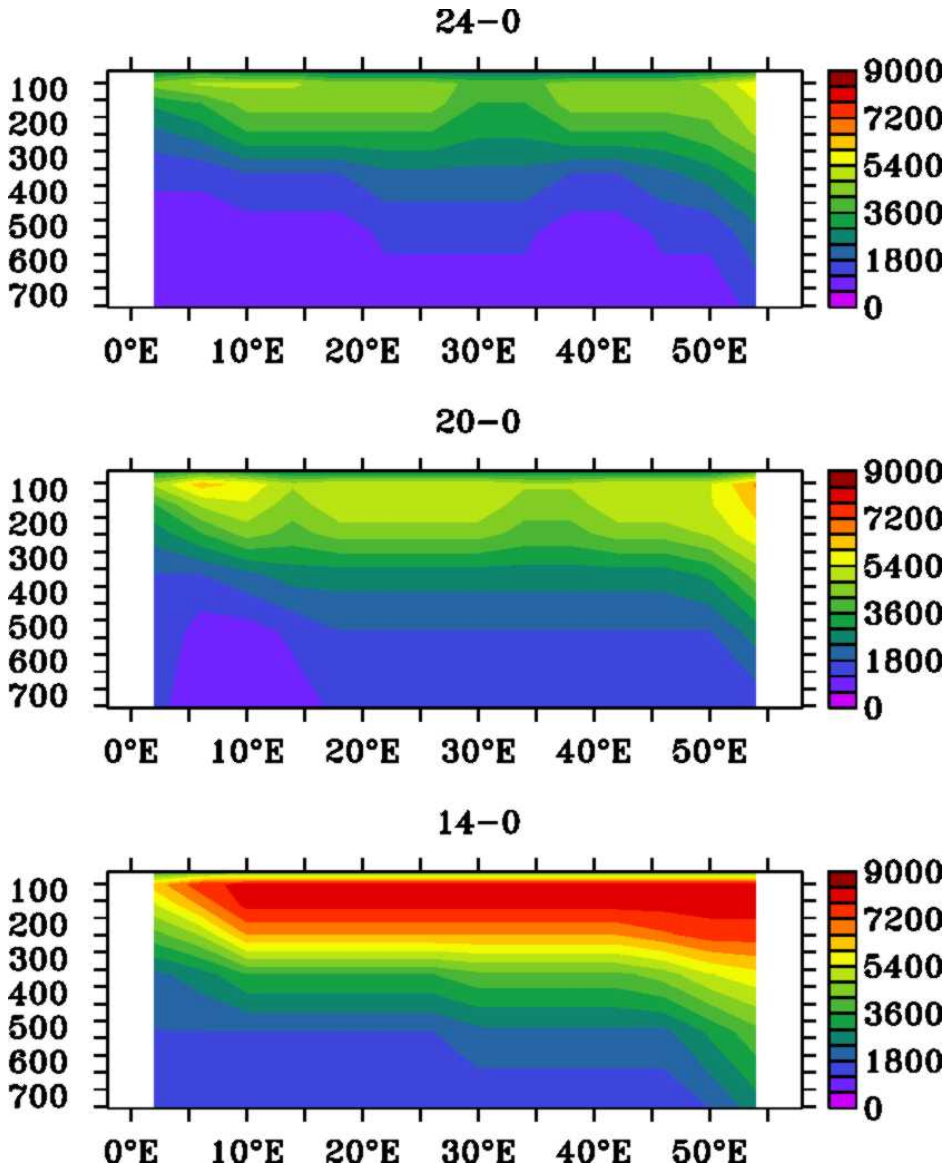

Figure3- 7: zonal distribution of the meridionally integrated convection index in the high latitudes (45^{o}-60^{o}N) from the surface to 700 metres for set 2

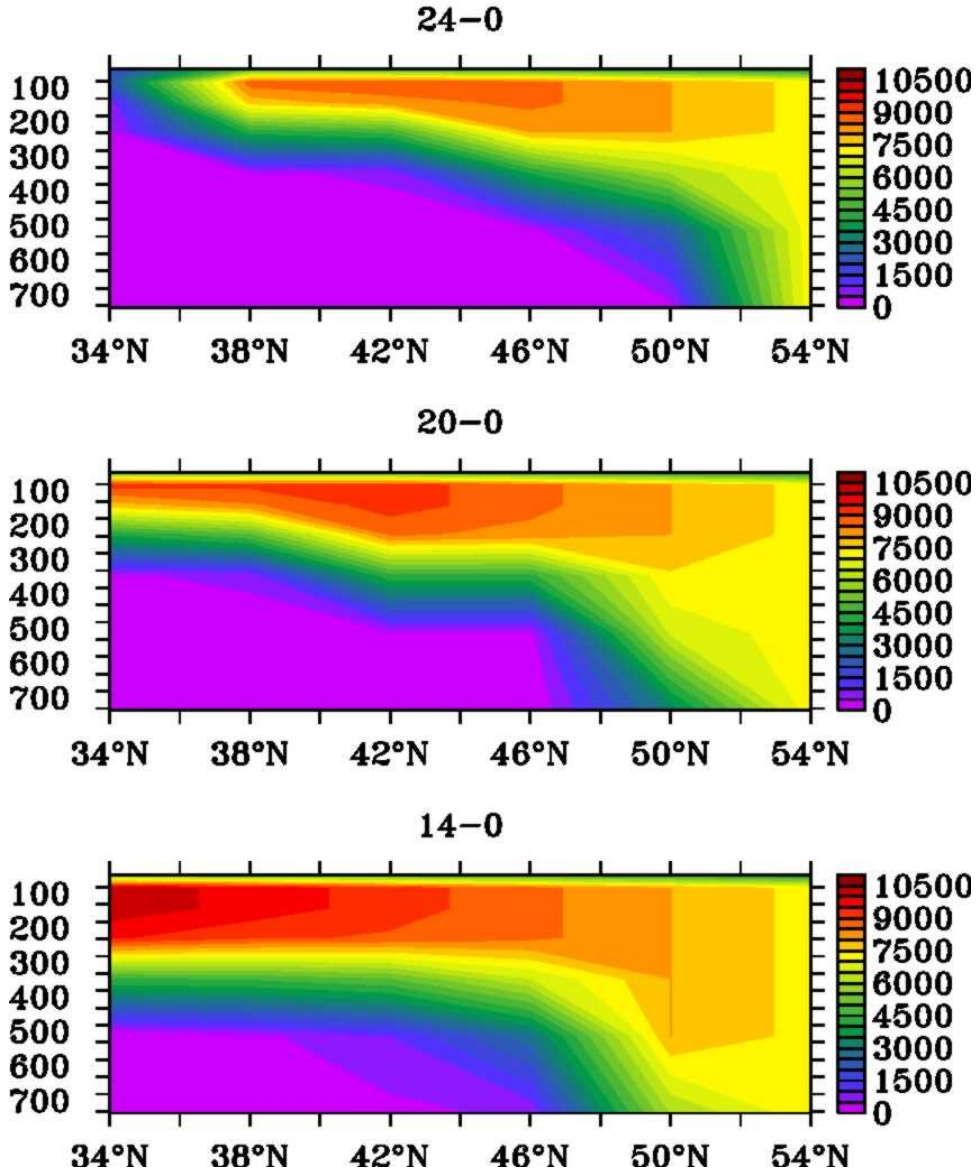

Figure3- 8: meridional distribution of the zonally integrated convection index in the high latitudes (45°-60°N) from the surface to 700 metres.

3.4.3) Difference in Behaviour between Set 1 and Set2:

One of the significant differences between the two sets of run is that for an equal north-south temperature gradient, set 1 exhibits a stronger overturning than set 2 (figure 3-2). This could be explained through the non- linearity of the equation of state used in the model. Simply put, a temperature difference of 24 degrees leads to a greater density difference if the maximum temperature is 28°C instead of 24°C as is illustrated in table 3-3. It is important to note that although the actual SST gradient is greater for 24-0 than for 28-4, the density difference behave in the opposite way.

	Equator Values		60° N Values		Gradient	
Restoring	SST	ρ	SST	ρ	SST	ρ
28-4	26.89	1022.8	5.484	1027.7	21.406	4.9
24-0	22.97	1024	1.469	1028.1	21.501	4.1

Table 3- 2: SST and density at the equator and northernmost latitude for a temperature gradient of 24 °C.

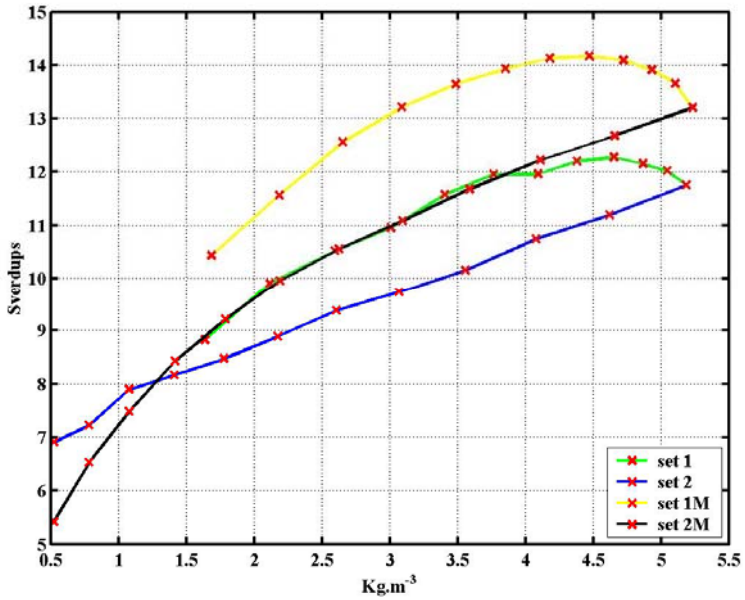

Figure3-9: Overturning against density gradient for the 4 sets.

However, it is not the density difference observed that explains the difference in the strength of the overturning. As is evident from the results of set 1 and 1M, a smaller density difference does not always lead to a smaller overturning. As shown in Figure3-9, a plot of the overturning against the density gradient for set 1, 1M, 2 and 2M. The non-linearity of the equation of state does not explain the behaviour observed in set 1 and 1M as the same behaviour is observed when plotting the overturning against the density gradient. It also does not account for the fact that, for the same density difference, set 1 and 1M have a greater overturning than set 2 and 2M respectively. The way in which the ocean adjusts to the two forcing must be examined closely.

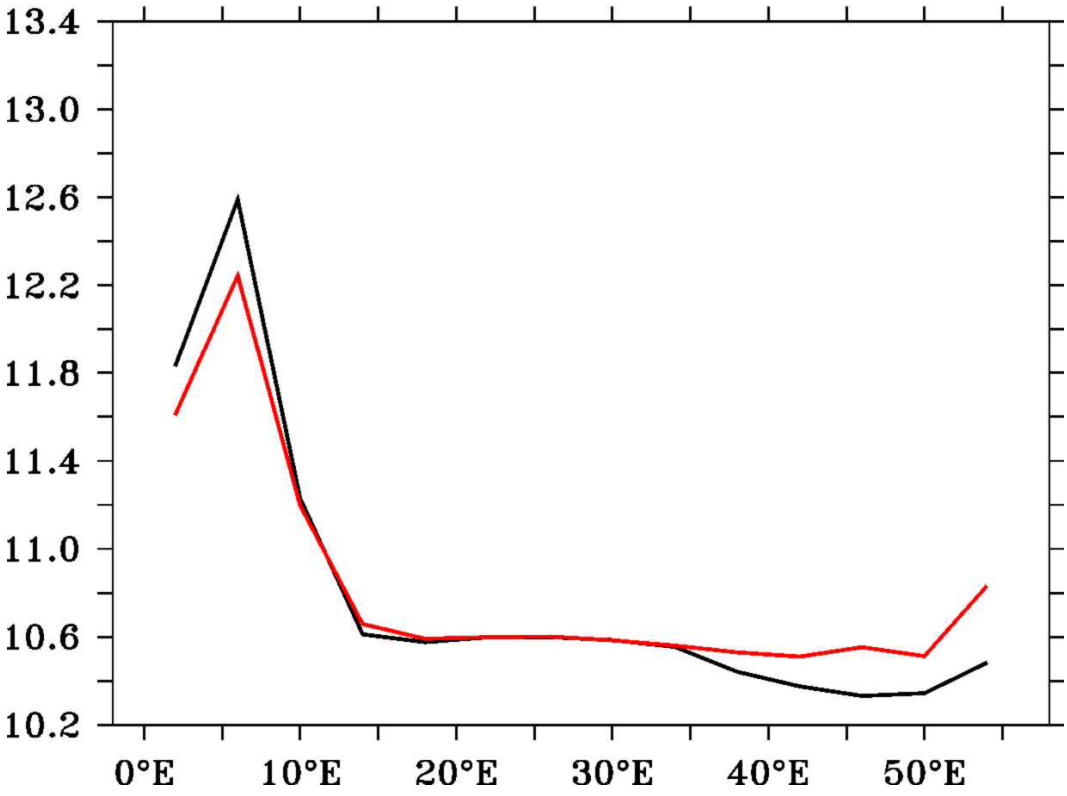

Figure3- 10: Meridional SST gradient in ^{o}C between 45^{o}and 60^{o}N for 28-4 (black) and 24-0 (red).

The circulation features of the two experiments are therefore analysed in greater detail to try and understand how the overturning and its strength are set-up. By looking closer at the 24 gradient case, in figure3-10, it is clear that the temperature gradient between 45^{o}N and 60^{o}N on the western side of the basin is smaller for the 24-0 case than for the 28-4 case. Figure3-11 suggests that this weaker temperature gradient is due to the fact that in the 24-0 case, there is more convection in the Northwest (greater index) than for 28-4. As a result, the surface temperatures will be slightly warmer. The weaker temperature gradient means that the eastward flowing high latitude current, the WBC once it has separated, is weaker in the 24-0 than in the 28-4 case. This is illustrated by figure3-12, a plot of the surface currents for both experiments and the difference between the two. The end result is that in the 24-0 case, less warm waters are being brought to the NE corner of the basin and so less water sinks because of convergence.

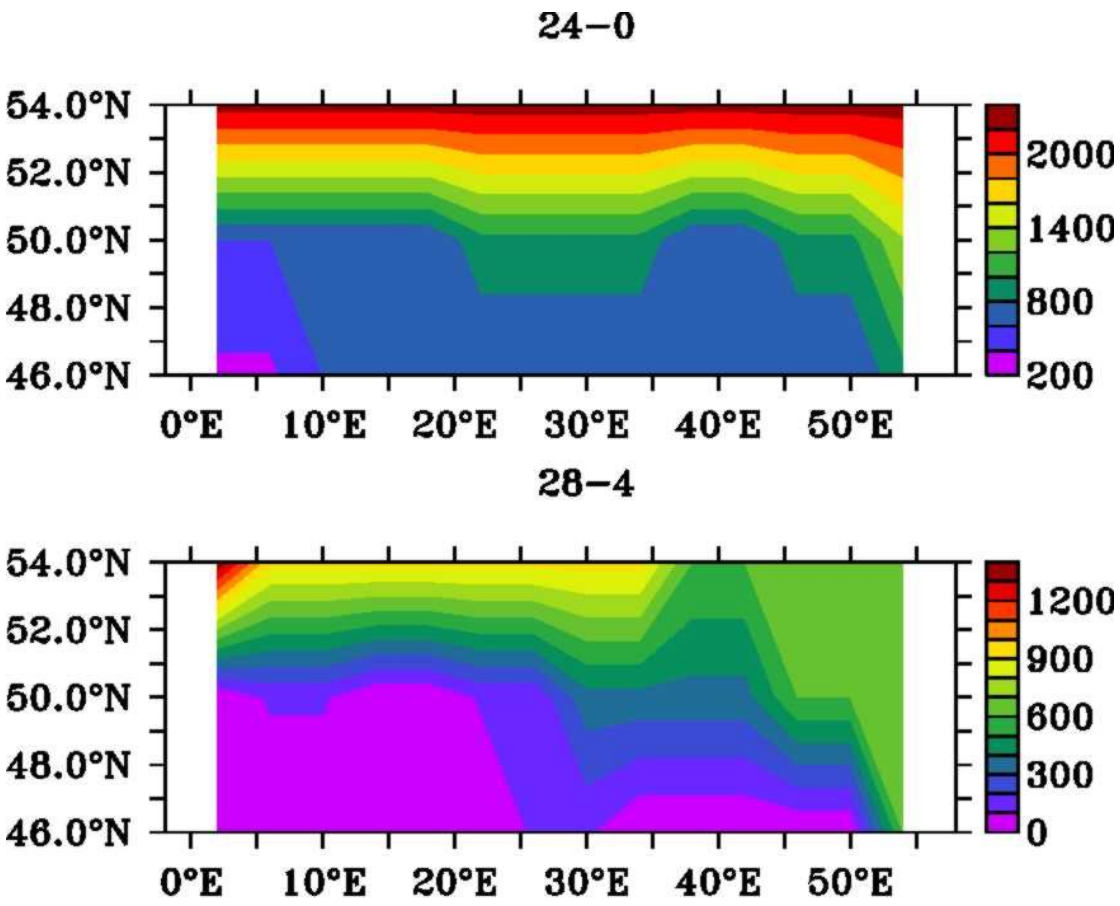

Figure3-11: Depth integrated distribution of the convection index in the high latitudes (45°-60°N) from the surface to 700 metres for 24-0 (top panel) and 28-4 (bottom panel).

Another way of looking at the problem is simply to observe that the convection distribution at high latitudes shows a greater western bias in the 28-4 case than in the 24-0 case. As is explained in section 3.4.4, such a distribution leads to a greater east-west density gradient and thus a stronger overturning for 28-4. In effect, the biggest difference between the two experiments is how the convection is distributed in the high latitudes and how that distribution affects the east-west density gradient. However, for temperature gradients smaller than 20, there is a significant difference in that the set 1 experiments no longer have any convection while in set 2, the amount of convection is increasing as the temperature gradient decreases.The distribution of convection argument described previously no longer holds. The difference between the two sets in the value of the north-south density gradient for a given temperature gradient is now more significant. This is clearly illustrated in table 3-4, where, for a temperature gradient of 14, the actual density gradient for set 1 is twice the density gradient for set 2. For the latter set,

the zonal distribution of convection becomes more uniform as the location of maximum convection moves southward as the density gradient decreases. This weakens the overturning by decreasing the east-west density gradient (discussed in section 3.4.4).

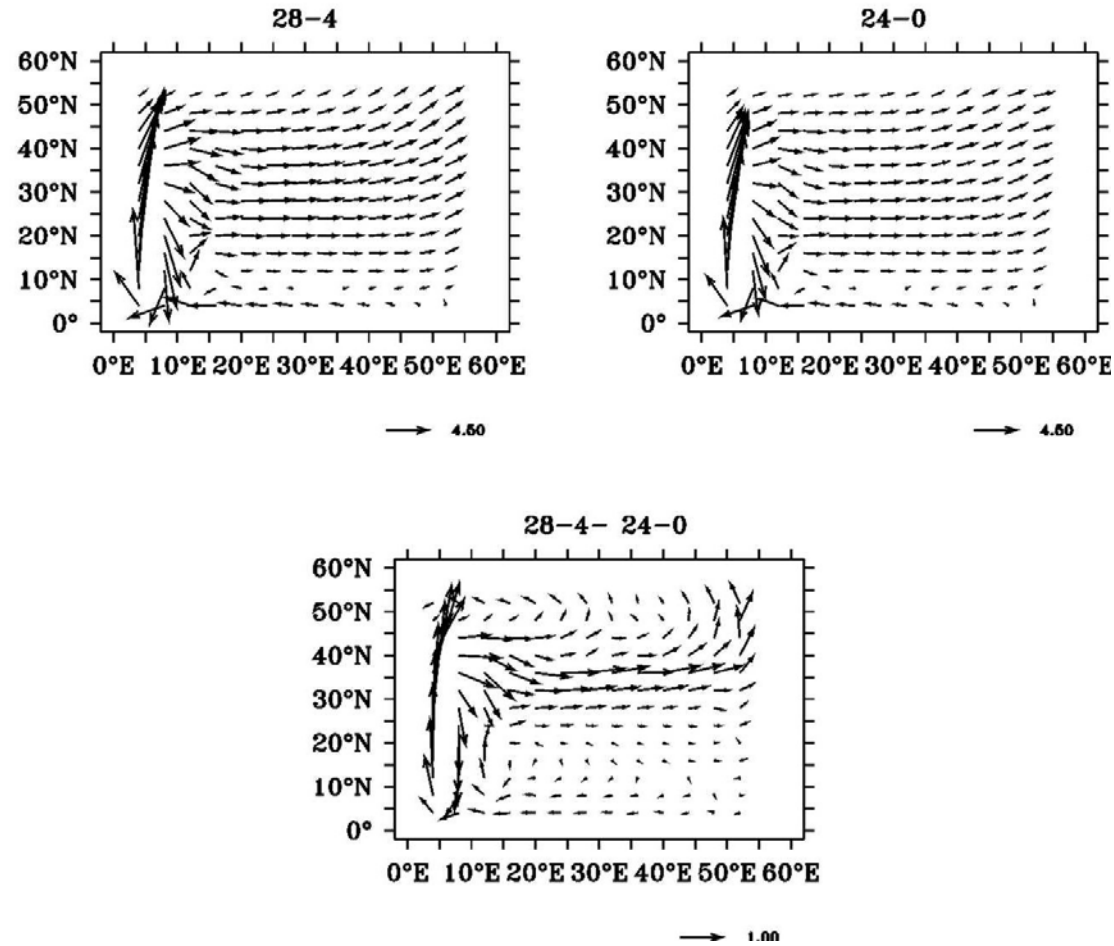

Figure3-12: Vector plot of the surface current in cm/s for a temperature gradient of 28-4 (panel A) , 24-0 (panel B) and the difference between the two (panel C).

	Equator Values		60^{o} N Values		Gradient	
Restoring	SST	ρ	SST	ρ	SST	ρ
28-14	27.40	1022.7	14.91	1026.1	12.49	3.4
14-0	13.56	1026.4	0.8305	1028.1	12.72	1.7

Table 3- 3: SST and density at the equator and northernmost latitude for a temperature gradient of 24 degrees Celsius.

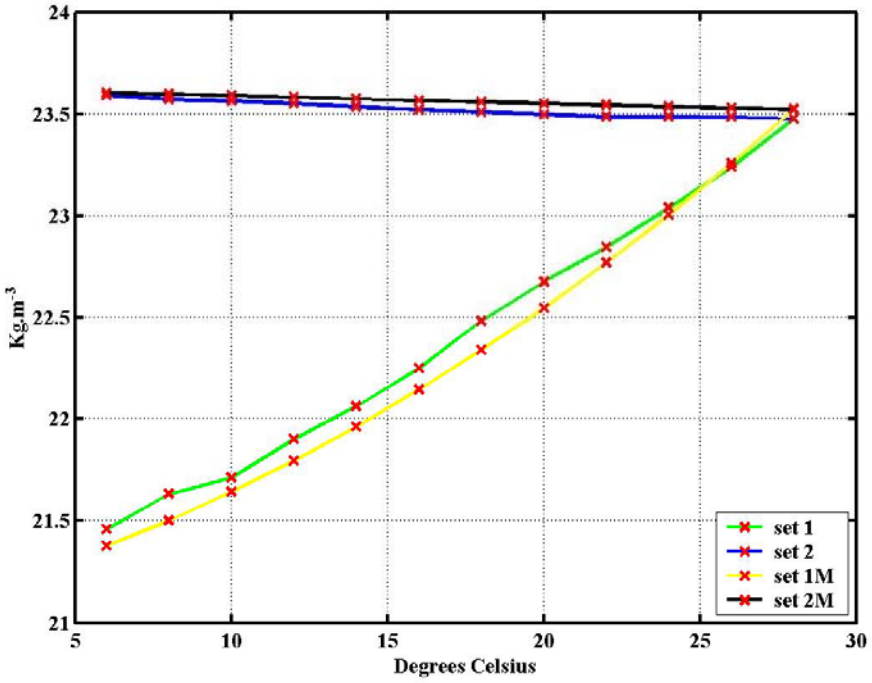

Figure3-13: Bottom to surface average density difference at 60°N against restoring temperature gradient for the 4 sets of experiments.

It is not clear why the two sets of experiments have such a different convective behaviour (in set1, as the temperature gradient increases, convection disappears while in set 2, as the temperature gradient decreases, convection intensifies).As is shown in figure 3-13, although locally, convection mixes the water column, the basin wide effect of the convection is to increase the amount of stratification (since it creates cold deep waters) and this in both models. In set 2 and 2M, as the temperature gradient decreases, convection increases and the bottom to surface density difference increase, indicating higher stratification in the northern latitudes. The experiment with the smallest density difference, 6-0, has the most convection, the highest high latitude stratification and the weakest overturning. To a certain extent, these results agree with the conclusion of Marotzke & Scott (1999), who found that increasing the convective mixing lead to a decrease in the overturning and that the overturning circulation could be strong, even in the absence of convective mixing.

In set 1 and 1M, the opposite situation occurs. As the temperature gradient decreases, the convection decreases and the high latitude stratification decreases.

In these set of experiments, the experiment with the smallest density difference, 28-2, has the weakest convection, the weakest stratification and the weakest overturning.

It was not possible to conduct experiments in set 1 and 2 with smaller gradients due to instabilities appearing in the MOMA model, the MIT model proved far more robust even for very small gradients (0.1^{o}C). As shown in figure3-14, when the gradient tends towards zero, the overturning also tends towards zero. This is the expected behaviour in an ocean with uniform temperatures.

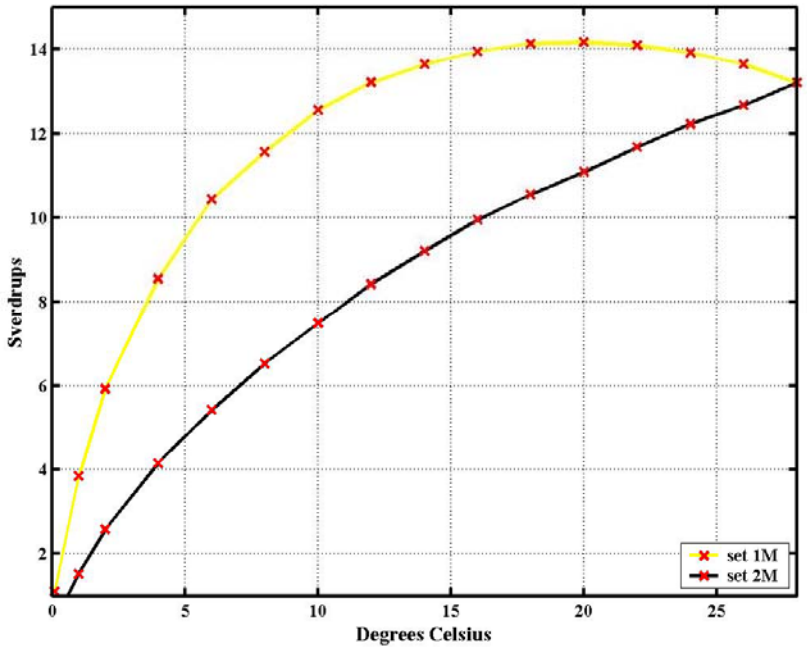

Figure3-14: overturning against temperature gradient for set 1M and 2M.

These experiments show that the ocean basin can follow two routes as the temperature gradient decreases: one that favours diffusion, in the case of a fixed northernmost temperature, one that favours convection, in the case of a fixed southernmost temperature. Both end up in an identical state when the temperature gradient is zero.

3.4.4) The effect of convection on the isopycnal in the high latitudes:

The analysis of the results has demonstrated the high variability of convection at high latitudes in these experiments. This variability of the convection has a

substantial impact on the overturning circulation, but the precise mechanisms involved are not clear. Consequently, it is necessary to look more closely at the effect of convection in the model.

The thermal wind equation gives a relation between the vertical shear in meridional velocity and the zonal density gradient:

$$\frac{\partial v}{\partial z} = \frac{-g}{\rho_o f}\frac{\partial \rho}{\partial x} \qquad (3.11)$$

The velocity gradient is therefore inversely proportional to the longitudinal density gradient.

Figure 3-15 shows a schematic of a mid-depth isopycnal (black curve) in the high latitudes for all the runs using the MOMA model.

The effect of convection is to cool the water column. Hence if the convection occurs on the eastern side of the basin (region A), the zonal temperature gradient will decrease (red curve) and as a result the vertical shear in the meridional velocity will decrease. All other things being equal, this will lead to a weakening of the overturning. If the convection occurs on the western side of the basin (region B), the zonal temperature gradient will increase (blue curve) and as a result the vertical shear in the meridional velocity will increase. This is clearly shown in figure 3.11 and 3.16. In 3.11, one can see that the mid-depth convection is relatively greater on the eastern side of the basin for experiment 24-0 from set 2 whereas experiment 28-4 from set 1 has more convection at high latitudes on the western side of the basin. As a result, the temperature anomaly is cooler on the western side and warmer on the eastern side for 28-4 than for 24-0 as is shown in figure 3.16. This leads to a stronger overturning for 28-4 than for 24-0.

When convection is distributed right across the basin, the temperature gradient is submitted to two competing effect, a weakening due to convection occurring on the eastern side and a strengthening due to convection occurring on the western side. The details of the circulation structure will determine which of these two effects dominates.

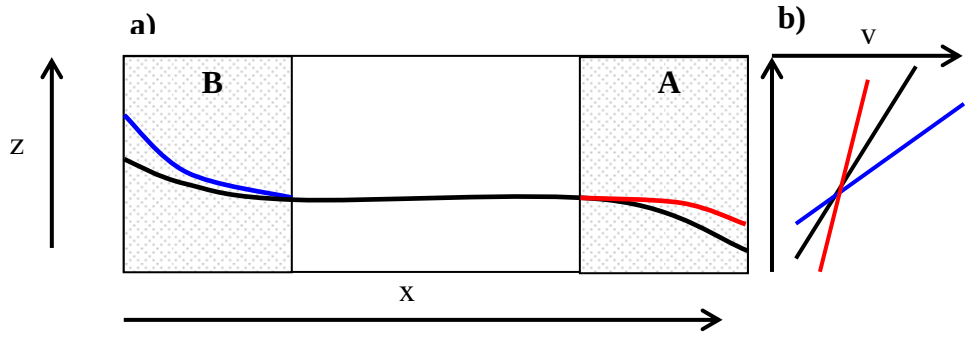

Figure3-15: a) Schematic of the effect of shallow depth convection on the isopycnals at high latitude. The black curve is the initial shape of the isopycnal, the red curve is the modified portion of the isopycnal after convection has occurred in zone A, and the blue curve is the modified portion of the isopycnal after convection has occurred in zone B. b) zonal mean meridional velocity, black initially, red after convection in zone A, blue after convection in zone B.

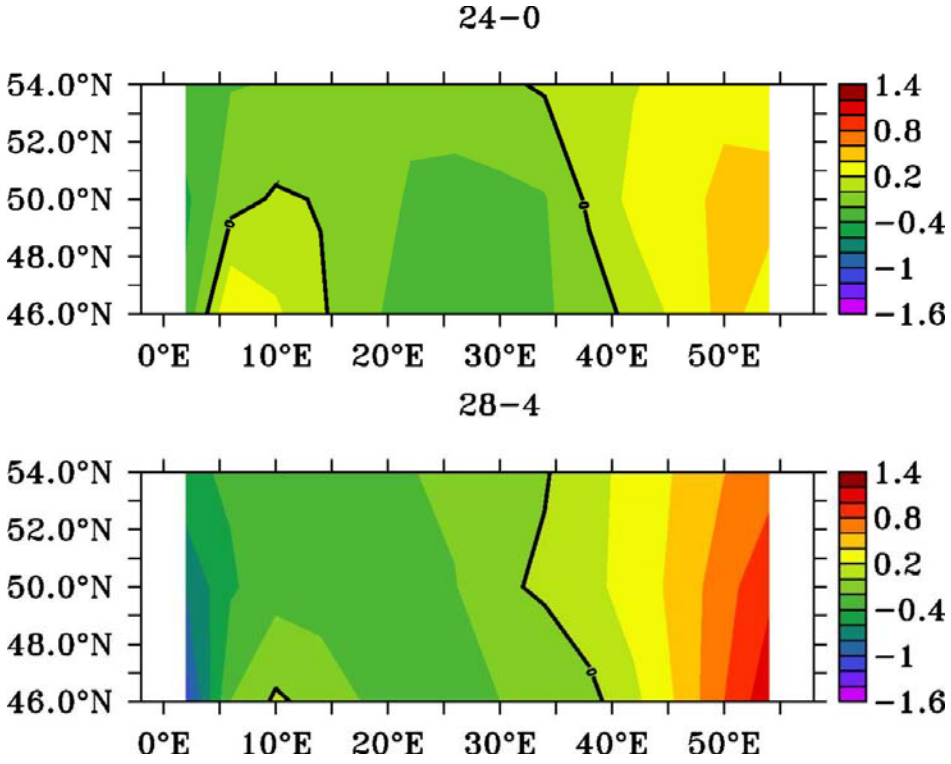

Figure3-16: Temperature anomaly in ^{o}C relative to the zonal mean at 800 metres for experiment 24-0 and 28-4 in the high latitudes.

It is worth noting that the further south the convection maximum is situated, the more zonally uniform its distribution becomes. This is because the SST distribution is more zonal towards the low latitudes (figure3-17).

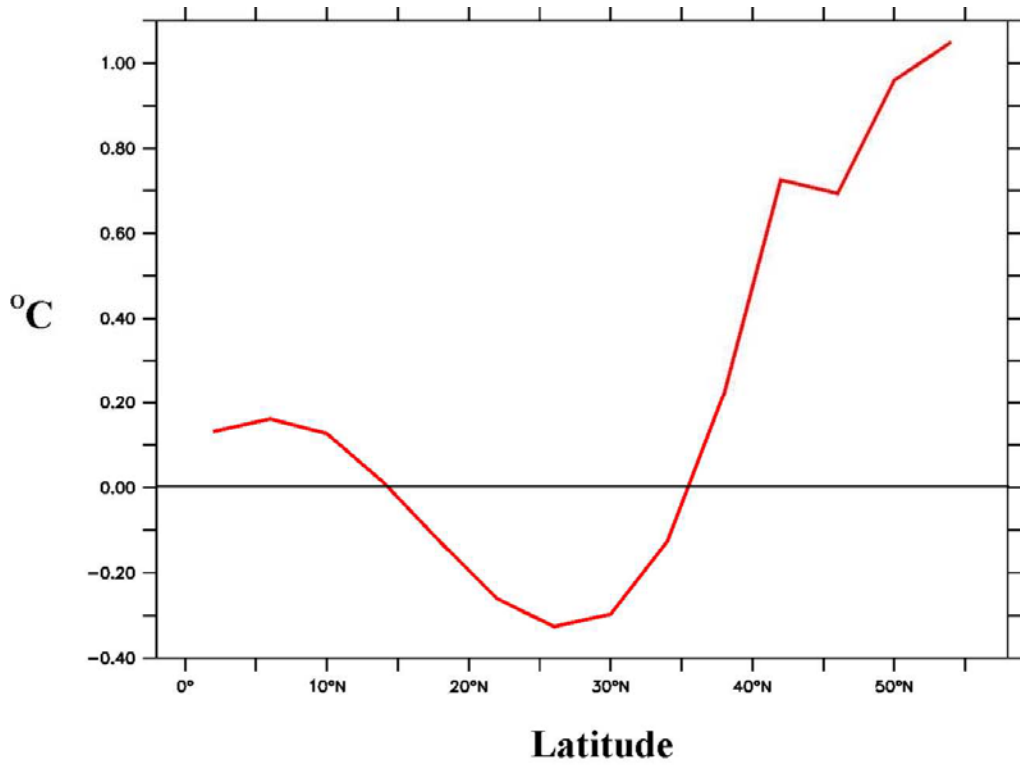

Figure3-17: Zonal SST difference distribution (Te-Tw).

The upshot of this is that when the convection maximum is in the high northern latitudes, its distribution will be skewed towards the western side of the basin as the SSTs there are warmer and the restoring temperature gradient is zonally uniform.

This analysis shows that the spatial distribution of the shallow to mid-depth convection is more important than its strength in controlling the strength of the meridional overturning stream function.

3.5) Conclusion:

These two sets of experiments clearly underline the fact that the behaviour of the system is too complex to be adequately represented by a simple scaling law. Indeed, self-similarity, which is necessary for the scaling law to be applicable (Park &Bryan 2000) does not hold for the first set of experiments. Indeed in set 1, as the temperature gradient decreases, the ocean basin evolves from one, which adjusts to the restoring through diffusion and intense convection in the high latitudes to one, which adjusts through diffusion alone. As a result, the

strength of the overturning increases with decreasing temperature gradient until a north south temperature gradient of 20 degrees followed by a decrease in the overturning for smaller gradients.

In set 2, as the temperature gradient decreases the distribution of the convection changes, shifting westward and southward. To a certain extent, self-similarity holds but the theoretical scaling law does not apply, as the decrease is linear. In effect it follows $\Delta\Psi \sim \Delta T^{1}$.

The results for the MIT model confirm that this behaviour is not specific to the MOMA model and might be generic to OGCMs.

In any case, this study has highlighted the complex behaviour of numerical models and demonstrated the hazards of applying a simple scaling law to the system in order to predict its behaviour. It has also shown that the spatial distribution of the convection is more important than its strength in controlling the strength of the overturning.

Implications

It has been shown here that the convection distribution varies and plays an important role in determining the strength of the overturning. This means that 2D models fail to capture an important aspect of the oceanic circulation, one that plays an important role in determining the strength of the meridional overturning.

Furthermore, the way convection is distributed means that the whole system resists change in the meridional overturning circulation in response to variation in the northernmost buoyancy value. Hence in set 1 (and 1M), it is very hard to produce a significant decrease in the overturning. A drop in the restoring temperature of at least 16 ^{o}C is necessary to observe some form of measurable reduction in the strength of the overturning. At 0^{o}C, this represents a freshening of 3 PSU to obtain the same density decrease. It is not clear whether this accurately represent the sensitivity of the real ocean circulation to sea surface buoyancy variations. In any case, this weak sensitivity could well be a feature of most OGCMs.

Chapter 4: The response of an idealised ocean basin to variable buoyancy forcing

Published as: Lucas, M. A., J. J. Hirschi, J. D. Stark, and J. Marotzke, 2005: The response of an idealized ocean basin to variable buoyancy forcing. *Journal of Physical Oceanography*, in press.

Summary:

The response of an idealised ocean basin to variable buoyancy forcing is examined. A general circulation model that employs a Gent-McWilliams mixing parameterisation is forced by a zonally constant restoring surface temperature profile, which varies with latitude and time over a period P. In each experiment, 17 different values of P are studied, ranging from 6 months to 32,000 years. The model's meridional overturning circulation (MOC) exhibits a very strong response on all timescales greater than 15 years, up to and including the longest forcing timescales examined. The peak-to-peak values of the MOC oscillations reach up to 125% of the steady-state maximum MOC and exhibit resonance-like behaviour, with a maximum at centennial to millennial forcing periods (depending on the vertical diffusivity). This resonance-like behaviour stems from the existence of two adjustment time scales, one of which is set by the vertical diffusion and another, which is set by the basin width. Furthermore, the linearity of the response as well as its lag with the forcing varies with the forcing period. The considerable deviation from the quasi-equilibrium response at all timescales above 15 years is surprising and suggests a potentially important role of the ocean circulation for climate even at Milankovich timescales.

4.1) Introduction

The response of the meridional overturning circulation (MOC) to pure buoyancy forcing has been the subject of relatively few studies. Those that exist have concentrated on the scaling behaviour between the equator-to-pole temperature gradient (ΔT) and the strength of the maximum overturning (Zhang et al. 1998; Huang 1999), based on the work of Bryan and Cox (1967), whose principal aim however had been to develop a scaling relationship between horizontal currents and the vertical diffusivity. Deriving the scaling law that links the MOC to the north-south surface temperature gradient implies that the meridional temperature gradient is proportional to the zonal temperature gradient. Marotzke (1997) presented theoretical arguments that this proportionality did indeed exist, and his conclusions were supported by the numerical results of Park and Bryan (2000). However, Scott (2000) cast doubt upon the robustness of the scaling law: his results suggest that the scaling law varies with latitudes and that it fails to capture the geographical displacement of the overturning cell as ΔT varies. He did not, however, study in detail the structure of the circulation or how it is affected by changes in ΔT. Park and Bryan (2001) also looked at the effect of different vertical coordinate systems on a purely buoyancy-forced ocean basin.

In contrast to these relatively few studies, there have been many model studies investigating MOC variability on the interdecadal time scale, both in pure ocean models with constant forcing (e.g., Marotzke,1990; Weaver and Sarachik, 1991; Weaver et al. 1993; Winton 1996; Greatbatch and Peterson 1996; te Raa and Dijkstra, 2002), in coupled ocean-atmosphere models (e.g., Delworth et al., 1993; Delworth and Greatbatch, 2000; Delworth and Mann, 2000) and in response to North Atlantic Oscillation (NAO)-style forcing (Visbeck et al., 1998; Hurrell et al., 2001). Theoretical arguments for the emergence of MOC variability have been put forward by Colin de Verdiere and Huck (1999), te Raa and Dijkstra (2002) as well as Eden and Greatbatch (2003).

There have also been efforts to study the oceanic response to Milankovitch orbital forcing. Brickman et al. (1999) conducted a study using a 2.5-D atmosphere ocean model run for 3.2 Ma. They found that the strongest response was in the obliquity band while the response in the eccentricity band was

suppressed. Their explanation for this was that the main effect of obliquity was to control the seasonal contrast, and as deep water formation happens in winter, the harsher the winter, the greater amount of deep water formed and the stronger the overturning. Their results also showed that in the obliquity band, the global ocean average temperatures were negatively correlated with the atmospheric ones, due to a rectifying effect by the ocean.

The present paper addresses a gap in all previous works, in that it investigates the effect of pure *variable* buoyancy forcing on the MOC under three-dimensional dynamics. We use very idealised forcing, which varies sinusoidally in time, and tune through a wide range of periods, following the strategy sketched in Visbeck et al. (1998).

In Section 4.2, we describe the model and the experimental set-up. Section 4.3 gives a descriptive account of the main results. An in-depth analysis and discussion are successively provided in Section 4.4 and Section 4.5, dealing with the effects of diffusion and the influence of the basin width, respectively. Section 6 compares boundary current velocities and the meridional overturning, and Section 7 briefly presents conclusions.

4.2) Model description and experimental set-up

4.2.1) Model description

The model used is a parallelised version of the GFDL MOM model which can distribute the various processes on an array of processors (Webb, 1996). The free surface numerics have been updated by including the free surface numerical code of OCCAM (Webb, 1995). The model also includes the eddy parameterisation scheme of Gent and McWilliams (1990) as implemented by Griffies (1998).

The domain is a 60^o wide basin with solid boundaries and 15 levels in the vertical, extending from the equator to 60^oN of latitude. The horizontal resolution is 4^ox4^o. Table 4-1 lists the default parameters.

In the initial conditions, the salinity is set to 35 psu throughout the model and the salinity fluxes are set to zero. The wind effect is removed by setting all the

surface wind stresses to zero. The temperature fields are initialised by setting the surface temperature to 20ºC at all latitudes and longitudes and decreasing it by one degree at each level. Thus, the coldest temperature is at the bottom and is 5ºC.

Parameter	Value
Basin Width, length	60^o, 60^o
Basin depth	5000 m
Number of vertical levels	15
Longitude, latitude grid spacing	4^o, 4^o
Vertical, horizontal diffusion coefficient	$1 \cdot 10^{-4} m^2 s^{-1}$, 0 $m^2 s^{-1}$
Isopycnal thickness diffusivity	$2 \cdot 10^3 m^2 s^{-1}$
Lateral eddy diffusivity, viscosity	$1 \cdot 10^5 m^2 s^{-1}$, $2 \cdot 10^3 s^{-1}$
Isopycnal tracer diffusivity	$2 \cdot 10^7 cm^2 s^{-1}$
Temperature restoring time scale	40 days
Momentum time step	14400 s
Tracer time step	150000 s

Table 4-1: Summary of numerical parameters

The temperature is forced using a Newtonian relaxation scheme, where the restoring period is set to 40 days. In the initial spin up, the sea surface temperature is restored using a zonally uniform cosine function with a peak-to-peak amplitude of 26^{o}C and a value at the equator of 28^{o}C . The spin up lasts 8000 model years, until the value of the maximum MOC becomes virtually constant.

4.2.2) Experimental strategy

In the time-varying experiments, a sinusoidal restoring temperature profile is used. It varies with latitude and time according to:

$$T(\Phi,t) = (13 + \cos(\frac{t}{P} \times 2\pi)) \times (\cos(\Phi \times 3) - 1) + 28$$

where T is the restoring temperature, Φ is latitude, t is time, and P the forcing period (figure 4-1). As a result, the north-south temperature gradient is modified by varying the northernmost temperature, not the equatorial temperature, as done previously (Scott 2000). In our experiments, we vary the SST at 60°N by 4°C, giving us a 4°C variation in the meridional temperature contrast. As is shown in figure 2, taken from the NCEP re-analysis (Kalnay et al, 1996), such a variation is smaller than today's seasonal range. However, as we propose to examine the effect of very long-period oscillations, we need to have an idea of the past amplitudes in SST.

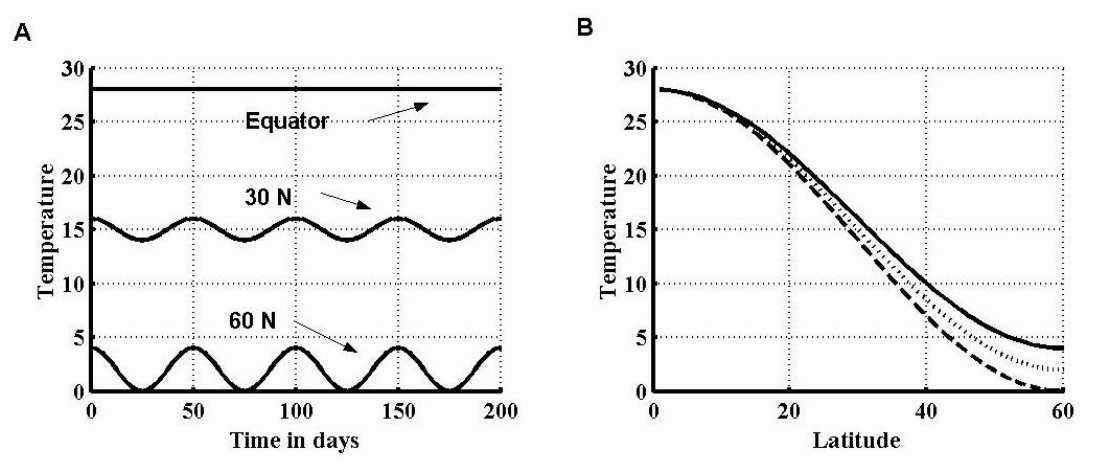

Figure 4- 1: Summary of variable forcing set-up. The left hand panel shows the evolution of the restoring temperature in °C at 3 latitudes for a forcing period of 50 days. The right hand panel shows the maximum (solid line) and the minimum (dashed line) forcing profile in °C as well as the forcing profile used to spin up the model (dotted line).

By analysing the $\delta^{18}O$ isotope records from various sites in the North Atlantic for the last 1.1 MA, Ruddiman et al. (1986) concluded that maximum SST variations at about 60°N was in excess of 10°C for summer and winter temperatures. This is

also the estimate obtained by the Climex project in their world maps of the last two climatic extremes, namely 18,000 years ago, the last glacial maximum, and 8,000 years ago, the Holocene optimum (CGM, 1999). These studies show that the 4°C range we use is modest compared to the range of naturally occurring values.

Six different experiments are carried out, with different values for the vertical diffusion coefficient, varying topography and basin width as well as one run which includes winds. Furthermore, a run with fixed fluxes is also carried out. Table 4-2 provides a brief description of each of the experiments carried out.

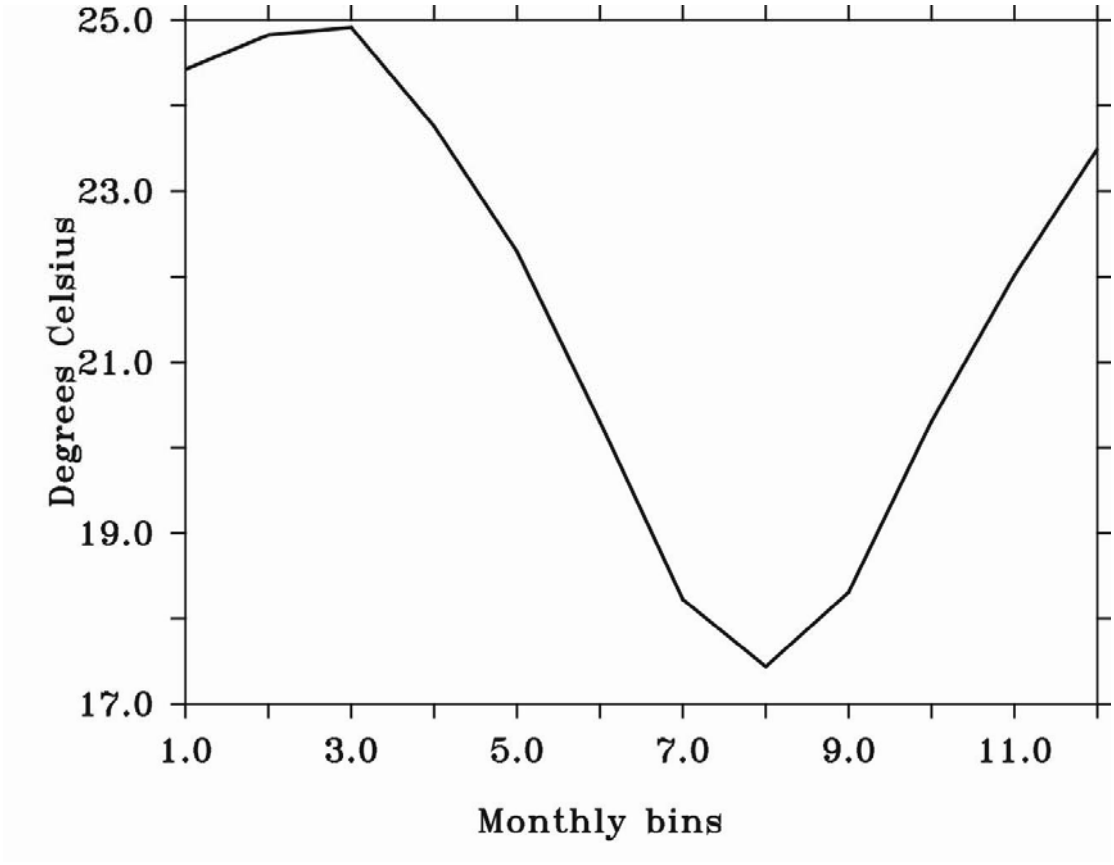

Figure 4-2: Monthly temperature gradient between the equator and 60°N in the Atlantic, obtained from NCEP data for the last 50 years.

Experiment	Vertical Diffusion	Basin width	Note
R1	1 cm^2/s	60^o	
R2	2 cm^2/s	60^o	
R5	5 cm^2/s	60^o	
T1	1 cm^2/s	60^o	Mid-ocean topography
D1	1 cm^2/s	60^o	Winds included
W1	1 cm^2/s	120^o	Wide basin
F1	1 cm^2/s	60^o	Constant fluxes.

Table 4-2: Summary of Experiments.

0.5	**1**	**2**	**4**	**8**	**15**
4,000	*4,000*	*4,000*	*4,000*	*4,000*	*4,000*
30	**60**	**120**	**250**	**500**	**1000**
4,000	*4,000*	*4,000*	*4,000*	*6,000*	*10,000*
2000	**4000**	**8000**	**16,000**	**32,000**	
12,000	*20,000*	*48,000*	*80,000*	*96,000*	

Table 4-3: List of forcing periods (bold) and integration time (italic) in years used in the experiments.

During the runs of the restoring experiments, R1, R2, R5, T1, D1 and W1, the forcing period P is gradually increased from 6 month to 32,000 years. For each value of P, the model is run until a cyclo-stationary state has been reached. Table 4-3 lists the actual periods used.

4.2.3) Asymptotic forcing

The constant restoring profiles of 28ºC to 0ºC and 28ºC to 4ºC can be seen to correspond to a time varying profile of infinite period as they represent a

infinitely slow change in the forcing. They can therefore be deemed to represent the asymptotic behaviour of the system.

Both experiments are started from the end of the spin up and run for 4000 years. Once equilibrium is reached, the maximum overturning takes the value of 12.16 Sv and 11.76 Sv respectively. This increase in the strength of the overturning when the meridional density contrast decreases is surprising. An in depth analysis of this behaviour is beyond the scope of this paper. However, it can be said that it occurs for a different reason from the one in Nilsson & Walin (2001) and Nilsson et al (2003) since here vertical diffusivity is prescribed (see chapter 3).

The asymptotic forcing experiments show that the 4ºC change in temperature between the two asymptotic experiments only leads to a 0.4 Sv change in the value of the maximum overturning. Therefore, any change in the overturning observed during the variable forcing beyond 0.4 Sv must be attributed to the oscillatory nature of the forcing.

4.3) Variable Forcing:

4.3.1) Overturning

Figure 4-3A shows the behaviour of the maximum overturning for R1. The system is profoundly affected by the oscillations in the forcing even for a forcing period of 32,000 years, which is within the Milankovitch cycle time band. The average maximum overturning value for each of the forcing periods is greater than the value of the maximum overturning during the spin up, which corresponds to the average forcing. The location of the maximum overturning is also very regular for each forcing period. For the maximum values, it is situated at about 53^{o}N and at about 2000 metres depth. As it decreases, it shallows and shifts southwards, to about 40^{o}N.

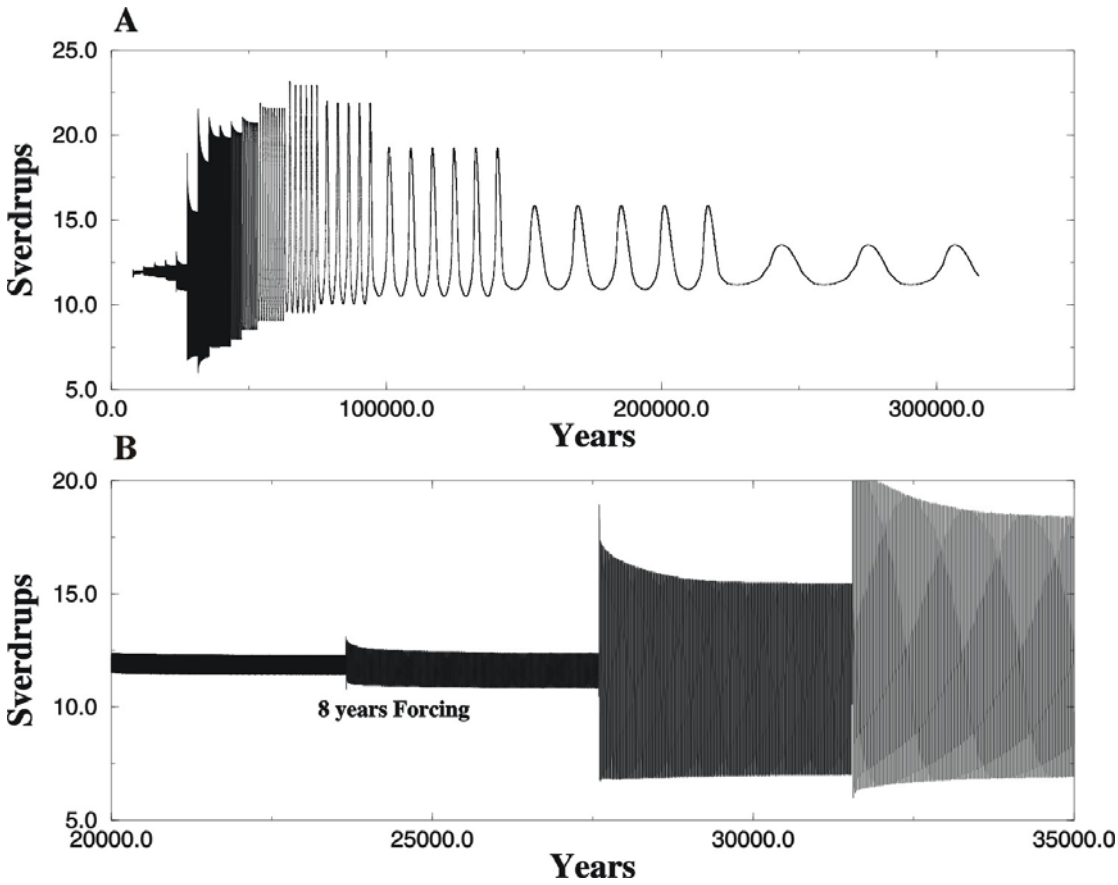

Figure 4-3: Panel A: Maximum overturning against time for experiment R1. Vertical diffusivity is 1 cm^2/s. The model is run for 17 forcing periods and for each until a cyclo-stationary state has been achieved. Panel B: Maximum overturning against time in experiment R1 for 4 successive forcing periods: 4, 8, 15, and 30 years. This figure highlights the jump in amplitude in the overturning as the period increases from 8 years to 15 years.

The maximum overturning curves also display a maximum range, which occurs for a period of 2000 years. At a forcing period of 30 years, the overturning reaches its absolute minimum value. From then on, the minimum value of the maximum overturning will continuously increase, even as the maximum eventually starts to decrease. The other notable feature is the presence of a significant increase in the amplitude when the forcing switches from a period of 8 to 15 years. This is clearly visible in figure 4-3B, a zoom of figure 4-3A on the transition between a forcing period of 8 years and a forcing period of 15 years.

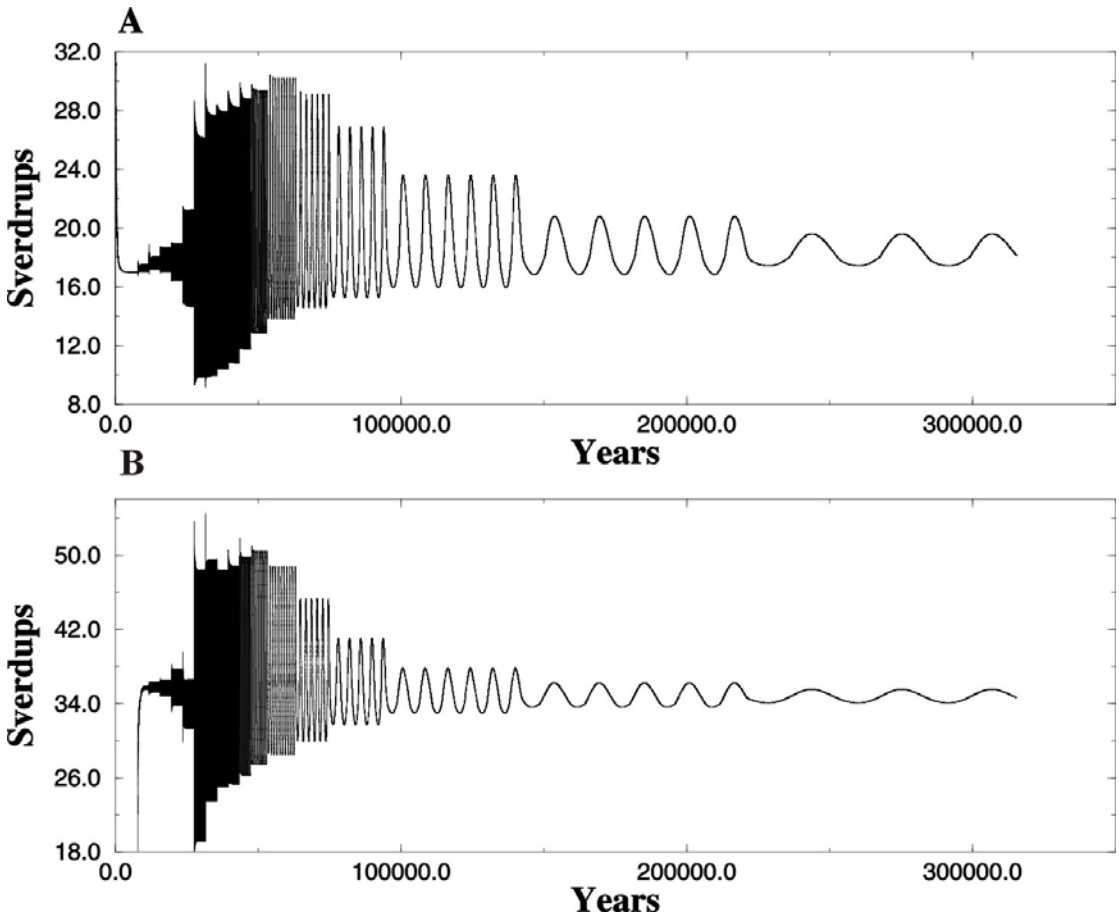

Figure 4- 4: Panel A: Maximum overturning against time for experiment R2. The diffusion is of 2 cm^2/s. The model is run for 17 forcing periods and for each until a cyclo-stationary state has been achieved.
Panel B: Maximum overturning against time for experiment R5. The diffusion is of 5 cm^2/s. The model is run for 17 forcing periods and for each until cyclo-stationary state has been achieved.

The following experiments are used to test the sensitivity of the system to vertical diffusivity and topography. Experiments R2 and R5 are identical to R1 except that the vertical diffusivity is set to 2 cm^2/s and 5 cm^2/s respectively. The results for the overturning are shown in figure 4-4. Generally, the values for the overturning are higher than for R1 and higher for R5 than for R2. This is consistent with experiments of constant forcing (e.g. Bryan, 1987; Colin de Verdiere, 1988; Park and Bryan, 2000). In both cases, the maximum amplitude in the overturning occurs for a period smaller than in R1. For R2, the maximum amplitude occurs for a forcing period of 60 years and for R5, it occurs for a forcing period of 30 years. As in R1, there is also a significant jump from a forcing period of 8 years to a forcing period of 15 years. Increasing the

diffusivity shifts the maximum amplitude in the overturning towards the smaller periods. It does not, however, affect the 8 years forcing period to 15 years forcing period jump in the amplitude of the maximum overturning.

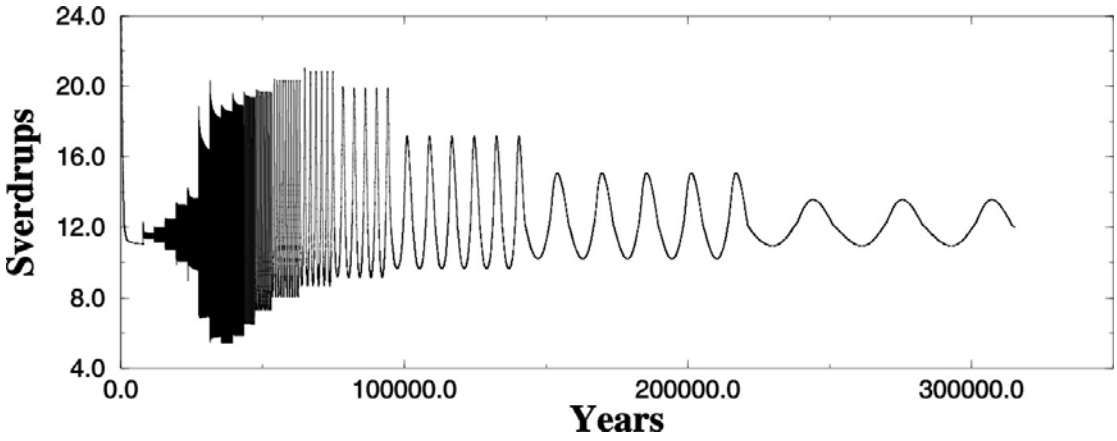

Figure 4-5: Maximum overturning against time for experiment T1. The diffusion is of 1 cm^2/s. The basin topography includes a north-south ridge 2500m high. The model is run for 17 forcing periods and for each until cyclo- stationary state has been achieved.

Experiment T1 is identical to R1 except for the introduction of an idealised north-south mid-basin ridge 2500 metres high and 4 cells wide. The result for the overturning is shown in Figure 4-5. Generally, the overturning is slightly weaker than in experiment R1. Furthermore, the maximum amplitude in the overturning occurs for a forcing period of 120 years. The jump between the forcing period of 8 years and the forcing period of 15 years observed in all the other experiments is still present. However, the absolute minimum is no longer so close to the jump in amplitude as it occurs for a period of 120 years.

Finally, Figure 4-6B shows the results for the overturning stream function in D1, which has an identical set-up to R1 except that a idealised wind forcing is applied. The actual wind stress values used are those of Weaver & Sarachik (1990) and are shown in figure 4-6A. Generally, the wind decreases the strength of the overturning. Most of this decrease is accounted for in a reduction of the strength of the western boundary current (not shown). Furthermore, the reduction in the strength of the western boundary current means that less warm water will be advected northward. As a result, at all times during a forcing cycle, the deep water formed is slightly colder than for a run without winds (not shown). This in

turn increases the stratification slightly and decreases the strength of the convection. The consequence of this is that the overturning is generally weaker throughout a forcing cycle for D1 relative to R1.

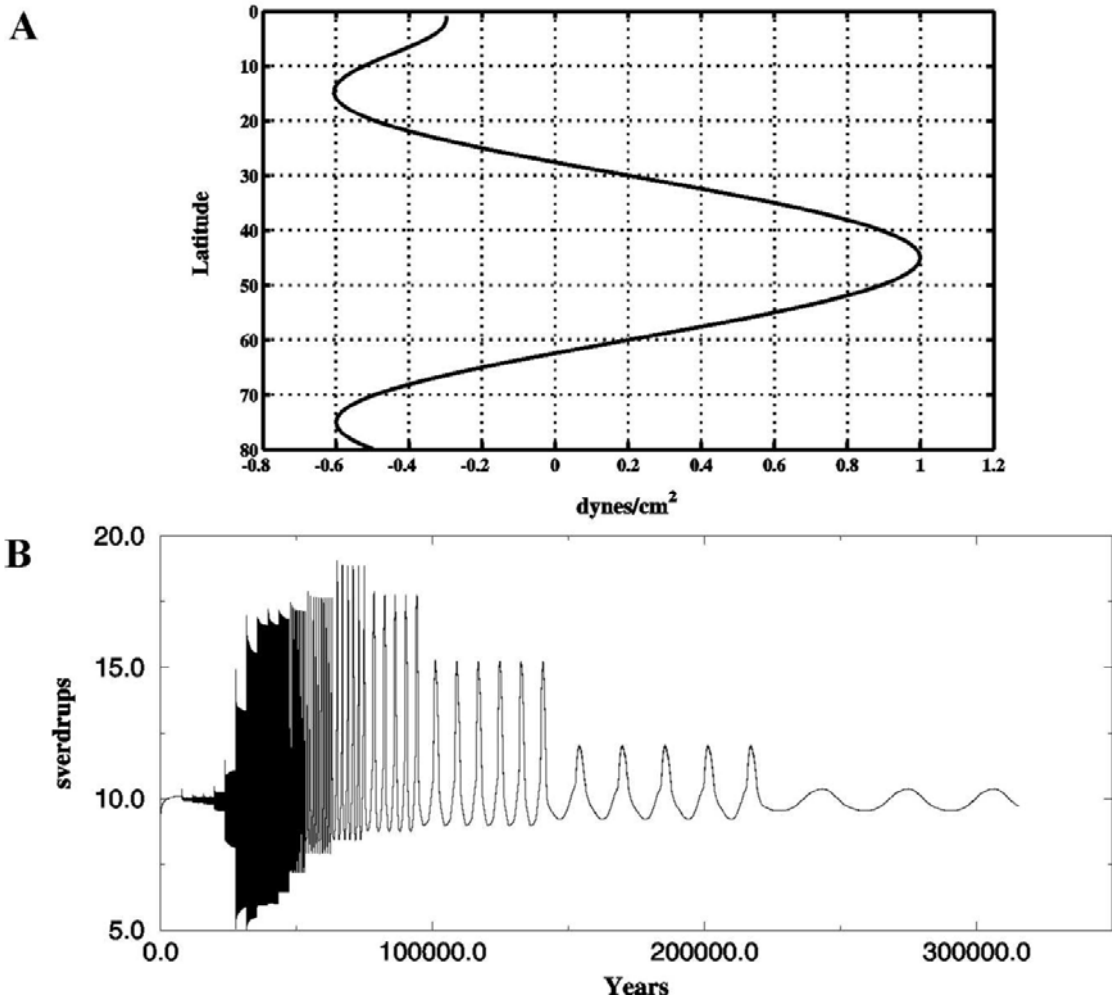

Figure 4-6: Panel A: wind stress distribution for experiment D1 after Weaver & Sarachik (1990).
Panel B: Maximum overturning against time for experiment D1. The diffusion is of 1 cm2/s.

The maximum amplitude is now of 10.6sv and occurs for a forcing period of 2000 years. Once again, the jump occurs between the forcing periods of 8 years and 15 years. As for R1, the absolute minimum is reached for a forcing period of 30 years.

Two robust and distinct features occur in all the experiments: a maximum amplitude in the overturning and a significant jump in the amplitude between the forcing period of 8 years and that of 15 years. To understand what brings about these features, we will thereafter focus on experiment R1.

4.3.2) Bottom temperature

Figure 4-7 is a plot of the forcing temperature at 60°N, i.e. the temperature to which the latitude of 60° is restored, and the minimum bottom temperature in R1. The bottom temperature displays some regular oscillations for all forcing periods although these have a very small amplitude for the forcing periods of 8 and 250 years, clearly showing that very little of the oscillatory behaviour of the forcing reaches the deep ocean. Changing the forcing period does have an effect as the mean value of the temperature in the deep ocean is lowered as the period is increased. This is partly because, the greater the forcing period, the colder the minimum temperature found in the surface ocean during a cycle as the vertical diffusivity becomes increasingly efficient in capturing the forcing signal the longer the forcing period becomes. It is this coldest water, which then fills the deep ocean. Furthermore, the longer the forcing period, the more time those cold waters have to fill the deep ocean before being removed by diffusive warming (see section 4).

As the period is increased, the amplitude of the oscillations increases slowly until, for the 32,000 years forcing, it reaches an amplitude of 2.5°C. The bottom temperature now closely follows the behaviour of the forcing temperature although it still has only half its amplitude. Clearly, the forcing signal now reaches all the way down to the bottom of the basin.

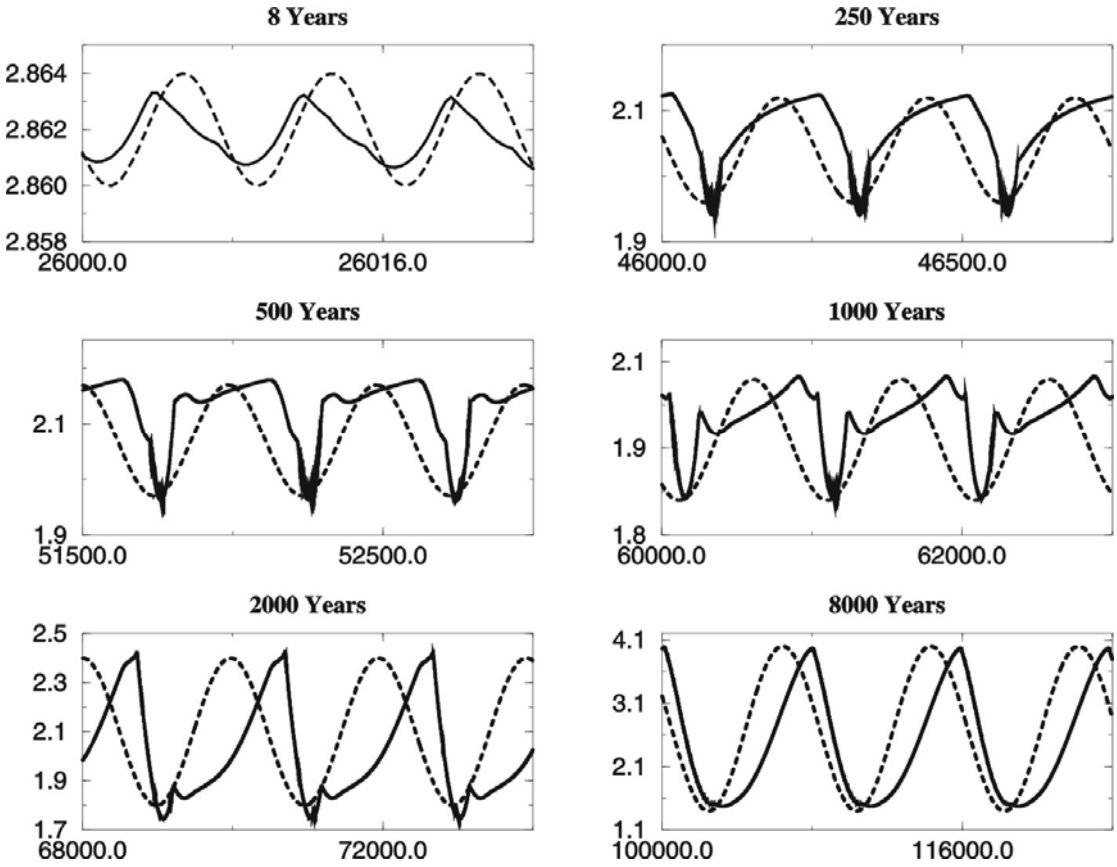

Figure 4-7: Evolution of the minimum bottom temperature (solid) and the forcing temperature (dashed) during experiment R1 over 6 different periods: 8 years, 250 years, 500 years, 1000 years, 2000 years and 32,000 years. The forcing temperature has been scaled down to the bottom temperature range. Consequently, no absolute values for the forcing temperature can be inferred from those plots. The forcing temperature is the restoring temperature of the northern most (60^o) latitude. Thus, when the forcing temperature is at a maximum, the north south temperature gradient is at a minimum. The x axis is time in years and the y axis temperature in ^oC.

We also observe that the bottom temperature signal displays two dominant components. One component, the narrow trough dominates the periods above 8 years and below 1000 years (figure 4-8). By this, we mean that the amplitude of the narrow trough accounts for most of the amplitude of the oscillations. The other component, the peak is clearly dominant for periods of 2000 years and above. The two components suggest that the response of the system is the result of its adjustments to the forcing through two processes, each requiring a certain time scale to become efficient. One of these processes has an adjustment time of decades while the other has an adjustment time in the millennial time band. The response of the system to a specific forcing period is a combination of the

adjustment of the basin to the forcing through those two mechanisms at that specific forcing period (see section 4 and 5).

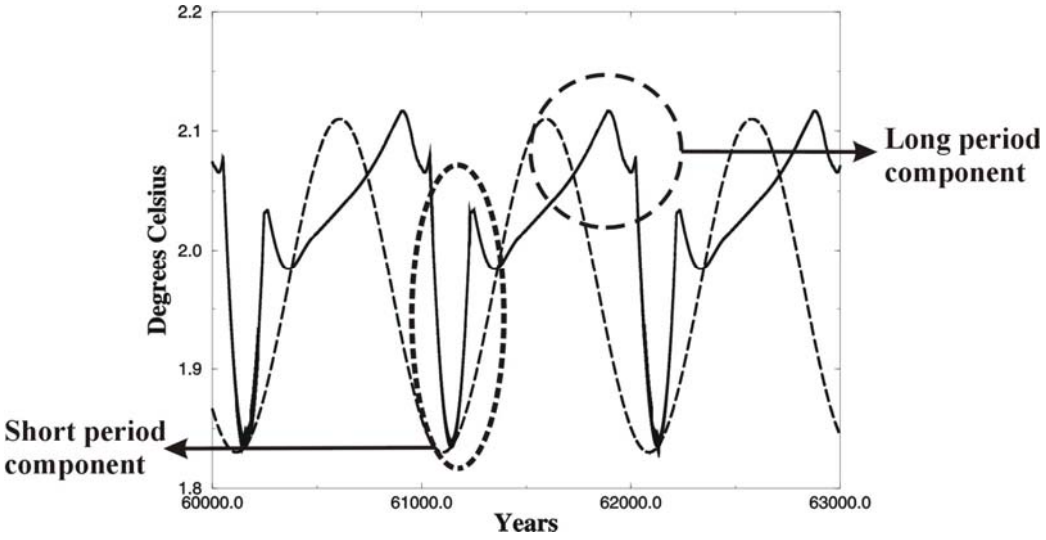

Figure 4-8: Evolution of the minimum bottom temperature (solid line) and the forcing temperature (dashed line) during experiment R1 over the 1000 years forcing. This figure shows the two components of the bottom temperature signal.

4.3.3) Phase lag

In figure 4-9, we can see the evolution of the phase lag between the forcing temperature at 60°N (the temperature to which the sea surface temperature is being restored), and the response of the meridional overturning. For the very long forcing periods, the two signals are slightly out of phase. As the forcing period decreases, the lag between the forcing temperature and the response increases: for a forcing period of 4 years, the lag is of one full period (a lag of 0). This means that in our model, the minimum temperature gradient, thus the maximum forcing temperature, leads to the maximum overturning and vice versa which is consistent with the results from the asymptotic runs. This figure also clearly demonstrates that the system is far more complex than a forced oscillator as, for the resonance like period, 2000 years, the lag is clearly not of $\pi/2$, as it would be in a forced oscillator but of π (see also section 6 on the velocities).

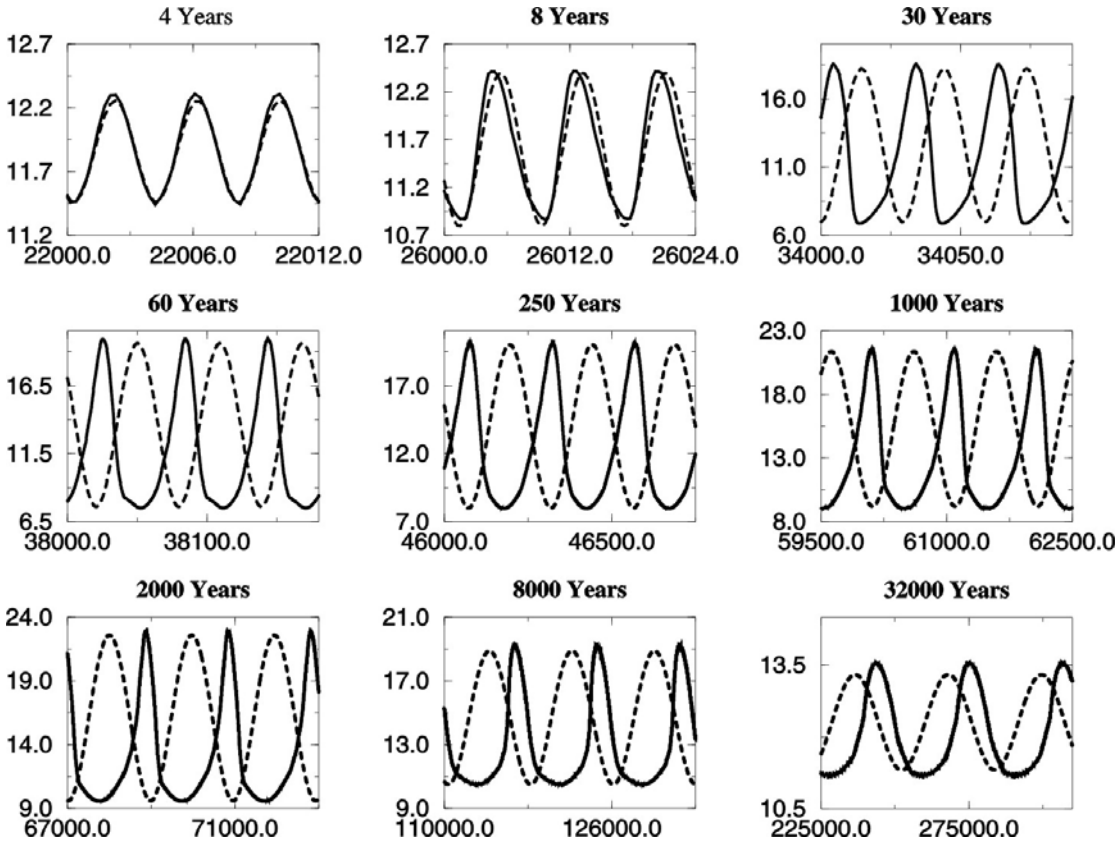

Figure 4-9: Forcing temperature (dashed line) and overturning response (solid) in R1 for 9 forcing periods. The forcing temperature has been scaled up to the overturning and as a result, no absolute value can be inferred. The forcing temperature is the restoring temperature of the northern most (60^o) latitude. Thus, when the forcing temperature is at a maximum, the north south temperature gradient is at a minimum. The x axis is time in years and the y axis temperature in ^{o}C.

We also observe that the non-linearity of the response varies with the forcing. For small periods, the response is quasi-sinusoidal whereas for a forcing period of 2000 years, the response is highly non-linear, with a very sharp peak and a longer trough. As the forcing period continues to increase, the peak becomes less pronounced and the response more linear again.

To understand how the phase lag is set up, it is necessary to look at other quantities. In figure 4-9, we see the evolution of the convection index, the overturning, and the surface-to-bottom temperature difference. The convection index is an average over the sampling period of the number of cells in the model which undergo convective mixing. The surface to bottom temperature difference is obtained by subtracting the minimum surface temperature to the minimum bottom temperature.

We have two different types of behaviour in the system, one for periods greater and another for periods smaller than 8 years. For the forcing periods greater than 8 years, the response of the overturning is almost perfectly in phase with the convection in the high latitudes. An increase in the strength of the convection index is followed by an increase in the strength of the overturning. As the period increases, the convection index plateaus for a longer time and the decrease in the strength of the overturning goes from lagging slightly the convection decrease to preceding it. For forcing periods below 8 years, the convection index and the overturning are out of phase.

The convection is well known for its abrupt changes once threshold values are reached (i.e. large convective areas are either switched "on" or "off", Lenderink, 1994). This explains why the convection index does not just follow the forcing and exhibits step like increases and plateaus. The latter occur when all the cells which in an area that can undergo convection are already convecting. For additional deeper cells to convect (i.e. for the convection index to increase), a substantial amount of water must become unstable. Similarly, if a deep cell is convecting, it must under go a substantial cooling to become stable. Once it reaches that threshold value, it will stop convecting.

Figure 4-10 shows that it is the difference between the surface and the bottom temperatures that determines the amount of convection that takes place. The maximum convection occurs when the minimum surface temperature is smaller than the minimum bottom temperature. It is therefore the surface temperature signal and how it penetrates in the deeper ocean, which determines the phase behaviour between the forcing and the response. The surface temperature signal is itself the result of the effect of the forcing and the various processes that occur in the ocean, such as convection, diffusion and advection (see section 4).

The response, that is, the strength of the overturning, clearly has a negative feedback on the surface ocean temperature as the stronger the overturning, the stronger the western boundary current and the more warm water is carried northward to the convection areas. Furthermore, the stronger the convection, the smaller is the surface to depth temperature gradient. As for diffusion, what matters is not only how deep the forcing signal penetrates but also with what amplitude. All this suggests that diffusion has a particular role to play in the

response mechanism of the ocean basin and needs be studied further. Its behaviour will be examined in detail in section 4.

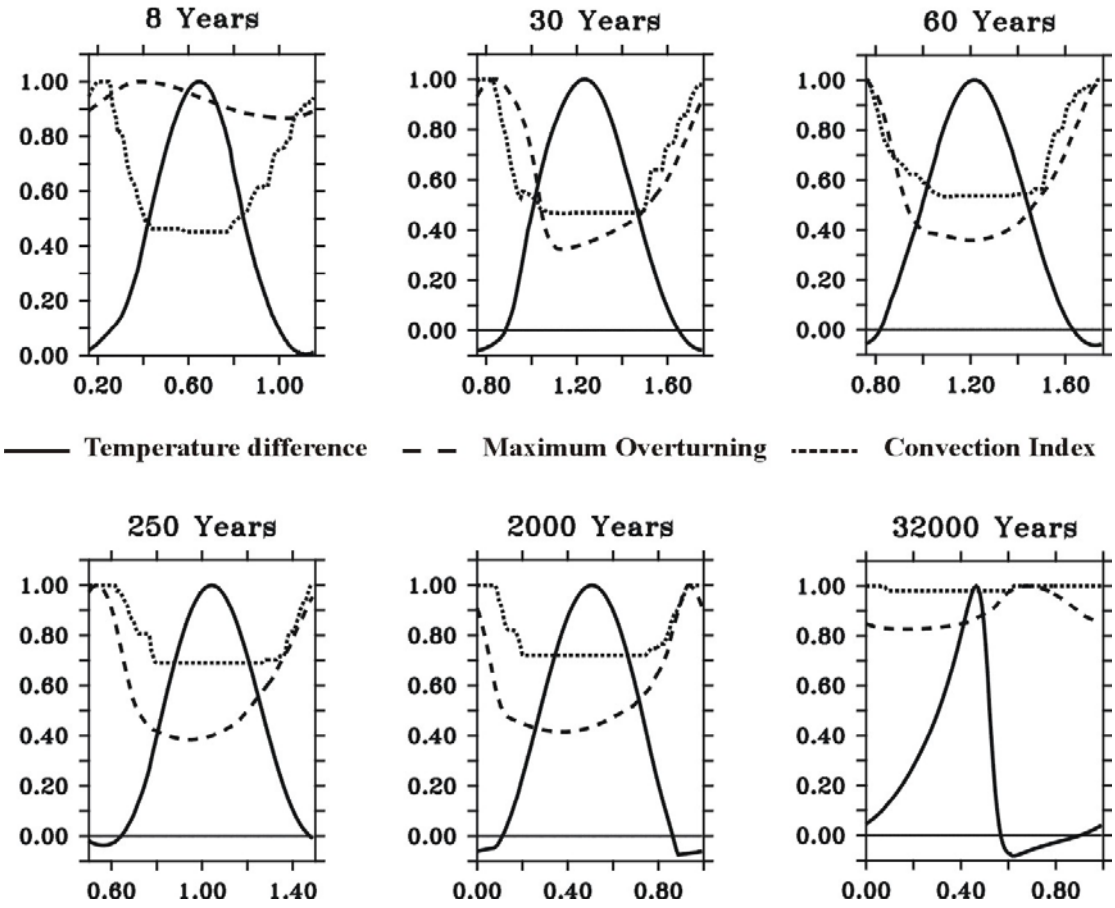

Figure 4-10: Evolution over one period of the total basin convection (dotted line), the Maximum overturning (dashed line) and the surface to bottom maximum temperature difference (solid line) for six forcing periods. All quantities have been normalised. The convection index is obtained by averaging over a sampling period the number of cells, which undergo convection. The x axis is time in fractions of a forcing period.

4.4) Diffusion

To obtain a deeper understanding of what happens as the period is increased, the behaviour of the system for four forcing periods in R1 is analysed: one small period, 8 years, one very long period, 32,000 years, and two periods in between, 250 and 2000 years. The 2000-year period is also important as it corresponds to

the maximum range in the overturning. Figure 4-11 shows the evolution of temperature and the meridional overturning at 52°N on the western side of the basin over one period of the forcing. For all the periods examined, the surface temperature displays a warm bias when compared to the forcing profile, resulting from the advection of warm water northwards by the boundary currents and the effect of convection.

For the very short periods the forcing signal does not penetrate below 1000 metres in the temperature field. As the forcing period increases, the forcing signal penetrates deeper and deeper, although the ocean remains fairly stratified. The amount of stratification is, however, clearly reduced in the 32,000 years forcing case. The surface temperature variation increases in amplitude as the forcing period increases, indicating that a greater amplitude of the forcing signal is captured by the surface ocean as the rate of change in the forcing decreases.

For periods of 250 and 2000 years, the warming at depth is slow and occurs while the overturning and the convective mixing are at their minimum. The cooling of the waters on the other hand, occurs at the same time as the maximum overturning and is particularly fast, relative to the warming, for the 2000-year period. For the 32,000-year period, the cooling and the warming have almost the same rate. This contrast between the rates of warming and cooling has already been discussed by Stouffer (2003), although the experiments presented here suggest that the strength of this contrast depends greatly on the forcing period. Finally, whereas for the short period (i.e. 250 years), the minimum temperature at depth occurs at almost the same time as the maximum surface temperature is reached, with increased forcing period this anti-phase behaviour is diminished and for 32000 years, the minimum deep temperature occurs at the same time as the minimum surface temperature.

The overturning stream function contour lines shows that it first strengthens and deepens from a forcing period of 8 years to 2000 years before shoaling and weakening for a forcing period of 32,000 years.

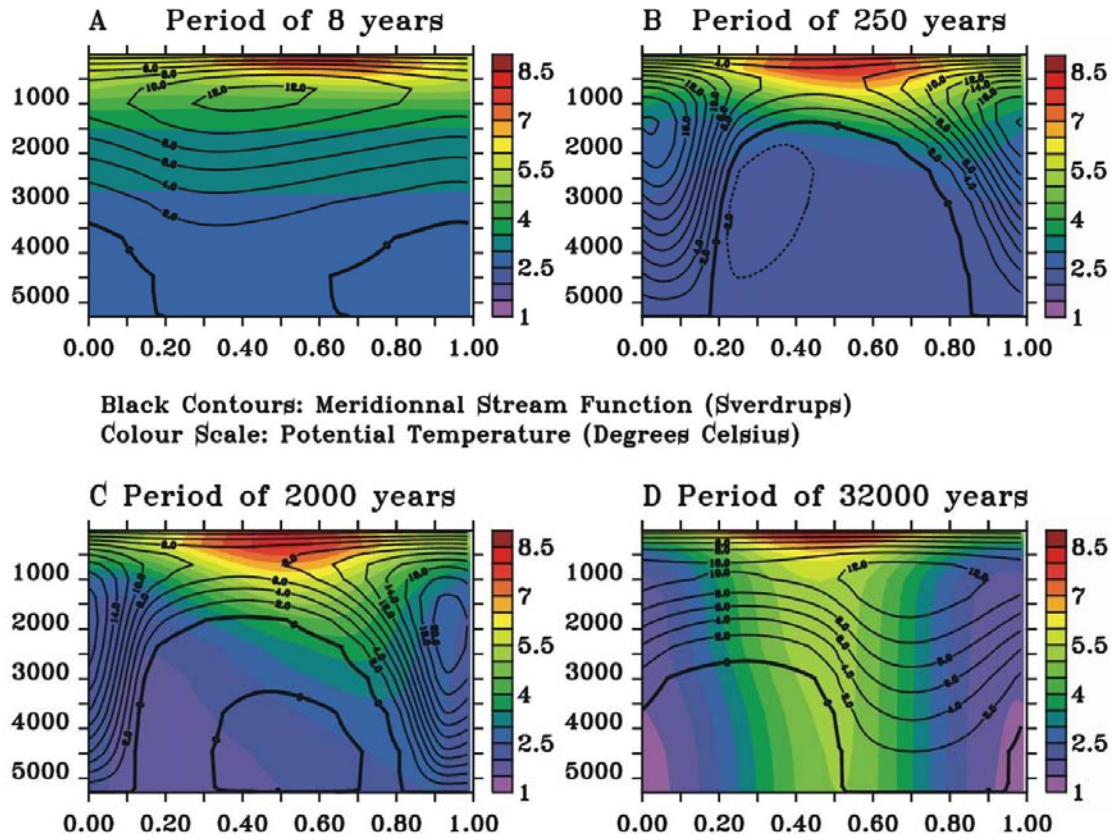

Figure 4-11: Evolution of the temperature (colour shading) and ψ (contours) over the four forcing periods: 8 (panel A), 250 (panel B), 2000 (panel C) and 32,000 years (panel D). The sampling period is set at 1/125 of the forcing period. The x-axis shows the normalised period and the y axis depth in metres.

Diffusion affects the system in two significant ways, firstly by controlling how much of the forcing signal the surface ocean will capture and secondly by determining how deep this captured signal will reach. The importance of the surface ocean in its ability to capture the forcing signal has already been suggested by Hasumi and Suginohara (1998). For small periods (below 250 years or so), the diffusion cannot keep pace with the changes in the forcing and thus only a small portion of the signal is captured by the surface ocean. Because the oscillation in the SST is so fast, the diffusion cannot transmit the forcing signal to the deep ocean and as a result, the amplitude of the deep ocean temperature oscillations is very small. As the period increases, more and more of the forcing signal is captured and transmitted to the deep ocean. Hence, for the forcing of 32,000 years, the warming and cooling are almost synchronous throughout the depth of the ocean. The depth to which the forcing signal

penetrates, even for the small forcing periods provides an explanation as to why the inclusion of wind in experiments D1 does not qualitatively alter the behaviour of the system. Indeed, we see in panel 4-11A that the forcing signal has a distinct signature up to a depth of 500 metres, which is deeper than the average wind mixed layer.

The maximum overturning occurs when enough of the forcing signal is captured to create buoyancy instabilities, which the diffusion is not efficient enough to remove. This creates convective mixing, which leads to an increase in the overturning. This allows for the fast removal of the instabilities and a rapid cooling of the ocean as is clearly shown in figure 4-11C where the warming of the deep ocean is slow and the cooling fast whereas the surface ocean cooling and warming have the same rate. Following the cooling, the warming of the surface ocean leads to the creation of a highly stratified ocean, which is very stable. This explains why the trough in the overturning increases relatively to the peak as the forcing period increases (figures 4-9 and 4-10). This fast cooling and slow warming also explains why the average bottom temperature increases for forcing periods of 1,000 years upwards. As the forcing period increases beyond the maximum overturning, the cooling, due to a combination of diffusion and convection has reached a maximum efficiency. However, the warming of the deep ocean becomes increasingly more efficient as diffusion has more time to have an effect (figure 4-7). Thus, the absolute minimum bottom temperature remains constant for periods greater than 1000 years but the absolute maximum increases leading to an increase of the average bottom temperature.

If we increase the value of the vertical diffusivity, we affect the systems capacity to capture the forcing signal and its response to it. This explains why the "resonance" shifts to the smaller periods when we increase the value of the vertical diffusivity: more of the signal is captured for the smaller forcing periods and the ocean is more capable of responding to it through diffusion alone. It must be noted that what we see in the response of the overturning is a combination of the adjustments to the forcing through the two processes. The observed resonance-like signal (i.e., when the greatest amplitude occurs) results from the interaction to those two responses. This is why increasing the diffusion shifts the main resonance signal so much towards the smaller periods.

Increasing the vertical diffusivity also alters the tail end of the curves displaying maximum overturning versus time (figure 4-3, 4-4 & 4-5). As the diffusion increases, for the long periods, the response of the system becomes more and more linear. This is also evident for a fixed diffusion and variable forcing periods (figure 4-8): as the forcing period increases past the maximum response in the overturning (2000 years for R1), the non-linearity in the response becomes less pronounced. This is because as diffusion becomes the dominant mechanism (either because it is increased or because it has more time to have an effect), the ocean basin has to rely less and less on the other mechanisms (convection, advection) to adjust to the forcing. Furthermore, the ocean becomes less and less stratified, thus less stable (figure 4-11D). As a result, the trough in the maximum overturning curve becomes less pronounced since the stratification is easier to break down and so the response becomes more linear. The linearity of the response of the ocean basin is therefore dependent on the forcing period and the value of the vertical diffusion.

To summarise, the ocean basin adjust to the effect of diffusion in two ways: firstly in the way the forcing signal is captured in the surface ocean and secondly in the way which this captured signal is transmitted to the deep ocean.

4.5) Basin width:

We still have to find an explanation for the sudden increase in response amplitude as the forcing period increases from 8 to 15 years. A plausible hypothesis suggests that the cross-basin travel time of baroclinic Rossby waves plays a role. To test this, we set up Experiment W1 identical to R1 in all but the basin width, which is twice that of R1, in other words 120^{o} of longitude. Once again, the system is spun up for 8000 years and then submitted to the same thermal forcing as R1.

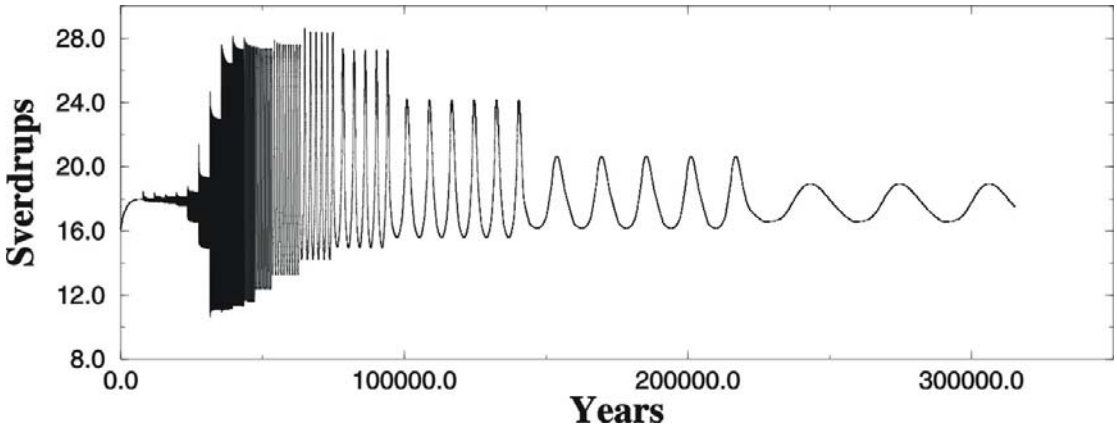

Figure 4-12: Maximum meridional overturning stream function for W1. The vertical diffusion is of 1 cm^2/s and the basin is 120^o wide. The model is run for 17 forcing periods and for each until cyclo-stationary state has been achieved.

Figure 4-12 shows the resulting behaviour of the maximum overturning. The average overturning is stronger but this is easily accounted for by the increase in basin width, implying stronger zonally integrated vertical diffusive fluxes and resulting in stronger vertical advection (Marotzke and Klinger, 2000). Broadly however, the behaviour is similar to that of the maximum overturning for R1. There is one important difference, however. The position of the jump in amplitude now occurs between a forcing period of 15 years and a forcing period of 30 years. Furthermore, in a fashion similar to R1, the absolute minimum in the overturning is found just after the jump, for the forcing period of 30 years. This is consistent with an important role of Rossby waves.

If we now examine the temperature anomaly in R1 on either side of the jump, for the forcing periods of 8 years and 60 years, at mid latitudes (30^oN) and just below the thermocline (800 metres depth), a westward propagating signal is visible (Figure 4-13). For 8 years, we see that there is some propagation of a signal from east to west but that it does not cross the whole basin. Furthermore, the temperature trend is not uniform zonally. We have instances of warming in the east while the west is cooling and vice versa. For 60 years, the picture is quite different. The warming and cooling trends are uniform across the whole basin, i.e. when the east is warming the west is warming too. Furthermore, the amplitude of the warming is almost an order of magnitude greater than for the forcing period of 8 years.

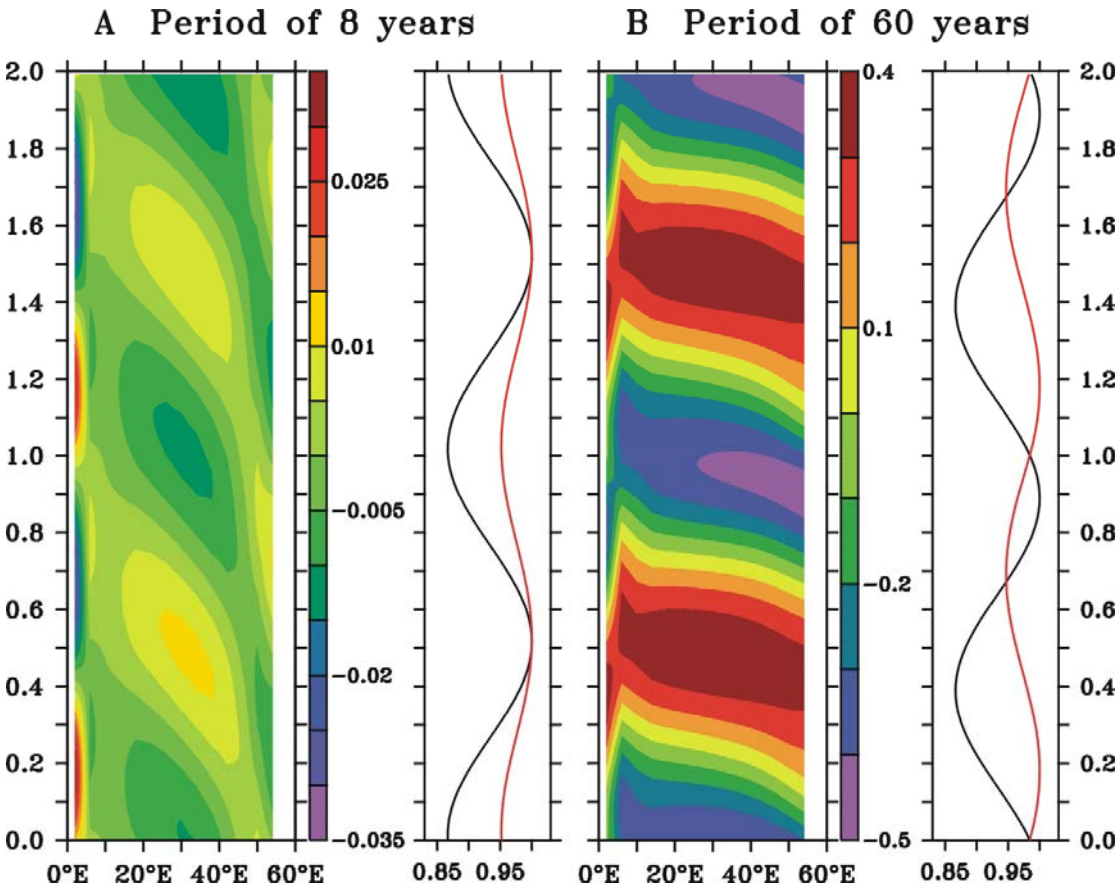

Figure 4-13: Hovmoeller plots of the temperature anomaly at 800 metres depth at 30°N ,the normalised average surface temperature (red line) and the normalised restoring temperature (black line) for forcings periods of 8 years (panel A) and 60 years (panel B). The colour contours are in degrees Celsius and the Y-axis shows 2 normalised periods.

The slope of the isotherms for the period of 60 years indicates that the anomaly crosses the whole basin in about 5 years. The shorter period of the jump in response amplitude in R1, as compared to W1, is therefore set by the basin width. Doubling the basin width doubles the period at which the maximum increase in the amplitude occurs. The analysis of figure 4-13 suggests that the westward propagation of the temperature anomaly results from the activity of a Rossby wave. Indeed, for the 8-year forcing period, the anomaly takes roughly 3.9 years to cross the basin from east to west while for the 60 years forcing period, it crosses the basin in roughly 4.2 years.

A very simple two layer model of the ocean basin with a thermocline at 800 metres and an average temperature of 14°C above the thermocline and of 4°C below the thermocline yields a gravity wave speed of 3.4 m/s, implying a mid-latitude (30°N) wave speed of long Rossby waves of 0.043m/s. Such a wave

takes 4.2 years to cross a 60^o wide basin. This means that for an anomaly to cross the basin in an uninterrupted fashion, the warming or cooling period must be greater than 4.2 years. This corresponds to a forcing period of 8.4 years.

The velocities have been calculated here for Rossby waves at 30^o North. As discussed by Cessi and Louazel (2001), it is the slowest Rossby waves that determine the basin adjustment time. We can therefore theorise that the northernmost Rossby waves are those that determine the adjustment time. However, in the high northern latitude, the signal generated by those waves is hard to pick out as it is the location of other processes such as convection.

For, the 8 years forcing period, the cooling and warming of the anomaly (Figure 4-13A) are exactly in phase with the behaviour of the surface temperature. In other words, we have an anomaly travelling across the basin and it is warmed and cooled by the forcing. The amplitude of the anomaly is very weak, about a 50th of what it is for the 60 years period (an amplitude 0.03^{o}C of versus an amplitude of 0.9^{o}C). For forcing periods above 15 years, the rossby wave signal swamps the direct effect of the surface forcing and therefore we do not see any evidence of the direct effect of the surface cooling and warming (figure13B). So in effect, we have an anomaly, which is built up by the activity of Rossby waves. If the forcing is fast, the anomaly has a very weak amplitude and is still sensitive to what happens at the surface. If the forcing is slow, the anomaly's amplitude is much greater and the surface forcing has no direct visible effect on it. Furthermore as the overturning is that much more stronger, the surface temperature does not follow so closely the forcing as we have stronger advective processes taking place.

The mechanism generating those Rossby waves is similar to that described by Cessi and Louazel (2001) and Johnson and Marshall (2002) in that we observe the propagation of boundary trapped waves along the western boundary which, when they reach the southern most boundary, travel eastward along it and then north along the eastern boundary. The northward propagation along the eastern boundary of these waves, created by the arrival of the equatorial boundary trapped waves as well as the oscillations in the surface forcing, generate the long Rossby waves, which propagate westward.

The boundary trapped waves propagating along the western boundary are readily visible in our model. They take roughly 3 years to travel from 60^{o}N to the equator (not shown). This is about ten times slower than the expected propagation time of Kelvin wave in a model with a 4^{o} resolution (Hsieh et al, 1983). Similar slow propagating waves were also reported by Marotzke & Klinger (2000). These have all the features of Kelvin waves but propagate much slower.

These Kelvin-like waves can also be followed along the equator for the short period forcing. Their crossing time is of the order of a year and the eastward propagation is clearly visible. For the longer periods (i.e., 60 years), their signature is swamped by that of the long Rossby waves and as a result, only a westward propagating signal is visible. Because they are closer to the equator, these Rossby waves should travel faster than those further north. Indeed, when we compare their speed with that of the waves in figure4-12B, the former cross the basin in about 3.4 years while the latter take roughly 3.9 years to cross it.

This analysis suggests that the basin possesses a characteristic time scale, which is determined by the speed of the slowest Rossby wave. If the period of the forcing is greater than twice that time scale, the Rossby waves build up a temperature anomaly, which crosses the basin. This anomaly increase the amplitude of the east-west pressure gradient, which in turn leads to an increase in the amplitude of the overturning. The greater the forcing period, the more efficient this adjustment becomes. As a result, the amplitude of the anomaly increases as the rossby waves have more time to build up the positive and negative anomalies. This process is one of the ways through which the basin adjusts to the changes in the forcing. In our experiments however, as the forcing period exceeds 1000 years, the adjustment to the forcing through the effects of diffusion swamps the effect of the adjustment to the forcing through the effect of rossby waves (figure 4-7).

If the period of the forcing is less than twice the characteristic time scale, the east-west pressure gradient is unaffected, as the wave signal is severely damped by the effect of the changing surface forcing. In this instance, as the anomaly does not reach the western side of the basin, or rather reaches it but in an

extremely damped form, there is no increase in the amplitude of the overturning. Furthermore, because this anomaly travels slower than the change in the surface forcing, if it is created during the warming phase, it will reach the western side of the basin during the cooling phase and will thus interact destructively with the cooling that is now taking place. For long enough forcing periods, the Rossby wave signal interferes constructively with the signal migrating southward along the western boundary, and much larger amplitudes are reached. All this suggests that baroclinic wave propagation plays an important role in the adjustment of the ocean basin to external oscillations, in contrast to the conclusion of Eden and Greatbatch (2003).

It must be noted that our model has a very coarse resolution and uses an Arakawa B grid. Furthermore, the time stepping is asynchronous. As a result, the wave processes, although present, are not well resolved. As suggested by Döscher et al. (1994), this means that the model might be overestimating the response time of the ocean to changes in the surface forcing. The implications for our study are that the jump (e.g. the sudden increase in the amplitude of the overturning oscillations) might be occurring for a greater forcing period than in a fine resolution model and that, due to the absence of very fast waves, the amplitude of the oscillations of the overturning for very small forcing periods (0.5, 1 & 2 years) might be underestimated.

There is the possibility that the internal variability of the model could affect the response to periodic forcing, particularly as it is usually of the same order as the timescale set by the basin width (Colin de Verdiere and Huck, 1999). Indeed, the internal variability, visible during run F1 with constant fluxes, has a period of 22.7 years (not shown). Although this is higher than the period for which the jump is observed, it is sufficiently close to the timescale set by the adjustment of the basin to the activity of Rossby waves to possibly contaminate the signal. However, the response in the amplitude of the maximum overturning shows no particular sensitivity to the internal oscillation time scale, even when a forcing period of exactly 22.7 years is used. This is probably because the restoring is sufficiently strong to damp out completely the internal oscillations.

4.6) Boundary current velocities:

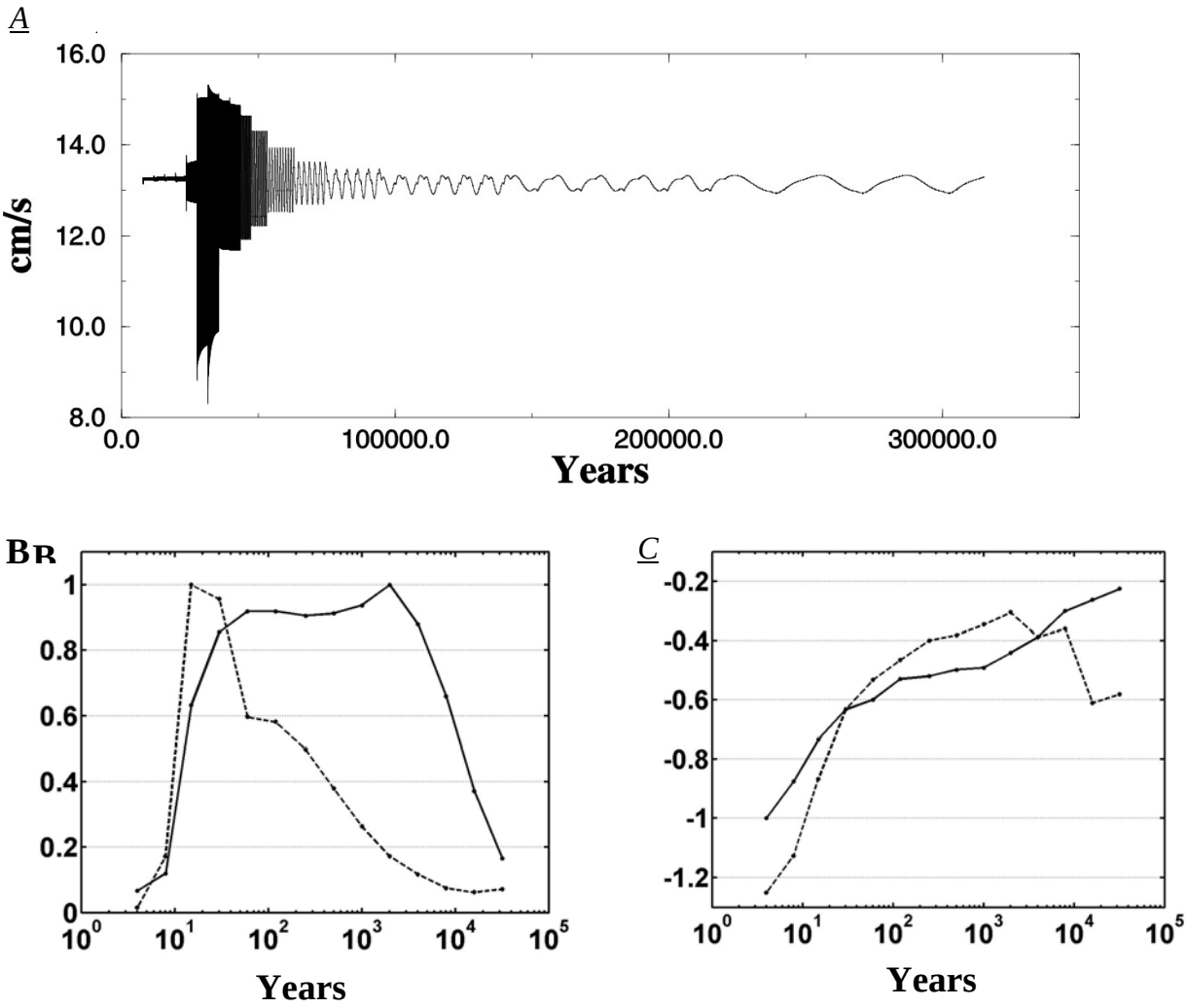

figure 4-14 :Panel A: maximum V velocity against time for Experiment R1: The vertical diffusion is of 10^{-4} m^2/s. The model is run for 17 forcing periods and for each until cyclo- equilibrium has been achieved.

Panel B: Normalised amplitude of the maximum overturning (solid line) and maximum V velocity (dashed line) in Experiment R1 against the forcing period.

Panel C: Phase shift in fraction of a period between the forcing and the maximum overturning (solid line) and maximum V velocity (dashed line) in Experiment R1 against the forcing period.

Figure 4-14A shows the evolution of the maximum meridional velocity, V, against time during Experiment R1. As for the overturning, V exhibits a resonance- like structure as well as the jump in amplitude. The curves, however,

clearly show that the response of V is far more non-linear than that of the overturning. This is particularly clear for the long periods, 4000 years and above. As illustrated in Figure 14B, the maximum amplitude occurs for a period smaller than for the maximum overturning, i.e., 30 years against 2000 years for the maximum overturning. This is surprising and suggests that the maximum overturning behaves differently to the western boundary current where the maximum value for V is found.

Furthermore, as is indicated in Figure 4-14C, the phase shift between the maximum overturning and the maximum V varies with the forcing period. In other words, within an oscillation, both quantities reach a maximum at a different time in the forcing cycle. This means that in an oscillatory system, care is needed when one wants to infer the strength of the MOC and the northward heat transport from velocity measurements in the WBC, as has been done in some palaeo studies (Lynch-Stieglitz et al., 1999) .

Figures 4-14B and 4-14C clearly illustrate the complexity of the system which cannot really be compared to a forced oscillator. Indeed, neither the velocity nor the overturning reaches a maximum amplitude when their respective phase shift with the forcing is of ¼ of a period ($\pi/2$).

4.7) Conclusions:

Even a very simple model ocean basin forced with highly idealised variable buoyancy forcing responds in a very complex way. It exhibits a very strong response in the meridional overturning stream function with large oscillations even for forcing periods of the order of Milankovitch cycles.

The amplitude of the oscillations presents a resonance-like behaviour, which stems from the existence of two adjustment time scales, one in the decadal band, and the other in the millennial band. The former is unaffected by changes in the vertical diffusivity or the introduction of simple topography or idealised wind

forcing and is set by the propagation speed of Rossby waves across the basin. Consequently, it depends on the basin width. The latter is controlled by the vertical temperature diffusion: the greater the diffusion, the smaller the period of the resonance. The basin adjusts to changes in the forcing through those two processes.

The relationship between western boundary meridional velocities and the meridional overturning is complex. This suggests that there is no simple inference of overturning and heat transport from local inferred palaeo-velocities.

Chapter 6: Conclusions

6.1) Summary:

The aim of this study was to investigate the response of the oceanic circulation to simple buoyancy forcing. In the first part of the study, a set of experiments with a steady restoring field was examined. In the second part, an oscillating restoring field with a range of periods was used and the response in a single then a double hemisphere examined as well as its sensitivity to diffusion, topography, wind and basin width.

In the first part, 4 sets of experiments were conducted with steady restoring forcing. 14 temperature gradients were investigated, with either a fixed equator temperature or a fixed northern most temperature with two models, the MOMA model (Webb, 1996) and the MIT model (Marshall et al, 1997). In effect, this study re-examined the scaling law between the North-South temperature gradient and the meridional overturning stream function. The results show that both models behave in a similar fashion. If the northernmost temperature is fixed, as the temperature gradient decreases, the overturning weakens. If the equator temperature is fixed, reducing the temperature gradient leads to a small increase in the overturning then to a decrease. The analysis shows that although the equator to pole density gradient is important, the spatial distribution of the convection rather than its actual intensity is crucial in determining the strength of the overturning cell.

In the second part, the restoring field is made to oscillate sinusoidally on a range of time scales from the sub-annual to the orbital, in all 17 different forcing period. The response of the overturning shows substantial oscillations and a very complex behaviour with, among other things, a maximum amplitude in the overturning for a specific forcing period and a sudden increase in amplitude

between forcing periods of 8 and 15 years. Examination of the bottom temperature signal underlines the complexity of the system. The analysis of the results shows that the resonance like period is principally determined by the choice of vertical diffusion and that the jump in amplitude is caused by the cumulative constructive interference of a temperature anomaly carried by Rossby waves and the surface forcing. Several interesting features were found such as the phase lag relation between the forcing and the response and the varying phase shift between the overturning and the maximum meridional velocity. Although the coarse resolution and the asynchronous time stepping used in the model are thought to have an influence on the wave related phenomena, the diffusion related results are considered fairly robust and suggest a previously unsuspected impact of relatively low amplitude oscillations on the oceanic circulation. They also show that millennial to orbital time scales cannot be ignored even when looking at the short time behaviour of the circulation.

The next part of the study involves switching to a double hemisphere basin. Two types of forcing are investigated, one where the forcings in both hemispheres are in phase and one where they are out of phase by half a period. Various oscillating temperature gradients are examined but in all cases, the densest waters are always produced in the northern hemisphere. The response of the oceanic circulation shows a similar resonance-like behaviour to that of the single hemisphere situation, with the same features and sensitivity to the diffusion. For the 0 lag forcing, the expected dominance of the northern hemisphere overturning cell is present; its strength and behaviour was similar to that of the single hemisphere circulation. However, major differences arose for long periods in the experiments with a lag of half a period in the forcing between the two hemispheres. The existence of two sources of deep water leads to a substantial increase in the amount of maximum stratification during a forcing cycle and as a result to a weaker minimum overturning. As a result, the amplitude of the oscillations in the maximum overturning stream function is much greater in both hemispheres at longer periods, in agreement with the behaviour suggested by the asymptotic runs. Although the experimental set-up is highly idealised, these results have some palaeo implications as they offer a explanation for the half precesionnal oscillations observed in the temperature proxy records as the

experiments with the pi lag forcing show a similar behaviour in the deep temperatures in both hemisphere for forcing periods above the millennial mark.

6.2) Analysis

6.2.1) Non linear response and convection:

Taken as a whole, this study underlines the complexity of the ocean system. A simple sinusoidal buoyancy forcing leads to very complex behaviour. The analysis of the bottom temperature signal in the variable forcing set-up emphasises this and underlines the non-linearity of the ocean system. What is more this non-linearity is itself a function of the period of forcing, suggesting that various processes have different characteristic time scales and thus the circulation as a whole respond differently depending on which of these processes dominate. In chapter 4, we identified two of the dominant processes, diffusion and the Rossby wave propagation. In all likelihood there are many other minor ones which all leave a characteristic signature on the deep ocean temperatures, the region of the ocean which is the most isolated from the direct effect of the forcing.

The issue of the phase lag between the forcing and the response is another element of interest. As we have seen in chapter 4, even the surface waters temperature signal substantially lags that of the forcing and that lag changes with the forcing period. Obviously, for very long forcing periods (8000 years and above), the lag is almost zero but for short forcing periods (125 years and below) the behaviour is far from straight forward as the surface waters are affected by other processes than the atmospheric forcing. These include advection as well as Rossby and Kelvin waves' activity.

Chapter 3 underlines the complexity of the convection process, particularly in terms of its location. The major upshot of this complexity is that the oceanic circulation does not appear to follow the theoretical scaling law, in other words $\Psi \sim \Delta T^{1/3} \kappa^{2/3}$ does not hold even in an OGCM with such a simplified set-up, with no topography, no winds and a purely thermal buoyancy forcing. To a certain

extent, this is not surprising in view of how intricate the system is and the number of processes affecting the circulation.

6.2.2) Diffusion:

The model's representation of the diffusive processes is very coarse. This could be a major limitation since most of the resonance behaviour stems from the existence of a delay in transmitting the thermal signal captured by the surface ocean to the deep ocean.

However, it is unlikely that a better representation of the diffusive processes would dramatically change the behaviour. Certainly, the exact period for which the resonance occurs would change but the processes highlighted in chapter 4 would still hold. If anything, the mid-depth diffusion values (10^{-4} m^2/s) used in this study are too high. Observations suggest that 10^{-5} m^2/s is closer to the actual value in the ocean. Using such a value would make it even more difficult for the ocean to transmit the surface thermal signal to great depth and thus exacerbate the surface to bottom temperature difference. This would lead to greater amplitudes in the oscillations and increase the impact of a minor temperature oscillation on the meridional overturning circulation. If anything, it would strengthen the importance of those results.

The issue of the diffusion value in the surface ocean is another matter. It is particularly important as it determines how much of the forcing signal is captured. As is clear from these results, although the restoring time scale is 40 days, it is the diffusion which really controls how much of the forcing signal will be captured by the surface waters. Although 10^{-4} m^2/s is higher than what is measured in the ocean, the models does not represent in any fashion the effect of capillary and gravity waves nor the effect of tides in shallow seas, all of which contribute to increasing the surface waters ability to capture and atmospheric thermal signal It is thought by some (Large et al, 1994) that the canonical value used in the surface ocean, 10^{-5} m^2/s is far too small as it does not take into account the existence of coherent structures such as Langmuir cell which might increase the surface ocean ability to capture a thermal oscillation. Furthermore, the temperature variation of 4^oC at 60^oN is quite small compared to either the

seasonal cycle or palaeo oscillations over the last 1 Ma (Ruddiman et al, 1986). Hence it could be argued that 10^{-4} m^2/s allows for an acceptable proportion of the atmospheric signal to be captured by the surface ocean in view of other parameters choices.

Lastly, it is known that the rough topography at depth enhances mixing through the breaking of internal waves. It is likely that 10^{-4} m^2/s is too small to adequately parameterise these processes. However, these processes occurs principally at great depth and the determining factor in creating a resonance like behaviour is how the temperature signal is transmitted from the surface ocean to the deep ocean, and not how the signal is diffused once it has reached depth of 3000 meters and below.

6.2.3) Resolution:

All of this study was conducted in models with a very coarse horizontal resolution. This was necessary due to the times scales that were being examined in chapter 4 and 5. As we have seen, most of the resonance behaviour found in those two chapters is due to processes that occur in the vertical, namely the decoupling of the surface and the deep ocean. In that aspect, the resolution can be deemed satisfactory.

However, the results from chapter 3 show that the horizontal distribution of the convective processes is crucial to explaining the unexpected behaviour of the models, where an increase in the equator to pole density difference leads to a decrease in the strength of the overturning. Would such behaviour still be present at higher resolution? Is there a resolution threshold beyond which this behaviour is no longer present? These questions would certainly benefit from further studies and would allow a greater understanding of some of the fundamental processes of ocean models.

6.2.4) Antarctic Circumpolar Current:

Chapter 5 has shown that having a secondary source of deep water in the subordinate hemisphere can profoundly alter the behaviour of the circulation during a forcing cycle. An unanswered question from this study is what impact

an ACC would have on this behaviour? The ACC would modify the water properties in the high southern latitude and would impede Rossby and Kelvin wave propagation; it is not clear what impact this would have on the secondary deep water production. The principal southern hemisphere overturning cell might as a result be weakened and with less deep water being produced, the temperature of the deep ocean would not be as low thereby weakening the maximum stratification that occurs during a forcing cycle. This could well mean that the amplitude of the oscillations would decrease. Conversely, the appearance of a narrow but dynamic secondary overturning cell in the high southern latitude might lead to the production of colder deep waters and thus the maximum stratification during a forcing cycle would increase. However, in view of the complexity of the system, it is difficult to predict the precise impact of the addition of an ACC. This suggests a need to conduct further numerical experiments with an ACC included.

6.3) Concluding remarks:

By its very nature, this process study is very idealised. Such idealisation allows the isolation and understanding of some of the fundamental mechanism of the oceanic circulation. To a certain extent, this is bucking the trend. Nowadays, the inclination is towards the use of ever more complex coupled ocean atmosphere models, with the ultimate aim of creating earth system models which will incorporate all the known elements of the climate system. The increase in computer power and the development of alternative computer processing methods makes this a realistic ambition. However, if the basic mechanisms that govern each element of these climatic models are not known or understood, then it will become ever more difficult to critically appraise the outputs of those models, thereby severely restricting their usefulness to the scientific community and society as a whole.

Chapter 5: Response to variable buoyancy forcing in a double hemisphere basin

Summary:

Many studies have underlined the importance of the various parts of World Ocean such as the Indian Ocean or the South Atlantic, in the production of deep water in the North Atlantic. In this chapter, the basin domain is extended from that in Chapter 4 to a highly idealized South Atlantic. The forcing is similar but has the added complexity of either being in phase in both hemispheres (set A) or out of phase (set B). The set-up is such that the northern hemisphere always produces the densest waters. In each experiment, 17 different values of the forcing period are studied, ranging from 6 months to 32,000 years. The model's meridional overturning circulation (MOC) exhibits a very strong response on all timescales in both hemispheres, up to and including the longest forcing timescales examined for either set of experiments with the amplitude of the oscillations reaching up to 140% of the steady-state maximum MOC and exhibiting resonance-like behaviour, with a maximum at centennial to millennial forcing periods. This resonance like behaviour is identical to what has been observed in a single hemisphere and occurs for the same reasons. What is novel is that for set B, the amplitude of the response is substantially greater for large forcing periods (millennial and above), particularly in the subordinate (southern) hemisphere. This happens because for set B, the basin has in effect two sources of deep water. This leads to colder bottom waters and thus greater stratification, which in turn stabilises the water column and thus reduces the value of the minimum overturning. These results have some interesting palaeo implications and suggest an explanation for the half precessional time scale observed in the deep ocean temperature record.

5.1) Introduction:

One of the outstanding issues in physical oceanography today is how steady or not, the deep oceanic circulation is and how sensitive to known atmospheric and surface ocean variabilities it is. In today's ocean, most the deep water production occurs in the North Atlantic, which is therefore the more obvious location to investigate the impact of surface variabilities on the deep circulation.

In chapter 4, we conducted a systematic numerical study of the response of the oceanic circulation in a single hemisphere to variable surface forcing which showed that the response of the deep circulation to surface oscillations can be in some cases significant and is dependant on the period of the oscillations.

However, when studying the North Atlantic, it is also important to include the South Atlantic as many studies have underlined the importance of the southern hemisphere in terms of the stability of the THC and in the production of NADW. For instance, Rahmstorf (1996) showed that freshwater budget north of 30^{o}S is crucial to what happens in the northern hemisphere, i.e. how salty the North Atlantic will be. Furthermore, in terms of modelling, some argue that actually, the oceanic circulation in a closed single hemisphere basin is representative of the globally integrated THC (NRC, 2002). Hence to get a proper hold on the circulation in a single hemisphere basin (i.e. the North Atlantic), the other hemisphere is essential. Finally, in terms of deep water production, a double hemisphere study has the important added complexity of theoretically allowing the existence of two high latitude deep water production sites, a situation much closer to what is observed in today's ocean with deep water production in the North Atlantic and to a lesser extent in the Weddell Sea (Pickard and Emery, 1990).

This study proposes of to replicate the approach of chapter 4 but in a double hemisphere basin. The lay out of this chapter is as follows. In section 5.2, the model set-up and the experiments conducted are described. In section 5.3, the results for the asymptotic forcing are presented. Section 5.4 deals with the results

of the experiments with an oscillatory forcing and in section 5.5, some of the fundamental aspect of these results are discussed. Finally, in section 5.6, the implications of this study are discussed.

5.2) Set-up:

5.2.1) Model configuration

The experimental set-up in this study is identical to that of chapter 4 except that the ocean basin is now interhemispheric

The model used is a parallelised version of the GFDL MOM model which can distribute the various processes on an array of processors (Webb, 1996). The free surface numerics have been updated by including the free surface numerical code of OCCAM (Webb, 1995). The model also includes the eddy parameterisation scheme of Gent and McWilliams (1990) as implemented by Griffies (1998).

The domain is a 60^o wide basin with solid boundaries and 15 levels in the vertical, extending from 60^oS to 60^oN of latitude. It has no circumpolar current. The horizontal resolution is 4^ox4^o. The ocean depth is everywhere 5300 metres depth and the thickness of the depth levels varies from 30 metres at the surface to 836 metres at level 15.

In the initial conditions, the salinity is set to 35 psu throughout the model and the salinity fluxes are set to zero. The wind effect is removed by setting all the surface wind stresses to zero. The temperature fields are initialised by setting the surface temperature to 20ºC at all latitudes and longitudes and decreasing it by one degree at each level. Thus, the coldest temperature is at the bottom and is 5ºC.

The temperature is forced using a Newtonian relaxation scheme, where the restoring period is set to 40 days.

5.2.2) Experimental strategy

In the time-varying experiments, a sinusoidal restoring temperature profile is used. It varies with latitude and time according to:

$$T(\Phi,t) = (F_H + \cos(\frac{t}{P} \times 2\pi + S)) \times (\cos(\Phi \times 3) - 1) + 28 \qquad (5.1)$$

where T is the restoring temperature, Φ is latitude, t is time, P the forcing period and F_H a parameter specific to each hemisphere and which varies from experiment to experiment. S is a parameter which allows a shift in the forcing of the two hemispheres of either 0, if S equals 0 or half a period if S= Л.

By varying F_H and S, a suite of experiments is created, with the northernmost temperature oscillating between values of 0 and 4 degrees Celsius and the southernmost temperature oscillating between 0 and 4, 1 and 5, 3 and 7, and 1 and 3.

The northern hemisphere is therefore the dominant one in all our experiments, and the southern hemisphere is the subordinate one. Table 5-1 gives the list of all the experiments. The experiment nomenclature is as follows: the first number refers to the maximum temperature in the northern hemisphere, the second number to the maximum temperature in the southern hemisphere and an A is added if the forcing has a phase lag of π between the two hemispheres.

Name of experiment	F_N	Northernmost temperature range in ^oC	F_S	Southernmost temperature range in ^oC	Lag in the forcing between the two hemispheres (radians)
4-4	13	0-4	13	0-4	0
4-5	13	0-4	12.5	1-5	0
4-4A	13	0-4	13	0-4	π
4-5A	13	0-4	12.5	1-5	π
4-7A	13	0-4	11.5	3-7	π
4-3A	13	0-4	12.5	1-3	π

Table 5- 1: Summary of experiments

Figure 5-1 shows the forcing extremes for experiments 4-4, 4-5, 4-4A and 4-5A. Over one forcing period, the restoring temperature oscillates between these extreme profiles. Table5-2 lists the forcing periods used and the integration time for each of them.

In the following sections, the results relating to experiment 4-5 and 4-5A will be presented and analysed in detail. The results from the other experiments will be briefly discussed in section 5.5 by analogy.

0.5 *4,000*	**1** *4,000*	**2** *4,000*	**4** *4,000*	**8** *4,000*	**15** *4,000*
30 *4,000*	**60** *4,000*	**120** *4,000*	**250** *4,000*	**500** *6,000*	**1000** *10,000*
2000 *12,000*	**4000** *20,000*	**8000** *48,000*	**16,000** *80,000*	**32,000** *96,000*	

Table 5- 2: Forcing periods (bold) in years and integration time for each (italic) in years.

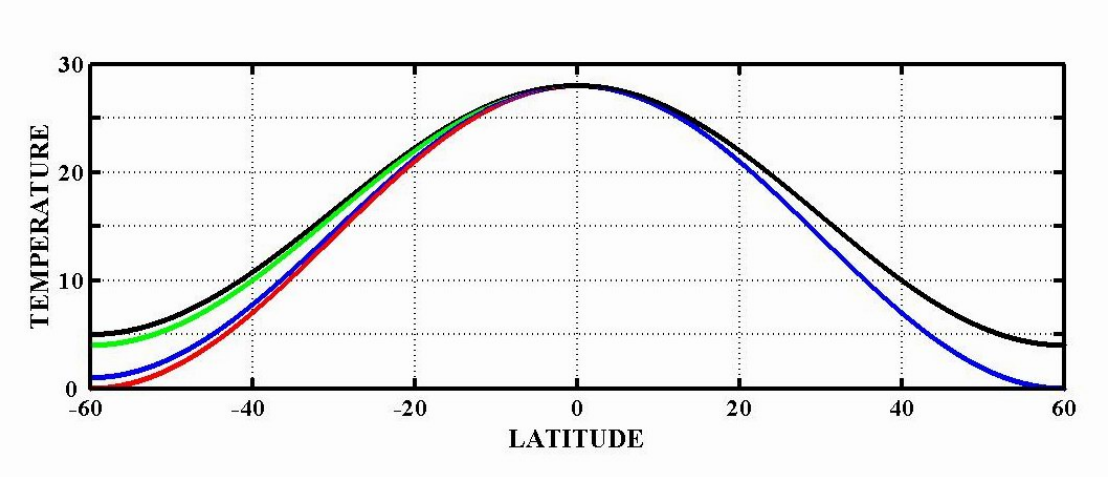

Figure5-1: Zonal extreme restoring temperature field in ^{o}C for experiments 4-4, 4-4A, (in red and green) 4-5, 4-5A (in blue and black). During a forcing period, the restoring temperature field oscillates between the curves.

5.3) Asymptotic forcing:

As in the single hemisphere case, experiments with a constant forcing field can be seen to correspond to an oscillatory forcing with an infinite period. In the double hemisphere case, the lag in the forcing between the two hemispheres must be taken into account when determining what the extreme forcing profiles are.

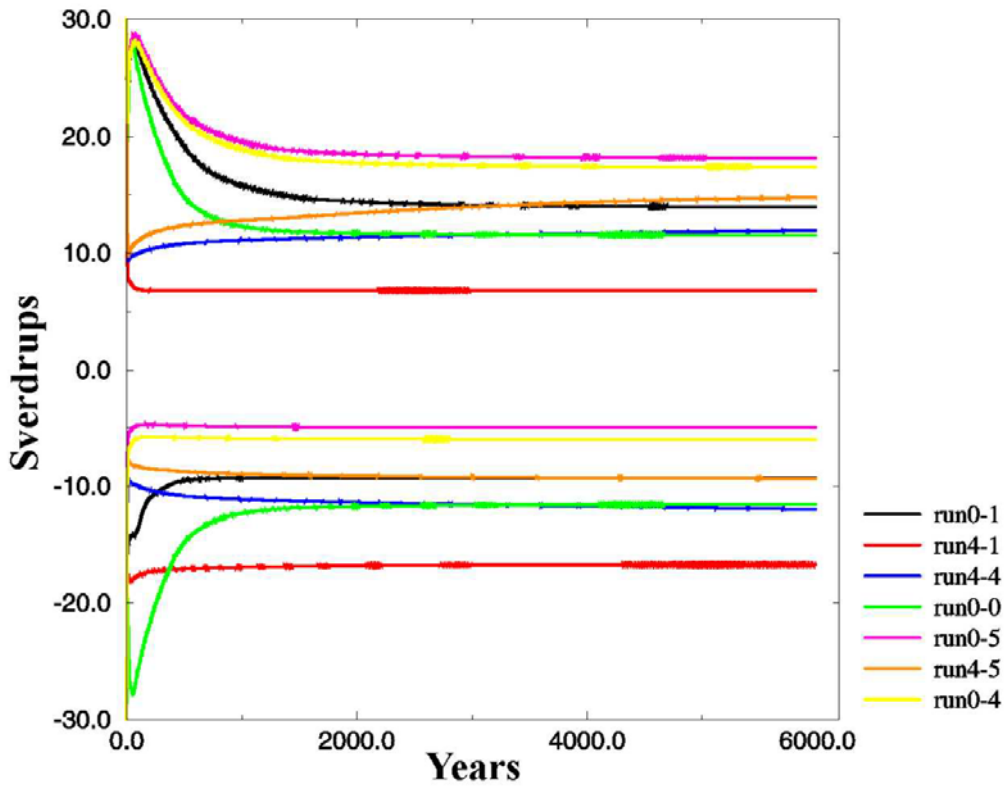

Figure5-2: Evolution of the maximum overturning stream function during the spin up of the asymptotic runs for a double hemisphere basin.

Figure 5-2 shows the maximum meridional overturning stream function during spin up for different forcing profiles. The positive curves show the behaviour of the northern hemisphere cell while the negative curves show the results for the southern hemisphere cells.

0 lag:

When there is no lag between the two hemispheres, the extreme forcing profiles are as follows for the 4-4 experiment: a temperature of 0 degrees at 60N and 0 at 60S, a temperature of 4 degrees at 60N and 4 degrees at 60S. The resulting overturning stream functions for those two profiles (run 0-0 and run 4-4) are almost equal in both hemispheres with a value of roughly 12 Sverdrups. As in the single hemisphere case, the weaker Equator to 60^{o}N temperature gradient leads to the slightly higher value for the meridional overturning stream function.

For the 4-5 experiments, the two extreme profiles are of 0 degrees at 60^{o}N and 1 degree at 60^{o}S (run 0-1) and 4 degrees at 60^{o}N and 5 at 60^{o}S (run 4-5). In the southern hemisphere, the overturning has the same value for the two profiles while in the northern hemisphere, the overturning is slightly stronger (about 0.7 Sv) for the latter profile.

These results suggest that for a very long period, in a zero lag forcing scenario, the amplitude of the oscillations in the overturning will be very small.

It is also interesting to note that, in slight contrast to what was found by Klinger and Marotzke (1999), the strength of the cell in the dominant hemisphere is set in part by the dominant hemisphere's surface forcing but also by the subordinate hemisphere surface forcing. Hence the value of the maximum overturning in the northern hemisphere is almost identical for experiments 0-4 and 0-5 (~20 Sv) but is distinctively greater than for experiment 0-1 (~15 Sv). In fact, the value of the maximum overturning for experiment 0-1 is very close to that of 4-5 which would suggest that the North-South surface density difference is in fact what controls the strength of the overturning cells in both hemispheres, dominant and subordinate. This idea is supported by the fact that the overturning cells in both hemisphere have the same strength (~12 Sv) when the forcing is symmetric about the equator, and this regardless of the lowest surface restoring temperature (exp 4-4 and 0-0).

Л lag:

In the case where there is a lag of half a period between the two hemispheres, the forcing now oscillates between the following extremes for the 4-4A experiments: a profile with a temperature of 0 degrees at 60^oN and 4 degree at 60^oS (run 0-4) and a profile of 4 degrees at 60^oN and 0 degree at 60^oS (not shown). In this case, there is a significant difference of 12 Sverdrups in the overturning in either hemisphere between the two forcing profiles.

For the 4-5A experiments, the forcing now oscillates between the following extremes: a profile with a temperature of 0 degrees at 60^oN and 5 degree at 60^oS (run 0-5) and a profile of 4 degrees at 60^oN and 1 degree at 60^oS (run 4-1). The difference in the overturning is 13 Sverdrups for the northern hemisphere and 12 Sverdrups in the southern hemisphere. These results suggest that for an experiment with a lag of half a period in the forcing between the two hemispheres at very long periods, there will be significant amplitudes in the oscillations.

5.4) Oscillatory runs:

5.4.1) Generic behaviour of the double hemisphere basin

Figure 5-3 shows the forcing for experiment 4-5 and 4-5A. The fundamental difference between the two runs is obviously in the southern hemisphere which is in phase with the northern hemisphere for experiment 4-5 but out of phase for experiment 4-5A.

For the same lag in the forcing, the main components of the circulation (overturning cells) in the double hemisphere basin respond qualitatively in a similar fashion for all forcing period. The differences in behaviour between the forcing periods are predominantly quantitative. Consequently, any forcing period will give a good indication of the generic behaviour of the basin during a forcing cycle. In this section, the evolution of response of the circulation over one

forcing period is examined. The forcing period is 2000 years (greatest amplitude in the response) and the figures show the state of the ocean every 8th of a period, hence year 0, year 250, year 500, year 750, year 1000, year 1250, year 1500 and year 1750.

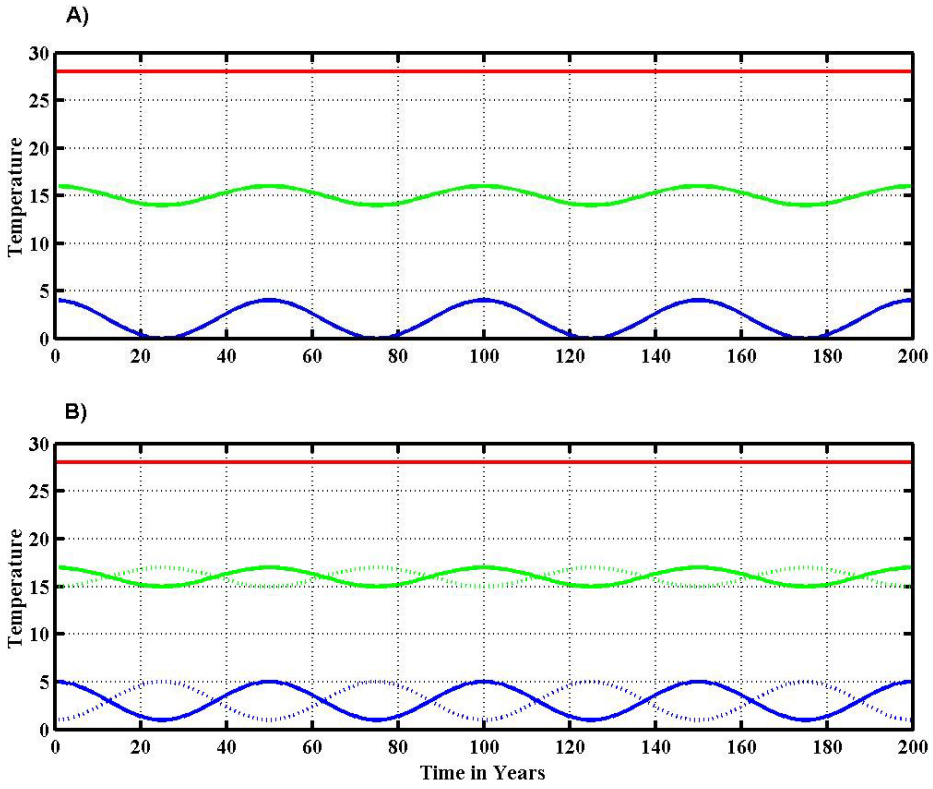

Figure5-3: Example of the restoring temperature in ^{o}C behaviour in the oscillatory runs for a forcing period of 50 years. Panel A shows the behaviour in the northern hemisphere, Panel B in the southern. The blue curves are the restoring temperature at 60^{o} of latitude, the green at 30^{o} and the red at the equator. The solid lines are for experiment 4-5 and the dashed for experiment 4-5A. Note that for that latter experiment, the dashed and solid lines are overlaid in the Northern hemisphere.

Figure 5-4 shows the evolution of the temperature and the meridional overturning stream function for a forcing period of 2000 years with no lag between the two hemisphere. The overturning stream function displays two cells in either hemisphere, which deepen between year 0 and 1000 of the forcing cycle. Furthermore, the northern cell also invades the southern hemisphere at

depth. Between the years 1000 and 1750, the cells shallow back to their original state.

0 Lag

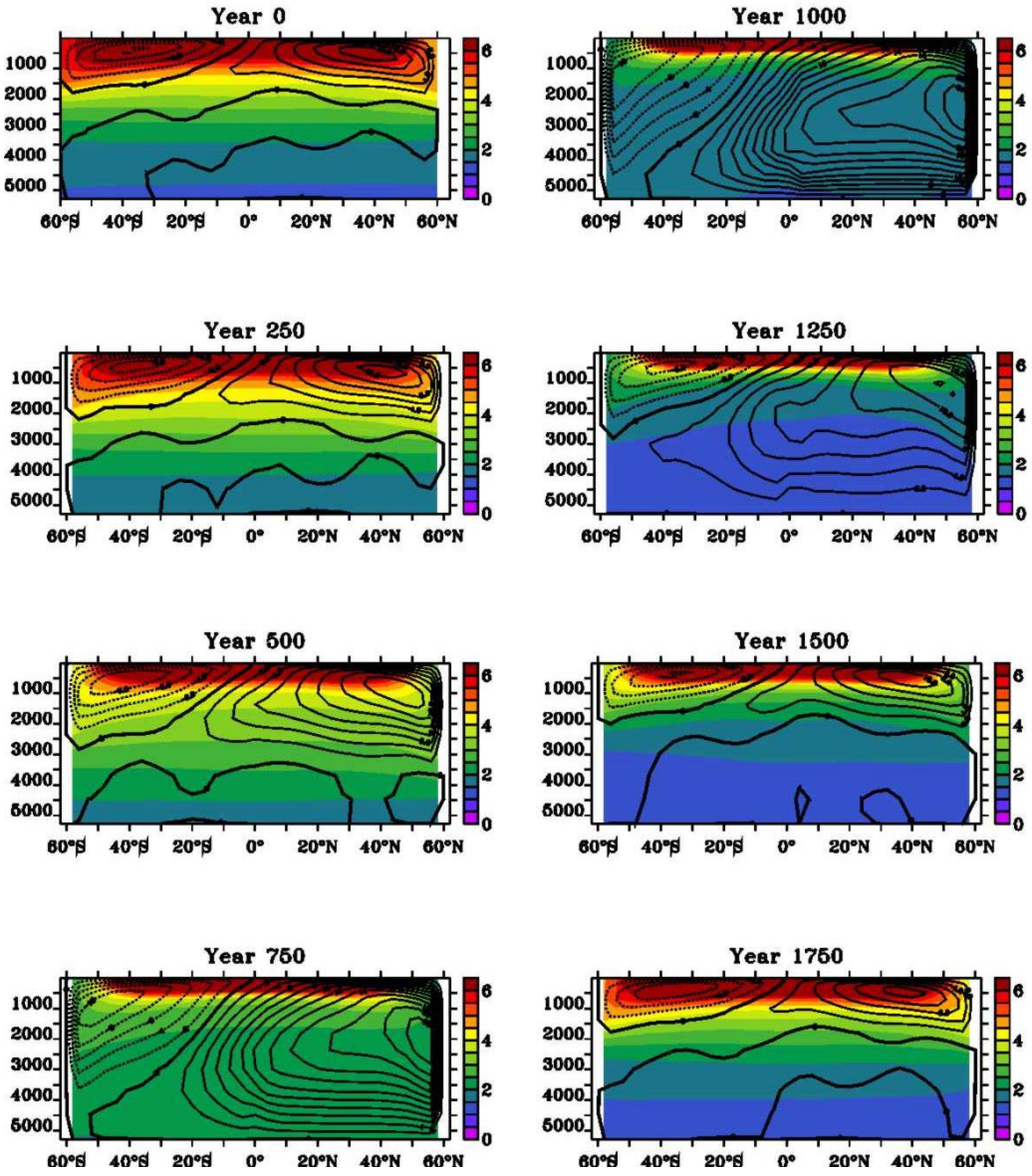

Figure5-4: Evolution of the PT in ^{o}C and the overturning stream function (Sv) through a cycle for experiment 4-5. The contour intervals are of 2 Sverdrups.

Л lag

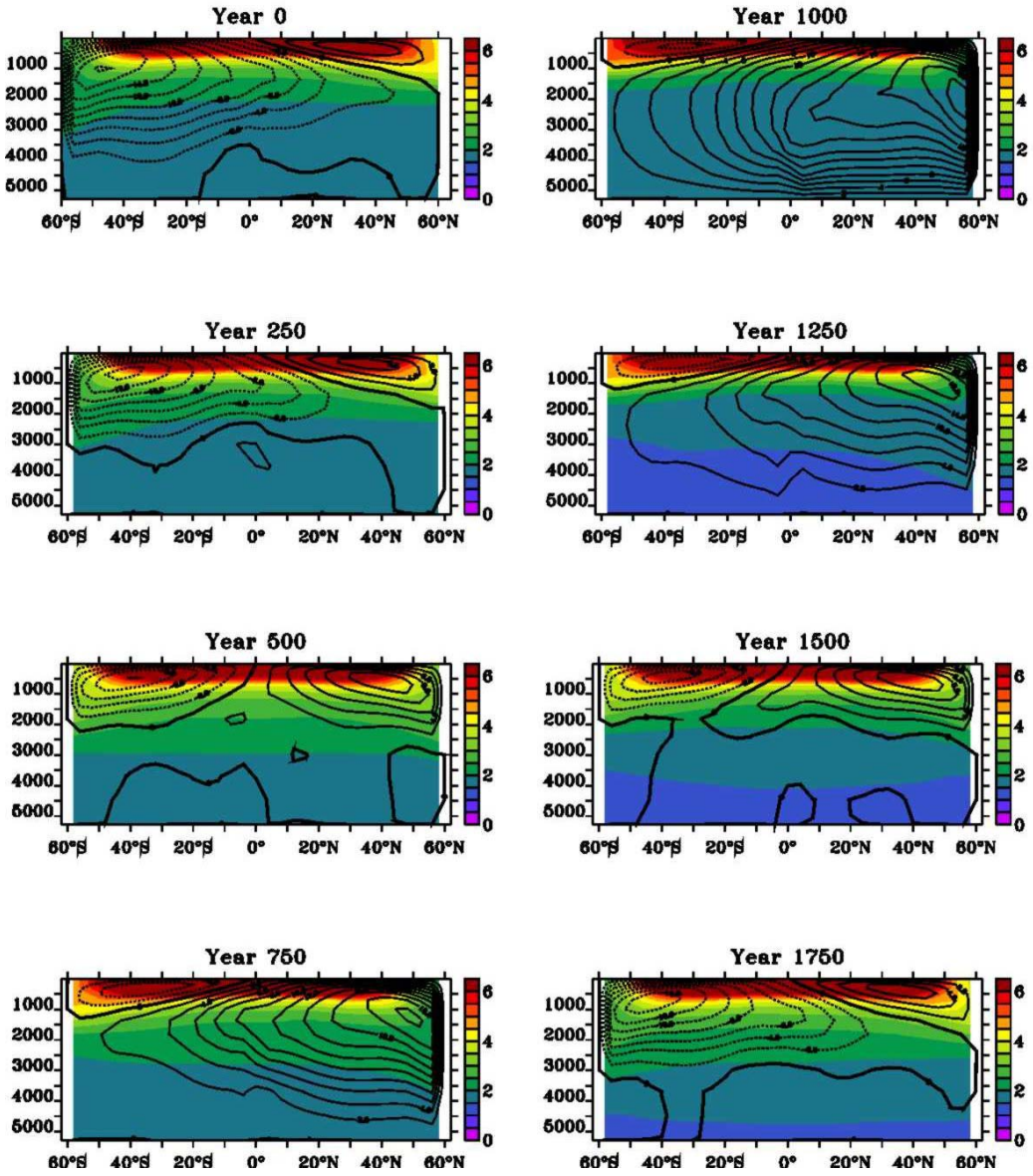

Figure5-5: Evolution of PT in ^{o}C and overturning stream function during a cycle in experiment 4-5A. The contour intervals are of 2 Sverdrups.

The zonally averaged temperature field shows the expected warming and cooling as the restoring temperature oscillates. It also shows that the only source of deep water is the northern hemisphere and that deep-water formation occurs between year 1000 and 1250. This deep water then remains almost throughout the cycle, gradually warming as the effect of the surface warming is transmitted to the deep ocean.

Figure5-5 shows the evolution of the temperature and the meridional overturning stream function for a forcing period of 2000 years with Л lag (half a period) between the two hemispheres. Again the cells in both hemispheres fluctuate in but this time, when the northern one is weak, the southern one is strong and vice versa. The slight dominance of the forcing in the northern hemisphere is reproduced in the maxima values of the two cells are as the northern cell at its maximum (year 1000) is far stronger than the southern cell when it reaches its maximum (year 0). Unlike the zero lag case, the southern cell never reaches the bottom. Below the depth to which the weaker cell penetrates, the basin behaves almost like a single hemisphere ocean with single source of deep cold water as only waters formed in the northern hemisphere fill the deep ocean.

The potential temperature shows similar fluctuations to that of the 0 lag case although the deep temperature is on average colder throughout the forcing cycle (2.4^{o}C for the Л lag case against 2.8^{o}C for a the 0 lag case). Furthermore, the deep water formed in the southern hemisphere penetrates to 3500 metres, much deeper than that produced in the southern hemisphere in the 0 lag case (2000 metres).

Trans-equatorial transport:

Of particular interest in these experiments is the cross equatorial transports as the Atlantic Ocean is unique in that, in its present state, there is a northward cross equatorial transport of heat by the MOC. As is clearly illustrated by figure 5-6, experiment 4-5 and 4-5A have a very different behaviour. In experiment 4-5, the transport is always northward and reaches a maximum at about 4000 metres depth. The transport near the surface is quite weak, reaching a maximum of about 5sv or so. Furthermore, there are substantial oscillations in the temperature field above 1500 metres.

For experiment 4-5A, the picture is quite different. The direction of the transport changes and the centres of the cores are shallower. In fact the southward core is substantially shallower than the northward one although it never is as strong. The

near surface temperature field shows less variability than in the 4-5 case but is on average cooler.

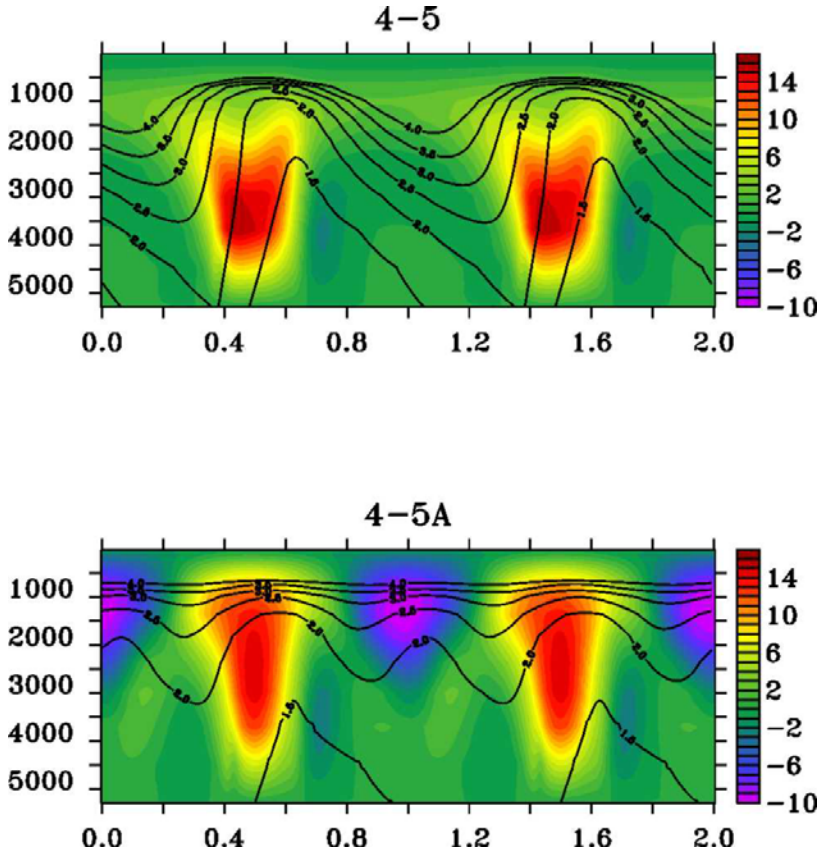

Figure5-6: Overturning in sv (colour shading) and zonally average Temperature in ^{o}C (black contour) at the equator over two periods, for experiment 4-5 and 4-5A for a forcing period of 2000 years. The y axis is depth in metres and the x-axis is time in fractions of a period.

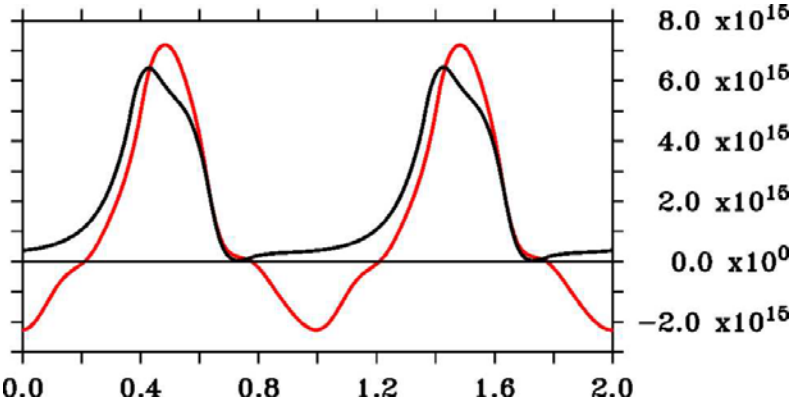

Figure5-7: Equatorial heat transport for 4-5A(red) and 4-5 (black) for a forcing period of 2000 years, over two periods. The y axis is in watts and the x-axis is time in fraction of a period.

The result is that the heat transport for 4-5A shows much greater variability than the heat transport for 4-5. This is clearly illustrated in figure 5-7. It is interesting to note that the heat transport at the equator is always northward for experiment 4-5 whereas for experiment 4-5A, it changes direction when the southern cell dominates

5.4.2) Results for all forcing periods:

Figure 5-8 is a plot of the maximum overturning against time for experiment 4-5. The time series of maximum overturning in both hemispheres show a behaviour similar to that of the single hemisphere experiment, with a jump in amplitude between the forcing period of 8 years and that of 15 years. Both hemispheres have a period for which the amplitude of the oscillations is at a maximum.

The main difference between the two hemispheres lies in the strength and amplitude of the overturning. The northern hemisphere is far stronger than the southern hemisphere with a maximum amplitude 17 Sverdrups while the southern hemisphere maximum amplitude is of 7 Sverdrups. The consequence is that the southern hemisphere seems almost to have reached its asymptotic behaviour for a forcing period of 32,000 years as the amplitude of the oscillations is less than a Sverdrups.

Figure 5-9 is a plot of the maximum overturning against time for experiment 4-5A. Again, both hemisphere seem to follow the generic behaviour of a single hemisphere basin in that the jump between forcing periods of 8 years and 15 years is present and that there is a period for which the overturning has a maximum amplitude.

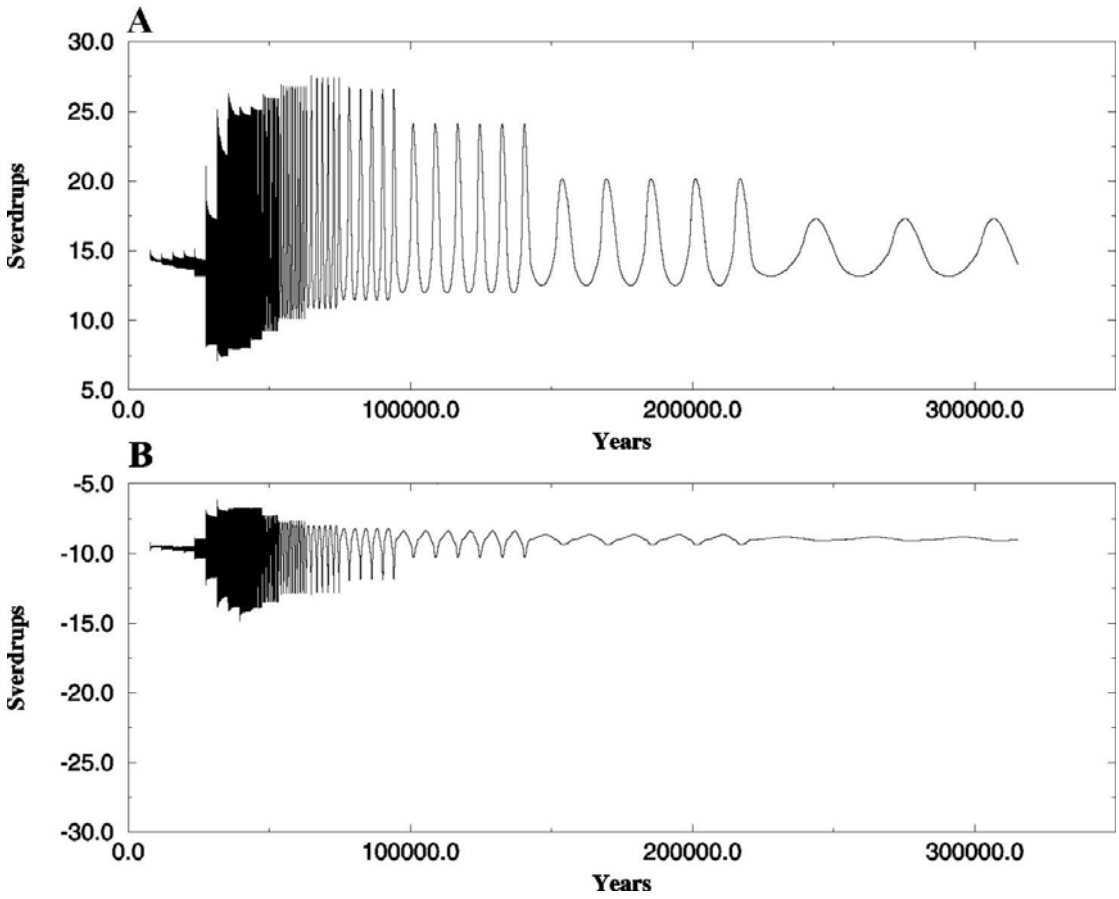

Figure5-8: maximum overturning stream function (Sv) for experiment 4-5, in the northern hemisphere (panel A) and the southern hemisphere (panel B).

There are however some striking differences. In the northern hemisphere, the amplitude is generally larger than for the 4-5 experiment and the system reaches a absolute minimum in the overturning which is constant for all periods above 250 years. In the southern hemisphere, the amplitude is far larger than in the 4-5 experiment (14 Sverdrups against a maximum of 7 Sverdrups) and again, the absolute minimum is constant for periods above 60 years. The amplitude is also fairly constant, suggesting that the system is near equilibrium for the southern hemisphere. Table 5-3 summarises the main features for all the runs conducted in this chapter

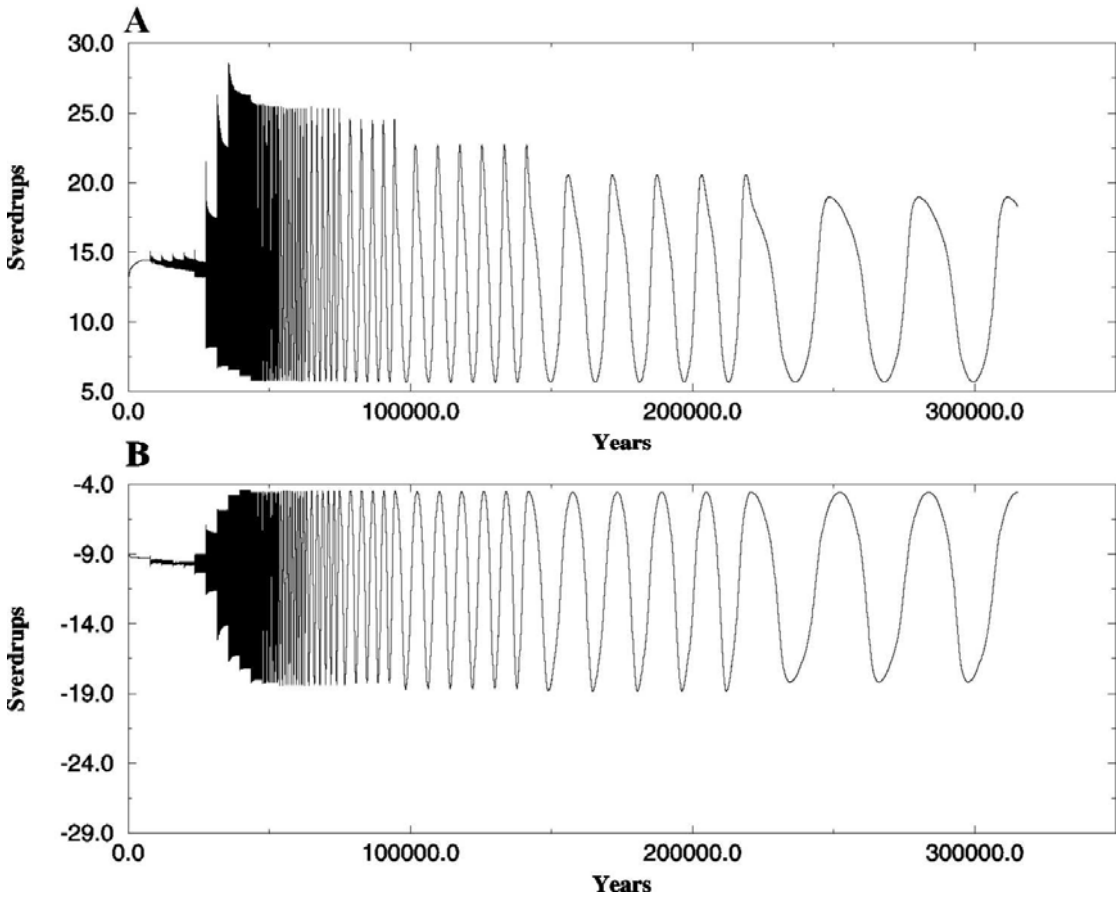

Figure5-9: maximum overturning stream function (Sv) for experiment 4-5A, in the northern hemisphere (panel A) and the southern hemisphere (panel B).

0 and Л lag forcing:

The results show that the greater the maximum temperature in the subordinate hemisphere, the greater the absolute maximum value of the overturning is in the dominant hemisphere. Furthermore, the smaller the minimum temperature in the subordinate hemisphere, the weaker the minimum overturning is in the dominant hemisphere

0 lag forcing:

In all the experiments conducted here (exp 4-4 and 4-5), it is evident that the amplitude of the response of the overturning in both hemisphere increases then decreases as the experiment progresses through the various forcing periods.

Towards the very long forcing period, as expected from the asymptotic behaviour described earlier, the amplitude in the overturning decreases.

Experiment	Northern Hemisphere					Southern Hemisphere				
	restoring	Φ_{min} (Sv)	Φ_{max} (Sv)	A_{max} (Sv)	P_{Amax} (years)	restoring	Φ_{min} (Sv)	Φ_{max} (Sv)	A_{ma} (Sv)	P_{Amax} (years)
0 lag (S=0)										
4-4	0-4	6	22	13	2000	0-4	-6	-22	13	2000
4-5	0-4	7.5	27	17	125	1-5	-7	-14	7	125
Л lag (S= Л)										
4-4A	0-4	4.8	22.5	17.3	250	0-4	-4.8	-22.5	17.3	250
4-5A	0-4	6	27	20	125	1-5	-4.8	-18.5	14	16000
4-7A	0-4	8	31.7	23.2	60	3-7	-3.6	-15.5	11.9	32000
4-3A	0-4	6	25.8	19	125	1-3	-7.5	-16	8.5	32000

Table 5-3: Summary of the main features for each of the oscillating experiments. Φ_{min} is the absolute minimum value that the overturning reaches, Φ_{max} is the absolute maximum value that the overturning reaches, A_{max} is the maximum amplitude that the overturning reaches and P_{Amax} is the period at which the maximum amplitude in the overturning occurs.

Л lag forcing:

In these experiment, generally, the dominant hemisphere overturning amplitude increases then decreases towards an amplitude equal to that suggested by the asymptotic values (exp 4-4A, 4-5A, 4-7A, 4-3A). The behaviour of the amplitude in the subordinate hemisphere is clearly dependent on its degree of subordination: the greater that is, the less likely it is to have reached a resonance like behaviour for the forcing periods examined. Indeed, in the last 2 experiments of the table (4-7A and 4-3A), it is unclear whether or not the

overturning has reached a resonance as its amplitude is still increasing towards that suggested by the asymptotic runs.

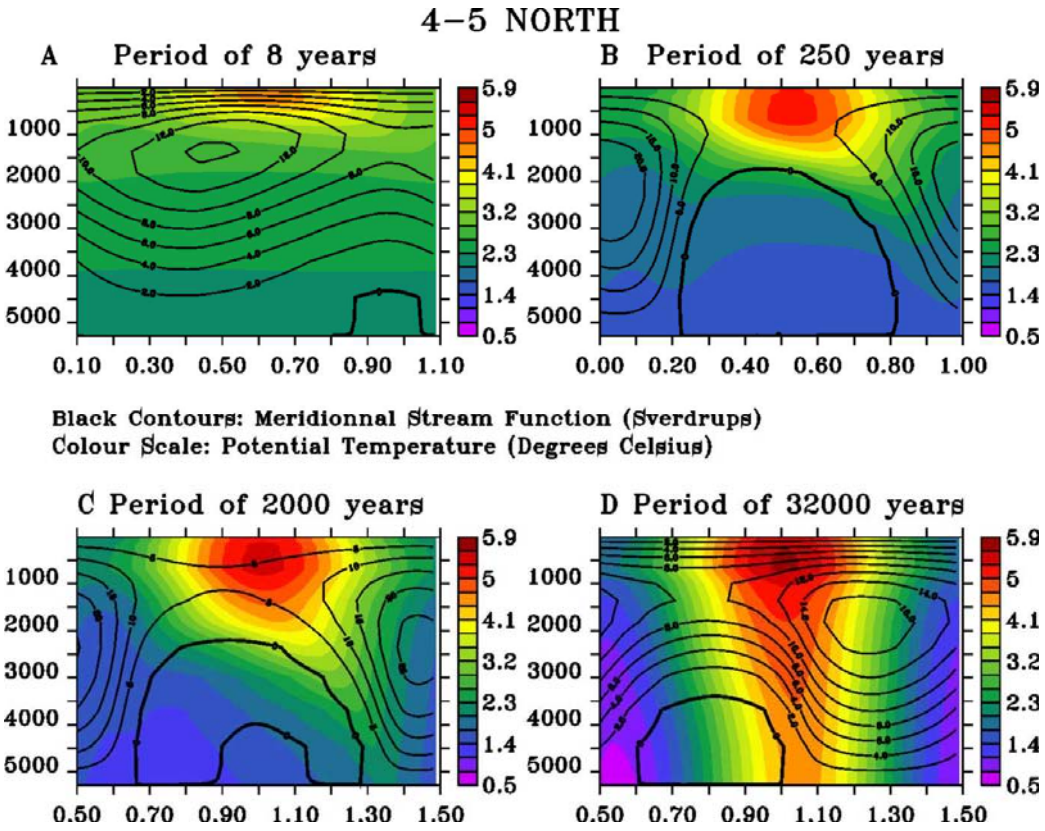

Figure5-10: Hovmoeller plots for the northern hemisphere in experiment 4-5 for 4 forcing periods. The y axis is depth and the x-axis is time in fractions of a period. The contour spacing is of 5 Sverdrups.

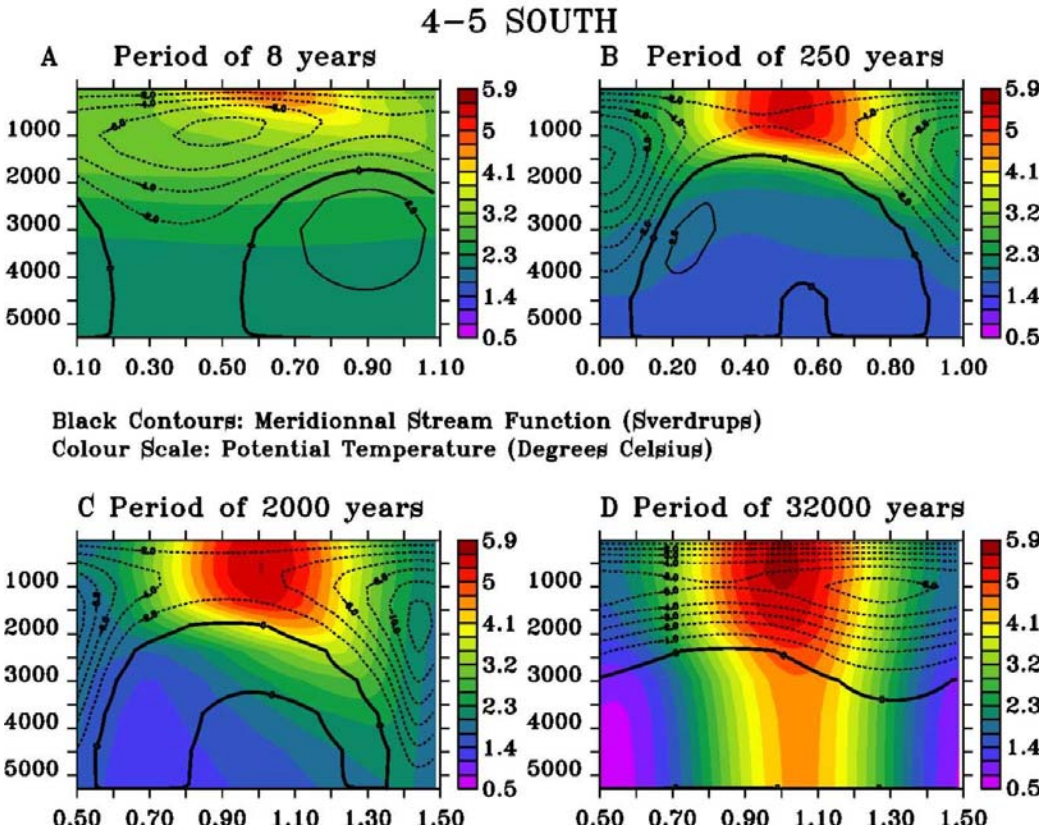

Figure5-11: Hovmoeller plots for the southern hemisphere in experiment 4-5 for 4 forcing periods. The y axis is depth and the x-axis is time in fractions of a period. The contour spacing is of 5 Sverdrups.

For the JI lag forcing, if the mean of the southern most value is increased but the range of the variability kept the same (exp 4-4A, exp 4-5A and exp 4-7A), the maximum amplitude in the dominant hemisphere increases and the resonance like period decreases from 250 to 60 years while in the subordinate hemisphere, the amplitude of the overturning decreases but the resonance like period increases, going from 250 years to above 32,000 years..

Decreasing the range (exp 4-3A) has the expected effect of decreasing the range in both hemisphere and increasing the period for which the resonance occurs in the subordinate hemisphere and the dominant hemisphere.

Figures 5-10 and 5-11 shows the evolution of the potential temperature and the overturning stream function at high latitudes in the northern and southern hemispheres for experiment 4-5. Both hemispheres behave in a similar fashion. As the forcing period increases, the forcing signal penetrates deeper and deeper.

It also grows in amplitude as more of it is captured by the surface ocean and transmitted to the deep ocean. The bottom temperature mean decreases with increasing forcing period and the amplitude increases. This behaviour is almost identical to that of a single hemisphere basin. The asymmetry between the basins is apparent in the top half of the water column with warmer temperatures in the southern hemisphere and increases with the forcing period. For the very long forcing period, 32,000 years, the deep water formed in the northern hemisphere, the temperature of which is below 0.8^{o}C (i.e. below 1^{o}C), is present in the southern hemisphere as is clearly visible in figure 5-11 D (light purple contour).

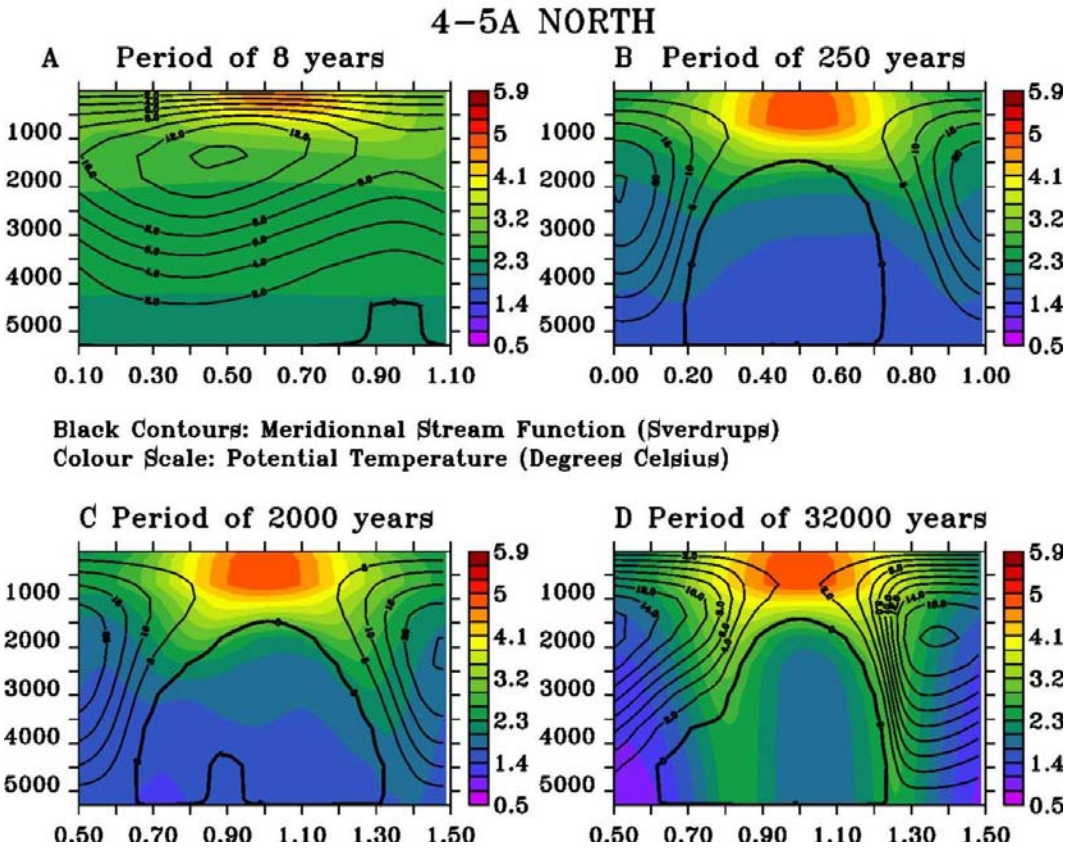

Figure5-12: Hovmoeller plots for the northern hemisphere in experiment 4-5A for 4 forcing periods. The y axis is depth and the x-axis is time in fractions of a period .The contour spacing is of 5 Sverdrups.

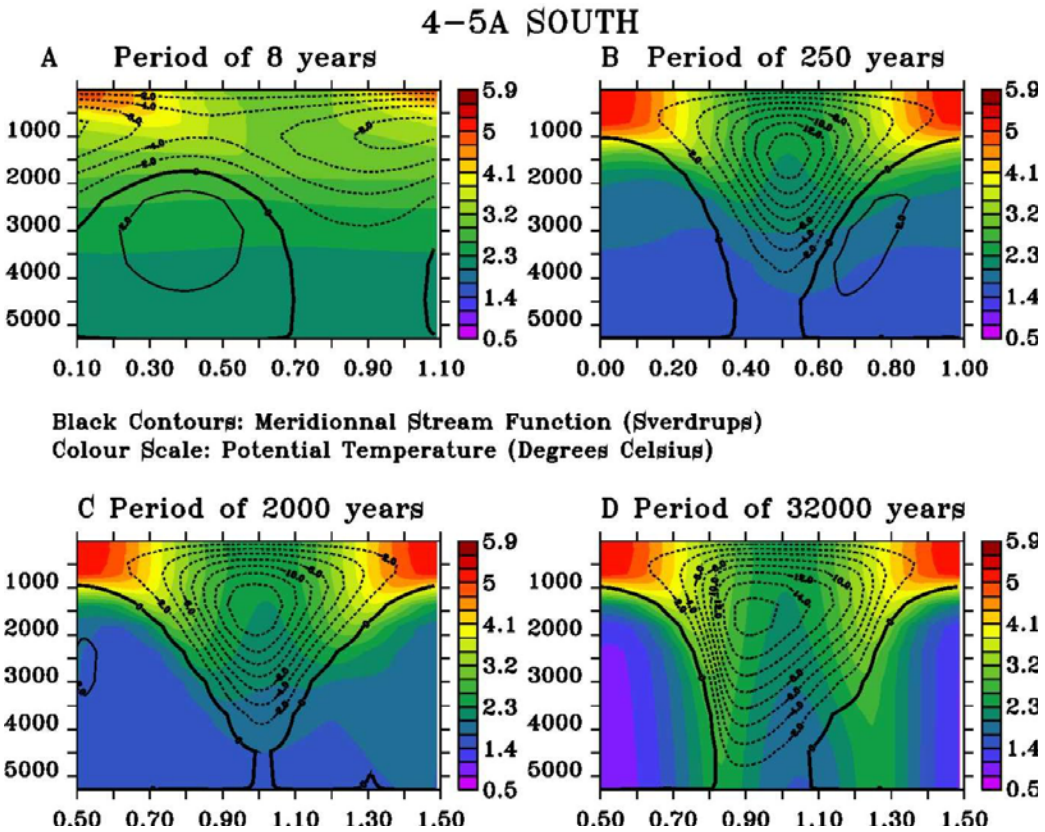

Figure5-13: Hovmoeller plots for the southern hemisphere in experiment 4-5A for 4 forcing periods. The y axis is depth and the x-axis is time in fractions of a period. The contour spacing is of 5 Sverdrups.

Figures 5-12 and 5-13 are the same graphs as 5-10 and 5-11 for experiment 4-5A. In the dominant hemisphere, there are no substantial differences between 4-5 and 4-5A for the forcing periods of 8 and 250 years. For 2,000 and 32,000 years, substantial differences with the 0 lag experiment (4-5) appear in the behaviour. The mean temperature of the bottom waters is much lower and the amplitude is smaller. There is also a clear decoupling between the surface and the deep waters. For instance, for the 32,000 years forcing the maximum temperature in the surface waters does not occur at the same time as the maximum in the deep waters.

The situation is very similar in the subordinate basin, with a similar decoupling between the surface and the deep waters. As in the 4-5 case, the surface waters in the southern ocean have a warmer temperature maximum than the northern.These results show that one of the biggest differences between 4-5 and 4-5A is how the deep ocean in each hemisphere is coupled to the surface waters.

In the 4-5A case, it is heavily influenced by what happens in the opposite hemisphere. The end result is that for some forcing periods, i.e. 2000 years, the deep ocean is always relatively cold.

Finally, figure5-14 underlines the main differences between the 4-5 and the 4-5A experiments in the potential temperature field's behaviour during a forcing period. For the very small period (8 years), there are little differences between the two. However the northern high latitudes bottom temperatures are slightly warmer for the 4-5A case than for the 4-5 case, while in the southern hemisphere, it is the opposite with the 4-5 being warmer than the 4-5A case.

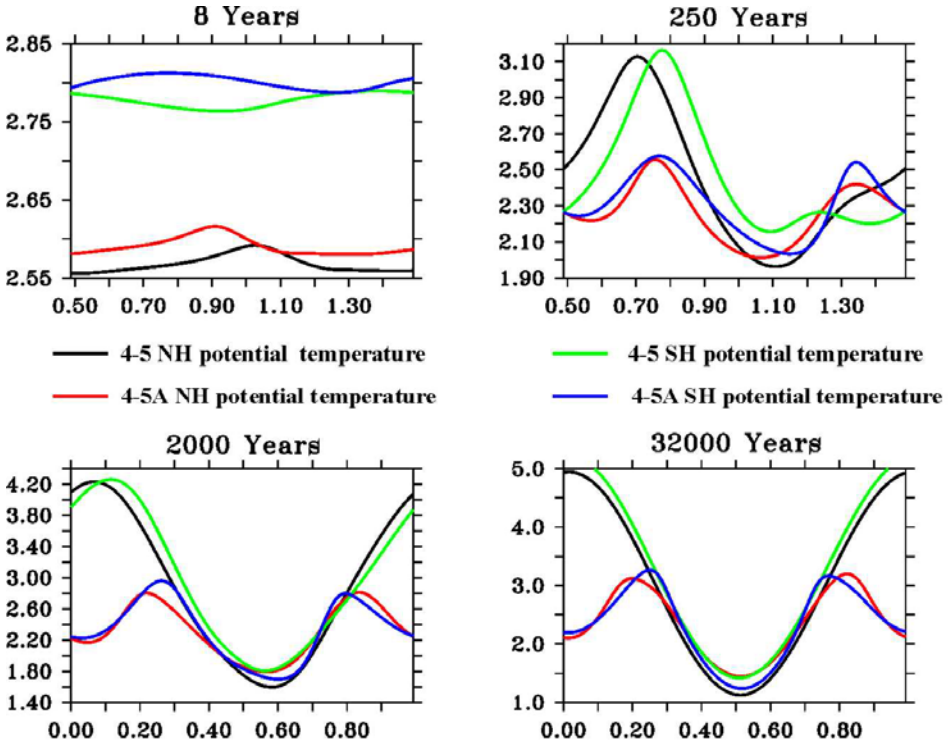

Figure5-14: average potential temperature at 2000 metres for both hemisphere in experiments 4-5, and 4-5A. The y axis is temperature in degrees Celsius and the x-axis is time in fractions of a period.

For the longer period, the differences between 4-5 and 4-5A are more acute. In particular, the 4-5A temperatures, in both hemispheres, show oscillations of half the period of the forcing. Furthermore, the mean temperature throughout a cycle is colder for the 4-5A case than for the 4-5 experiment and the amplitude

smaller. For all forcing periods, the 4-5 absolute minimum temperature in the northern hemisphere is slightly colder than the 4-5A absolute minimum temperature. In the southern hemisphere, the opposite happens.

5.5) Discussion:

Most of the resonance-like behaviour can be explained from the work done with the single hemisphere basin (chapter 4). There are however some aspects of the behaviour of a double hemisphere basin which need to be addressed.

5.5.1) Why is the southern cell so much weaker than the northern cell?

4-5 experiment:

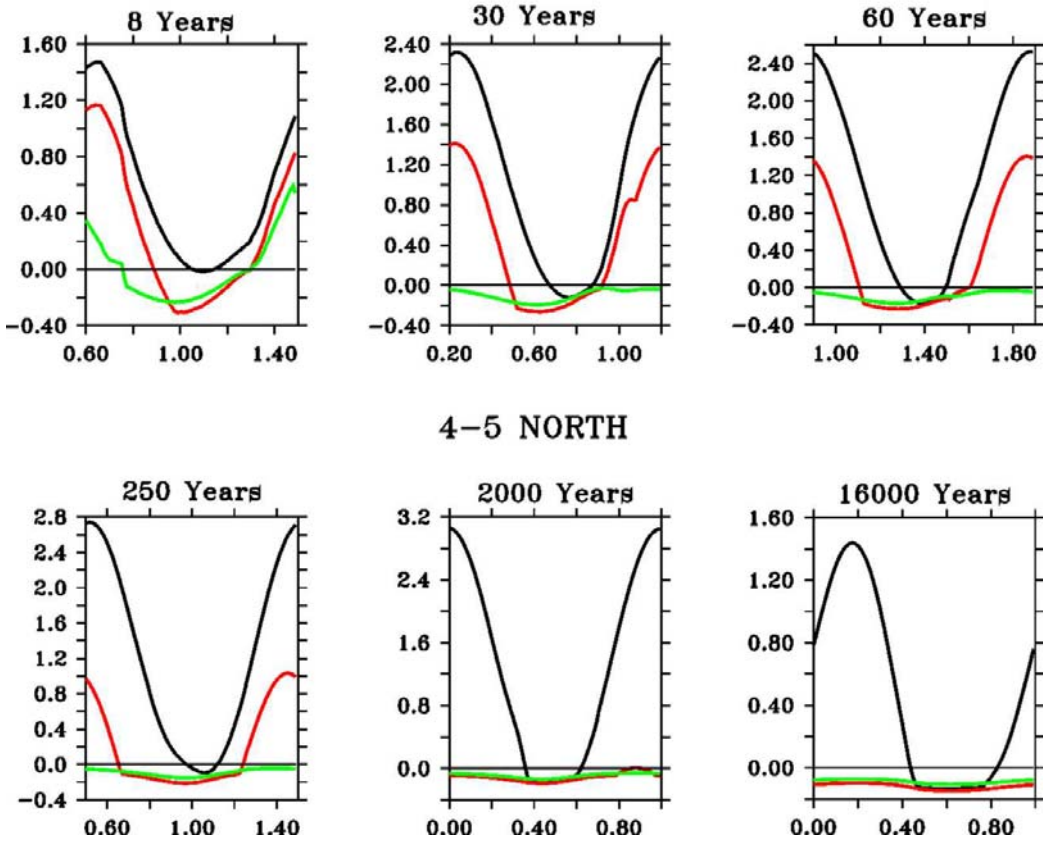

Figure5-15: Temperature difference between level 1 and 15 (black curve, level 1 and 8 (red curve) and level 1 and 5 (green curve) in the northern hemisphere. The y axis is temperature in degrees Celsius and the x-axis is time in fractions of a period. The negative values results from the model's convection scheme.

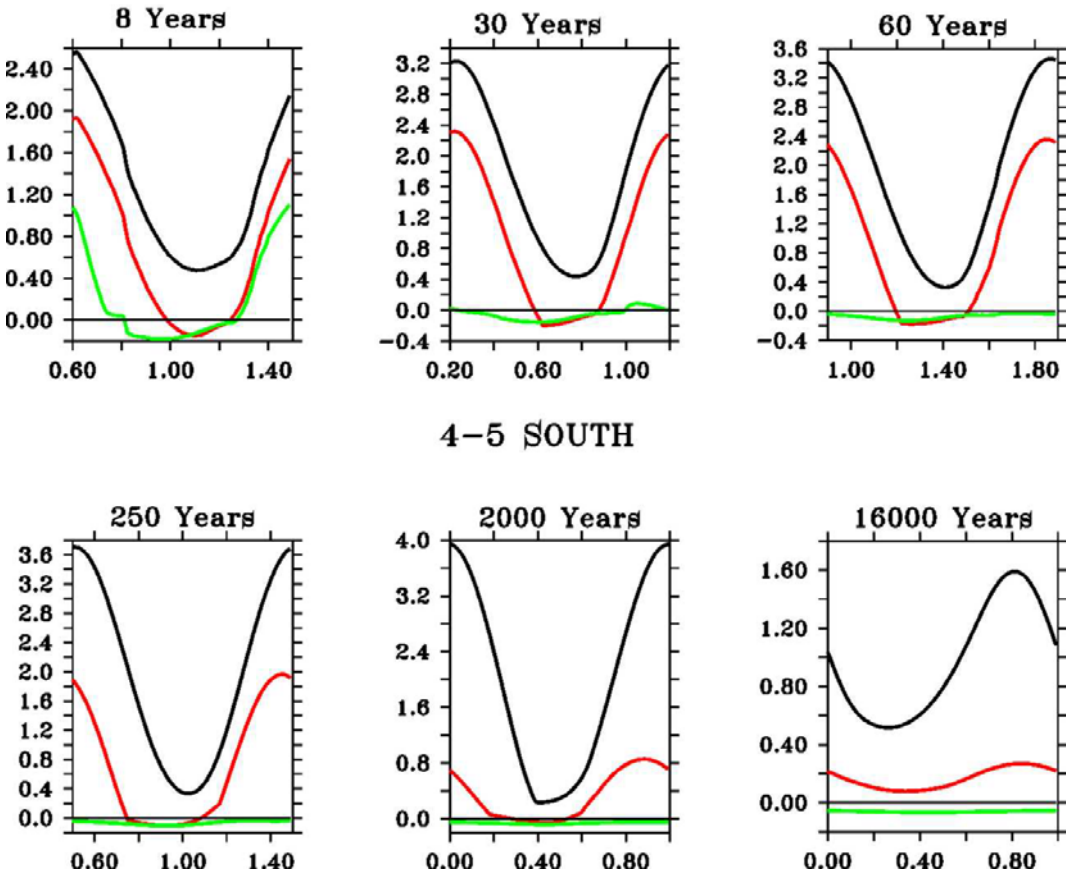

Figure5-16: Temperature difference between level 1 and 15 (black curve, level 1 and 8 (red curve) and level 1 and 5 (green curve) in the southern hemisphere. The y axis is temperature in degrees Celsius and the x-axis is time in fractions of a period. The negative values results from the model's convection scheme.

The southern hemisphere cell is much weaker than the northern hemisphere one principally because the southern hemisphere is far more stratified than the northern, due to the fact that the bottom water is produced in the NH. Figure 5-15 and 5-16 clearly illustrates this point. For all the periods, the maximum surface to bottom temperature difference is greater in the southern hemisphere than in the northern hemisphere. This means that during a cycle, the stratification in the southern hemisphere is greater than in the northern hemisphere. The consequence is that the southern hemisphere ocean is more stably stratified and the overturning weaker. Similarly, the minimum surface to bottom temperature difference is greater in the southern hemisphere than in the northern hemisphere. In fact, for the long periods, there is a small temperature inversion between the surface and the bottom in the northern hemisphere, which is absent from the southern hemisphere. This means that the water column becomes far more

unstable in the Northern hemisphere than in the southern hemisphere. Such a situation leads to high convection at high latitudes and thus strong overturning.

As demonstrated by figure5-15 and 5-16, this situation occurs throughout the water column as can be seen from the behaviour of the red and green curves.

Interestingly, the northern hemisphere maximum amplitude of the meridional overturning stream function is greater than that for a single hemisphere experiment. In fact, the overturning is always slightly greater, for all periods, suggesting that the effect of the southern hemisphere is to reduce the amount of stratification in the water column. This is confirmed by looking at the surface to bottom temperature difference (not shown), which is greater in the single hemisphere case than in the double hemisphere case even though the temperature of the deep ocean is cooler for the 4-5 experiment than for the single hemisphere experiment.

It is also interesting to note that the double hemisphere configuration leads to a colder minimum bottom temperature even if the forcing in the southern hemisphere has a minimum temperature of $1^{o}C$ and this regardless of whether or not there is a phase lag between the two hemispheres.

4-5A experiment:

For the pi lag forcing, the most obvious is difference in the results with respect to the 0 lag forcing experiment is that the amplitude of the overturning in the southern hemisphere is very close to that of the northern hemisphere. Figure 5-17 and 5-18 clearly show that both hemispheres behave in a similar fashion, albeit with the prescribed phase shift although the behaviour of the northern hemisphere is more non-linear. The southern hemisphere however still shows a greater maximum stratification as indicated by the black curve which for a forcing period of 16000 years reaches a maximum of 4^{0} C while in the northern hemisphere, it reaches a maximum of $2.4^{o}C$.

The northern hemisphere still has a stronger maximum overturning because for all forcing periods, the convection is stronger as it reaches deeper. This is evident when one examines the black and red curves in figure 5-17 and 5-18 which in the northern hemisphere become more strongly negative than in the southern hemisphere.

However, comparing the southern hemisphere with 0 lag forcing to the southern hemisphere with π lag forcing, shows that the amplitude of the surface to bottom temperature gradient is much greater in the π lag case than the 0 lag case. This suggests that the amount of stratification varies more in π lag the case than in the 0 lag case thus leading to greater oscillation in the overturning.

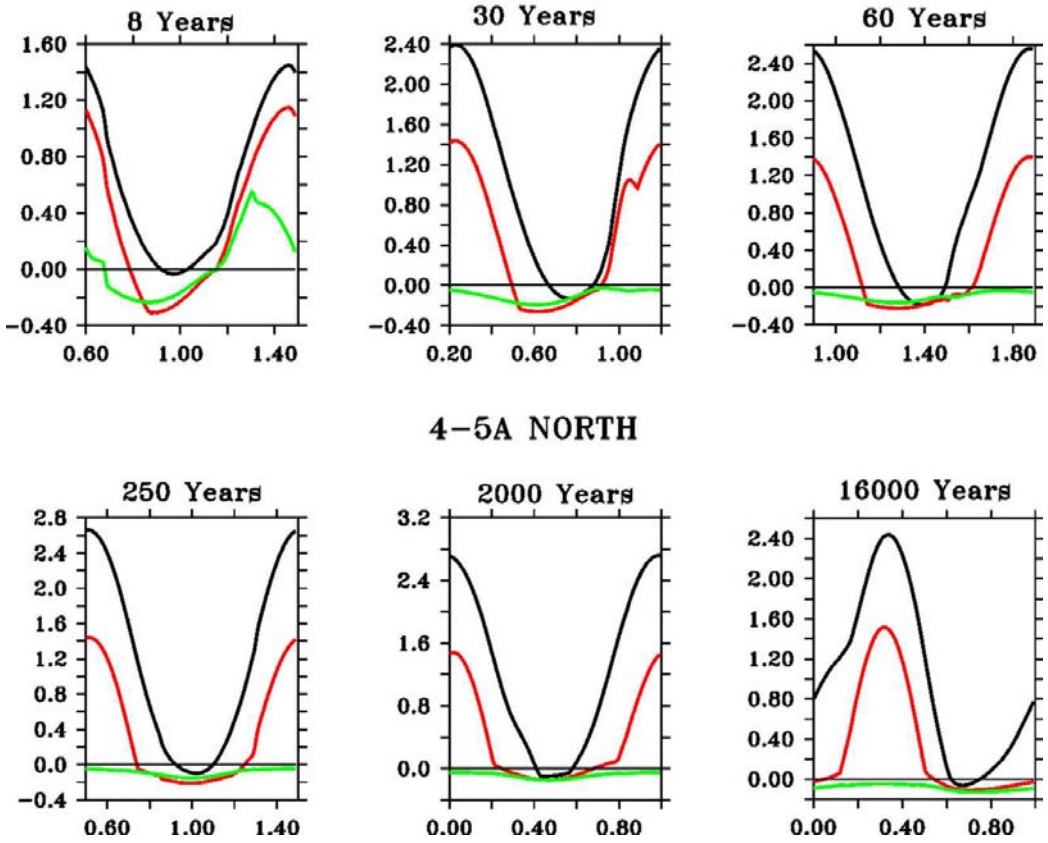

Figure5-17: Temperature difference between level 1 and 15 (black curve, level 1 and 8 (red curve) and level 1 and 5 (green curve) in the Northern hemisphere. The y axis is temperature in degrees Celsius and the x-axis is time in fractions of a period. The negative values results from the model's convection scheme.

In fact, the comparison of the 0 lag case with the π lag case demonstrates that the red curve shows far more variability in the pi lag case than in the 0 lag case,

indicating greater amplitude in the top to mid ocean convection. This means that in the π lag situation, the ocean becomes far more stratified than in the 0 lag case. This is why, particularly at long periods, the minimum in the maximum overturning stream function is smaller for the π lag case than for the 0 lag case. The amount of stratification reaches a maximum for the 4-5A experiment for a forcing period of 250 years. For larger periods, more of the forcing signal is captured but the diffusion is now efficient enough to transmit that signal to the deep ocean. Hence the surface to bottom temperature difference maximum remains fairly constant from a forcing period 250 years upwards.

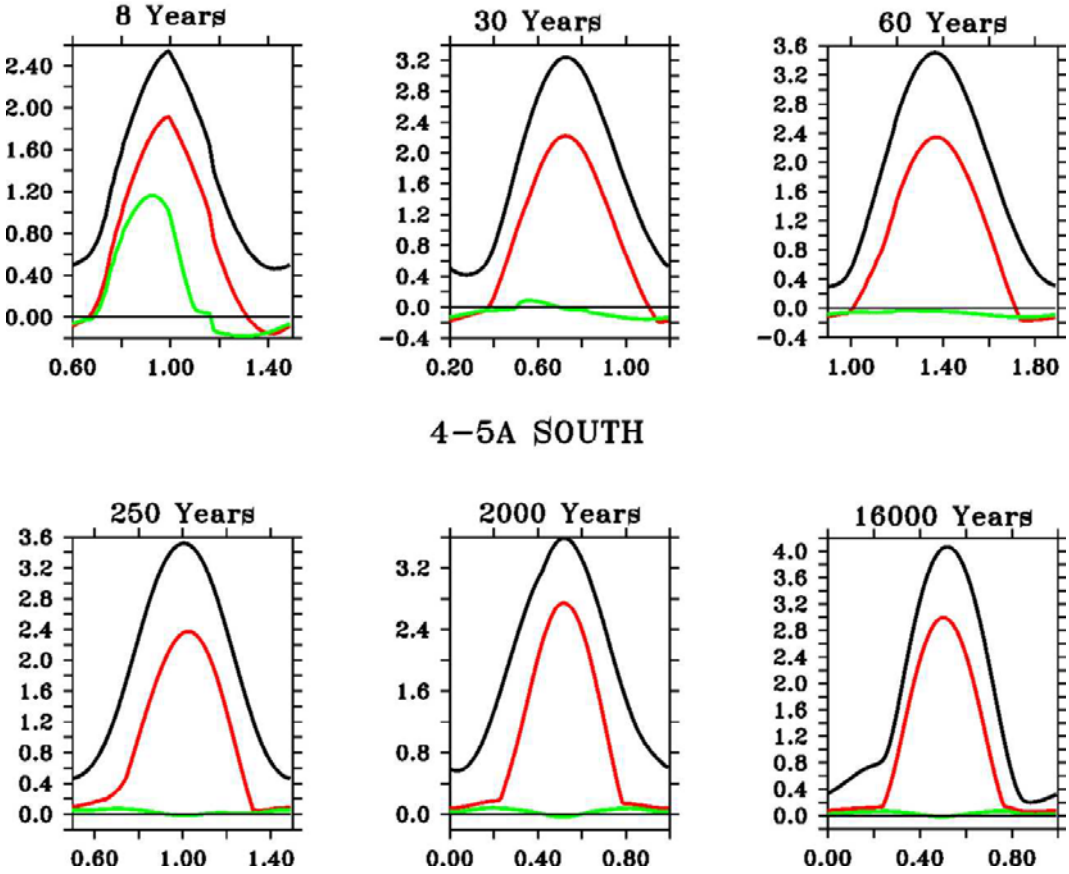

Figure5-18: Temperature difference between level 1 and 15 (black curve, level 1 and 8 (red curve) and level 1 and 5 (green curve) in the Southern hemisphere. The y axis is temperature in degrees Celsius and the x-axis is time in fractions of a period. The negative values results from the model's convection scheme.

5.5.2) Deep water production:

For the small periods, there are very little differences between 4-5 and 4-5A. Clearly, not enough of the forcing signal is captured to necessitate a substantial response from the ocean circulation. At longer periods, multi-decadal and above, differences between the two set-ups become more pronounced. To a certain extent, this has a lot to do with deep-water production.

In the pi lag forcing, there are two sources of deep water so to speak which result in near continuous production of deep water. This means that the deep never becomes warm (relative to the 0 lag experiment), even for the long periods (figure 5-10). As result, during a forcing cycle, there can be intense stratification in either hemispheres, as seen in figure 5-12 B, C, D, where the maximum warming of the surface waters coincides with deep cold temperatures. This intense stratification leads to very weak overturning; this explains the main difference between the 0 lag and π lag experiments. Indeed, figures 5-8 and 5-9 show that the maximum overturning has roughly the same value for experiments 4-5 and 4-5A. What gives the overturning in 4-5A a greater amplitude is the fact that the minimum overturning is so much weaker.

As the period becomes longer, the effect of the forcing becomes greater and the decoupling of the surface and bottom ocean more intense. In other words, the surface temperature in each hemisphere is controlled by the forcing in that hemisphere whereas the bottom temperature is controlled by the forcing in both hemispheres. This leads to a situation where the surface reaches a maximum when the bottom reaches a minimum. Hence for instance, the maximum surface to bottom temperature difference in the northern hemisphere is 1.42 degrees Celsius in the 4-5 experiment against 2.42^{o}C (figures 5-15 and 5-17, black curve).

The mid depth ocean (~1000 metres) responds in a similar fashion but the divergence in behaviour between 4-5 and 4-5A occurs for a smaller period (figure 5-15, 5-16,5-17,5-18, red curve). Indeed, by 250 years, the difference in temperature between the surface and 1000 metres (level 8) has a smaller maximum for 4-5 than 4-5A. At longer periods, the divergence in behaviour is

even more acute, with the surface to 1000 metres temperature difference being negative with a very small amplitude for 4-5 while its is mostly positive with a large amplitude for 4-5A. This leads to a greater variability in the overturning over a forcing period for experiment 4-5A than for experiment 4-5.

5.5.3) 4-4 run.

This experiment is very similar to experiment 4-5 but the forcing is absolutely symmetric on either side of the equator. As a result, there is no dominant hemisphere and the oceanic circulation is identical in both hemispheres. It behaves almost identically to the single hemisphere circulation, as it made clear by table 5-3: the maximum overturning amplitude and the period for which it occurs as well as its minimum and maximum values are those of the single hemisphere basin analysed in chapter 4.

5.5.4) 4-4A run.

The main difference between 4-5A and 4-4A is the temperature of the deep water formed in the southern hemisphere. It has the same value as the one produced in the northern hemisphere and as a result, the bottom temperature is on average colder. In the northern hemisphere, this leads to more stratification throughout the forcing cycle and as a result, the absolute maximum overturning will be weaker as will be the absolute minimum overturning. However in the southern hemisphere, because the model uses a non-linear equation of state, the lowering of the maximum temperature by 1 degrees Celsius will lead to a greater change in density than lowering the minimum temperature. The consequence is that the minimum overturning is almost unchanged whereas the maximum overturning increases significantly as the minimum amount of stratification during a cycle is reduced. Succinctly, reducing the average temperature in the subordinate hemisphere for a pi lag experiment has more impact on the surface waters in that hemisphere than the bottom waters, which are predominantly controlled by the dominant hemisphere.

5.5.5) 4-7A run.

In this run, the main difference with the 4-5A run is that the bottom water formed in the southern hemisphere is relatively warmer. This has implications for the dominant hemisphere as, when it cools, the underlying water will not be as cold as in the 4-5A case. As a result, convection will be stronger and the overturning will follow. Similarly, when the northern hemisphere is warming, it will never stratify as much as in the 4-5A case. The overturning will thus be stronger.

In the subordinate hemisphere, the stratification will be greater when the surface waters have reached their maximum, as the bottom of the ocean will be filled with cold water produced in the north. Similarly, when the surface waters are cooled, the surface to bottom temperature difference will be greater than in the 4-5A case. The consequence is that the water column will be more stratified and thus prone to less convection thus a weaker overturning.

5.5.6) 4-3A run

In this run, the southern hemisphere amplitude is only 2^{o}C. The deep water never gets as warm as in the 4-5A case. The result is that the convection is not as intense in the dominant hemisphere as the water column is slightly more stratified when the surface waters in the northern hemisphere reached their coldest temperature. The maximum stratification is of the same order as in the 4-5A experiment as the minimum surface restoring temperature in the southern hemisphere is the same, namely 1^{o}C, so there is little difference in the level of maximum stratification present in the model when the surface waters in the NH are at their warmest.

In the subordinate hemisphere, when the surface waters are at their warmest, the stratification is lower than in the 4-5A case since the surface forcing is not as strong. This leads to stronger overturning. When the surface waters are at their coldest, the surface to bottom temperature difference is slightly greater than in

the 4-5A case as the deep water never gets as warm as in the 4-5A case. This leads to a slightly weaker overturning.

5.5.6) Resonance behaviour

The presence of two sources of deep water also has significant impact on the resonance like behaviour of the system. As is shown in table 5-3, as the average temperature increases, the period for which the maximum amplitude occurs becomes smaller.

This is similar to what happens in a single hemisphere configuration when the vertical diffusion is increased. In that set-up, the resonance occurs when a substantial part of the forcing signal is captured by the surface ocean but the diffusion cannot keep up with the changes in the surface and as a result, the water column is either weakly stratified or strongly stratified (see chapter 4).

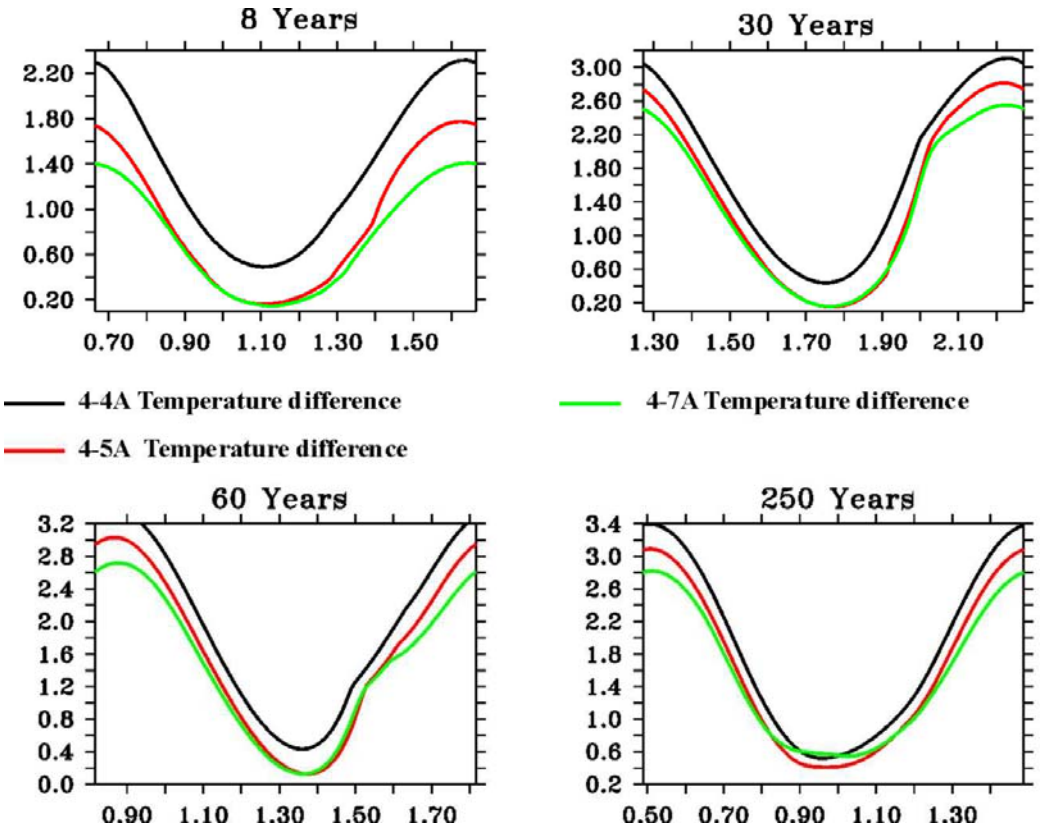

Figure5-19: Surface to bottom temperature difference for 4-4A(black), 4-5A (red) and 4-7A(green). The y axis is temperature in degrees Celsius and the x-axis is time in fractions of a period.

In the double hemisphere experiment, the mechanism is slightly different. Having a second source of deep-water means that in the dominant hemisphere, the minimum stratification is weaker than in the single hemisphere case, as the minimum bottom temperature when the surface forcing is at a minimum is warmer than in the single hemisphere case. Similarly, when in the dominant hemisphere, the surface waters are at their warmest, the deep temperature is colder than in the single hemisphere case and a result, the overturning will be weaker. The combination of those two situations will lead to a greater amplitude in the overturning. Succinctly, the presence of a second deep water source makes it easier for the system to reach extrema surface to bottom temperature differences.

As shown in table 5-3, the period for which the maximum amplitude occurs varies predominantly because of the changes in the maximum overturning value. The resonance shifts towards the smaller period mainly because the absolute maximum shifts towards them. This is because the minimum overturning during a forcing cycle very quickly reaches a value close to the absolute minimum overturning for the experiment. Furthermore, once it has reached it, the value of minimum overturning during a forcing cycle remains constant for subsequent forcing periods. The maximum overturning during a cycle show much more variability. Hence the behaviour of the resonance is principally controlled by the minimum stratification that occurs during a forcing cycle. This occurs when a substantial part of the forcing signal is captured but is not transmitted fast enough by diffusion to the deep ocean. The higher the average forcing temperature, the warmer the bottom temperature becomes (figure 5-19). As a result, the water column is less stratified. This means that a smaller forcing period is needed to create the minimum stratification since less of the forcing signal will need to be captured. The absolute overturning maximum occurs when the surface to bottom temperature difference reaches an absolute minimum. As is shown in figure 5-17, for 4-4A, the minimum temperature difference is still decreasing as the period increases from 8 years to 250 years. For 4-5A and 4-7A, the minimum decreases from 8 years to 60 years but increases from 60 years to 250 years, indicating that the absolute minimum occurs for a period between 60 years and 120 years. Furthermore, the range in the bottom to surface temperature

difference for these two experiments has also reached a maximum for a period between 60years and 250 years indicating that the resonance period is somewhere in between, as is shown in table 5-3

Changing the range in the southern hemisphere reduces the amplitude of the maximum overturning but not the period for which the resonance occurs. Although the strength of the stratification changes, the period for which the absolute minimum in stratification occurs does not.

5.6) Summary and Implications:

These runs have demonstrated the complexity of the response of a double hemisphere ocean basin to a very simple oscillatory buoyancy forcing. One of the most striking results is that when the forcings in both hemispheres have no lag, an asymmetry of $1^{o}C$ in the amplitude of the forcing profiles with stronger forcing in the northern hemisphere, leads to substantial differences in the response of the overturning with a clear dominance of the northern overturning cell for all forcing periods. Furthermore, when the forcing in the subordinate hemisphere lags the forcing in the dominant one by half a period, the system exhibits substantial oscillations, even at very long periods. In fact, the asymptotic behaviour (figure 5-2) suggests that these oscillations would persist for an infinite forcing period.

The strength of the amplitude of those oscillations stems from the presence of two sources of deep water which lead the water column to become either very stratified leading to a weak overturning or weakly stratified, which leads to a strong overturning. This result is to some extent in agreement with the conclusions of Marotzke & Klinger (2000) who stated that the export rate of NADW is controlled by the mixing and upwelling in the rest of the world ocean. Indeed, the present study has clearly shown that what happens in the southern hemisphere has a profound impact on the Northern Hemisphere deep water production, even when the Northern Hemisphere forcing is substantially dominant (experiment 4-3A & 4-7A).

These results have some important implications when one considers the precessional orbital forcing of climate variations. This is a 22,000 year forcing cycle which actually results from the combination of two forcing cycles, one of 19,000 years and the other of 23,000 years. It is an oscillation of the earth's rotational axis point and its effect is to strengthen or weaken the seasonal difference by determining how close to the perihelion or aphelion of the earth orbit the solstices occur. At one of its extremes, the winters in one hemisphere are very cold and the summers very hot (strong seasonal difference) while at the other, the winters and summers in one hemisphere are mild (weak seasonal difference). Crucially, when the one of the hemisphere has a strong seasonal contrast, the other has a weak one. Hence when we have a warm winter in the northern hemisphere, we will have a very cold winter in the southern hemisphere and vice versa. If we consider that the forcing we apply is equivalent to a winter forcing, when deep water production occurs, then our result suggest that the precession forcing can strongly influence the THC, even though it has a period of about 22,000 years.

In this study, the experiments with a Л lag forcing between the northern and southern hemispheres (4-4A, 4-5A) provide the best insight into how the ocean could respond to precesionnal forcing. The results clearly show that a forcing period of 22,000 years (in between 16,000 and 32,000 years), the response of the ocean would still be significant, with an amplitude of at least 10 Sverdrups in the subordinate hemisphere (and greater in the dominant)if the amplitude of the forcing was 4 degrees.

The single hemisphere experiments have demonstrated that the mixing of the upper waters by the wind driven circulation has little impact on the behaviour of the meridional overturning circulation when the ocean basin is submitted to variable buoyancy forcing (see chapter 4). They also suggest that the presence of simple topography in the form of a mid-ocean ridge has only a very minor impact. However, these experiments are highly idealised and the grid resolution is coarse. It is not clear whether or not the results from these experiments can be extrapolated to the real world. Nevertheless, they suggest an explanation for the recent palaeo results that have described a 10,000 years cycle, very close to the

half a precession time scale, in the palaeo proxy record (Turney et al, 2004). Indeed, we have also observed a signal of half the forcing cycles in the deep temperature for a forcing period of over 2000 years, as illustrated in figure 5-12.

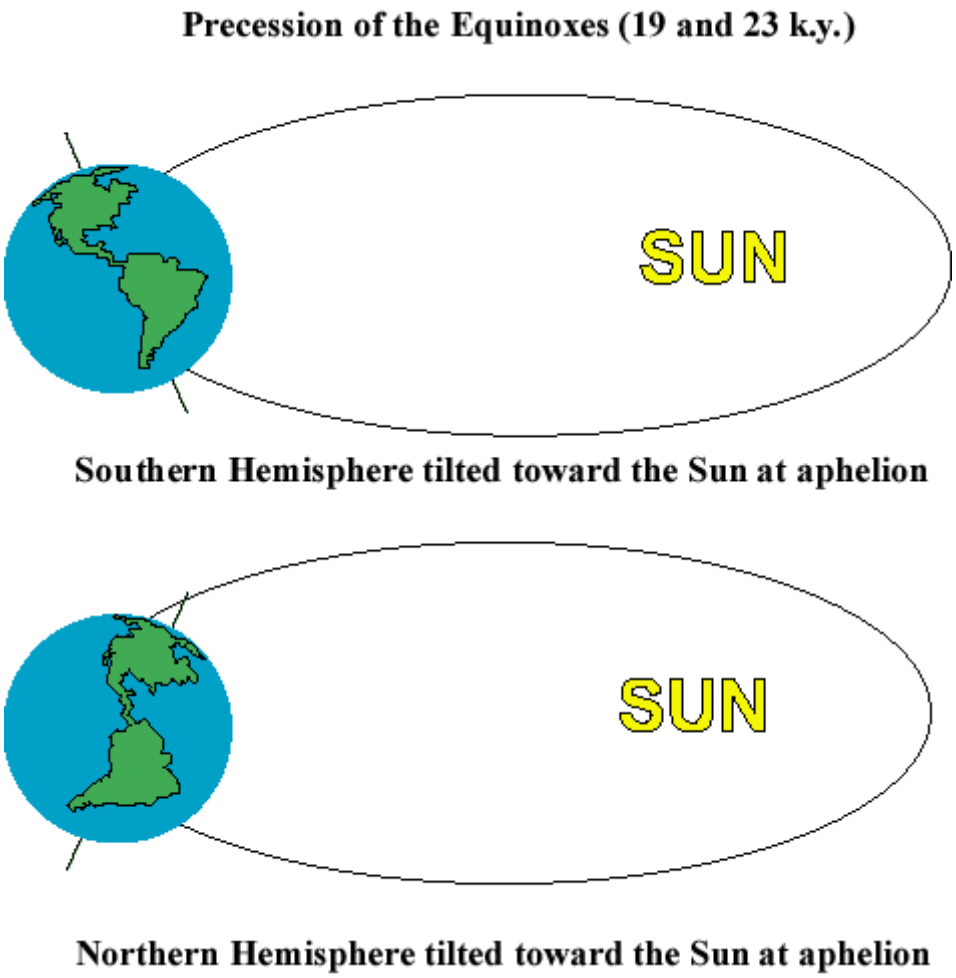

Figure5-20: Schematic of the effect of precession.
(http://earth.usc.edu/geol150/variability/images/orbit/precession.gif).

This study has shown that adding a subordinate southern hemisphere basin to the set-up of chapter 4 can profoundly alter the behaviour of the circulation in the northern hemisphere, particularly when the forcing in the southern hemisphere lags that of the northern by half a period.. In particular, it creates a secondary source of deep water which cools the deep ocean and increases the maximum

stratification that occurs during a forcing cycle.. This in turns leads to a much greater amplitude in the oscillatory response of the meridional overturning circulation, particularly for long forcing periods (2000 years and above). The impact of having a phase lag in the forcing on the southern hemisphere is even more pronounced; it leads to a dramatic increase in the amplitude of the oscillations of the meridional overturning stream function, with a range that is of the same order as that of the meridional overturning stream function in the dominant hemisphere.

Appendix: running the model

A-1)Inputs of the model:

The fundamental parameters of the models are all set in the data file ocean.in (see figureA-1) and can be changed without having to re-compile the model. These parameters include the integration time, the times step, the vertical diffusion as well as the output frequencies of snapshots and archive files.

Modifying the topography of the model requires creating a new ocean.kmt file (figureA-1) and adjusting within the model the latitude and longitude. This necessitates a re-compilation of the model code.

In this study, the surface boundary conditions are modified both in term of the temperature forcing and the wind forcing. In both cases, this involves modifying the model code in the setvbc.F file (figureA-1). Again, the model has to be recompiled. The model can then be run and will stop at once the end time set in ocean.in is reached or if the model becomes numerically unstable.

A-2) File format

The model output is of two kinds: ascii format and netcdf format. Two ascii file are generated during a run. They both store data received from a Fortran routine which calculates some of the models fundamental quantities such as the total heat, the maximum meridional overturning stream function and other extrema quantities such as the minimum and maximum temperature or the minimum and maximum velocities in both directions.

The netcdf files are of two types and archive the various fields within the model. (see tableA-1), an archive file, and a snapshot file.

The archive file allows the user to restart a run from a specific date. It usually has two successive time slices in order to restart the leapfrog scheme. The frequency of output of these files can be specified by the user. These files are usually 473718 bytes in size for the 60x60x15 basin. The fields written to the file are listed in tableA-1.

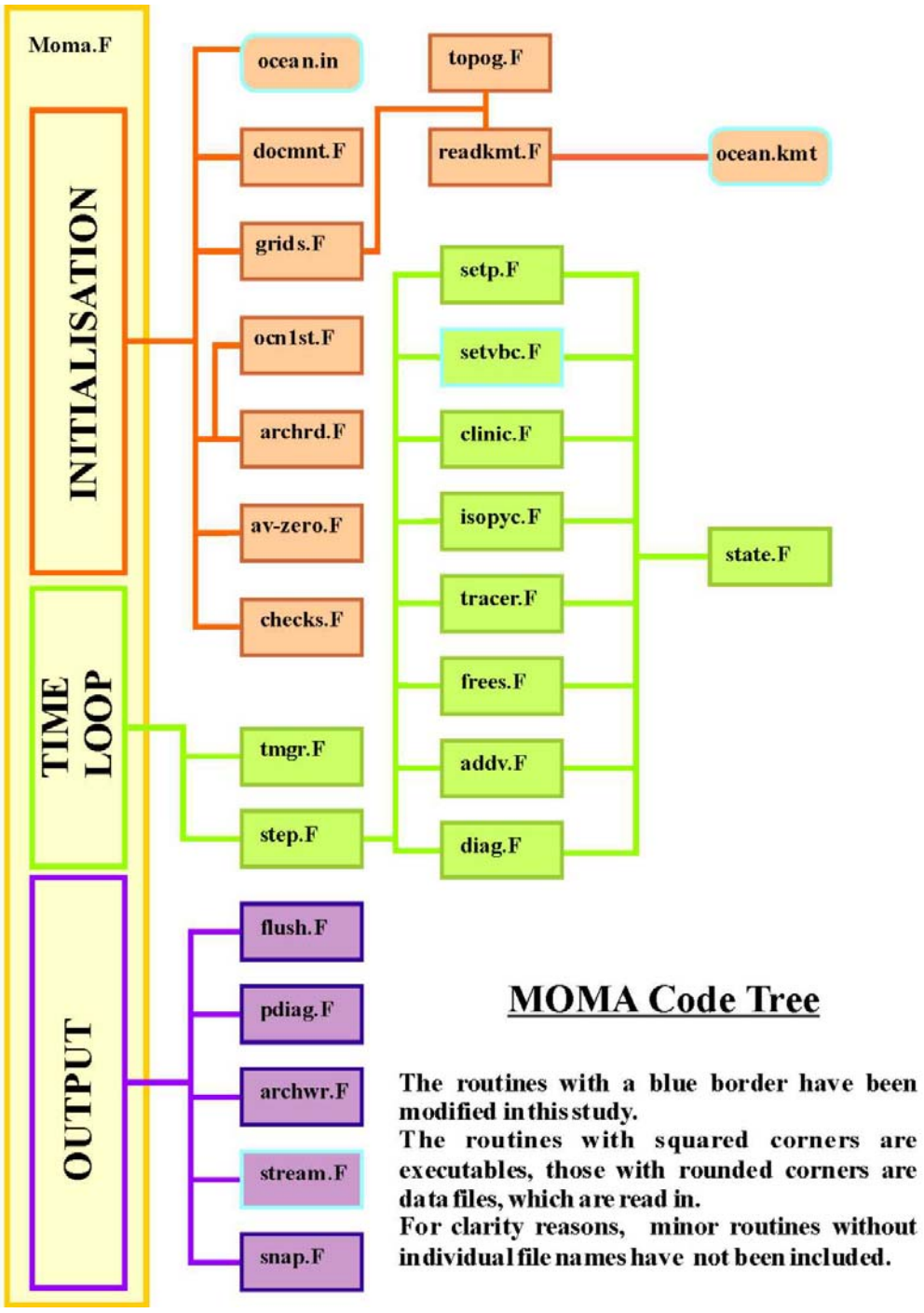

figure A-1: Code map of Moma.

Field	Abbreviation
Potential temperature	PT
Salinity	SAL
u-velocity (meridional)	U
v-velocity (zonal)	V
Barotropic u-velocity	BU
Barotropic v-velocity	BV
Free surface height	FSH
Elapsed model time	SECONDS
Elapsed model time	YEARS

Table A-1: output fields of netcdf files

The snapshot file is a succession of time slices of the model fields. Again, the frequency of writing to the file can be specified. This file contains all the field d the archive file as well as an additional variable CONV, which is a measure of the convection. This field is particular in that it averages the number of time a cell in the model undergoes convective adjustment between two sampling events. The model also allows the user to output the vertical velocity field to the netcdf files.